QATAR UNIVERSITY

COLLEGE OF ENGINEERING

AN EXPERIMENTAL COMPARISON OF PERFORMANCE BETWEEN FLAT SHEET AND HOLLOW FIBER MEMBRANE MODULES IN DIRECT CONTACT MEMBRANE DISTILLATION SYSTEM FOR DESALINATION OF SEAWATER

BY

AMIRA AL-KHATIB

A Thesis Submitted to the Faculty of

College of Engineering

in Partial Fulfillment

of the Requirements

for the Degree of

Master of Science in

Environmental Engineering

June 2016

COMMITTEE PAGE

The members of the Committee approve the thesis of **Amira Al-Khatib** defended on 29 May 2016.

_____

Prof. Farid Benyahia
Thesis Supervisor

_____

Prof. Hassan Arafat
Committee Member

_____

Dr. Samer Ahmed
Committee Member

_____

Dr. Fares AlMomani
Committee Member

_____

Dr. Ujjal Ghosh
Committee Member

Approved:

_____

Dr. Khalifa Al-Khalifa, Dean, College of Engineering

ABSTRACT

Membrane distillation desalination is an emerging technology with a promise to considerably reduce environmental impacts associated with traditional desalination technologies such as thermal and reverse osmosis. Various membrane module configurations have been reported in the literature. The most popular configuration reported in the literature was the direct contact and can be used for both flat sheet and hollow fiber membranes. The literature study has shown that the bulk of studies involved either flat sheet or hollow fiber modules separately and no single study involved both configurations in a single research work. This investigation was therefore aimed at comparing the flux performance of flat sheet and hollow fiber direct contact modules under similar conditions using real seawater from the Qatar coastal area of the Arabian Gulf. Our work has shown that the flat sheet direct contact membrane distillation module gave consistently higher fluxes than the hollow fiber module. The highest flux measured for the flat sheet module at 65 C and 3 L/min was 37.1 $L/m^2.h$ compared to 5.2 $L/m^2.h$ for the hollow fiber module under identical experimental conditions. The large difference in flux between the flat sheet module and the hollow fiber module was explained in terms of difference in flow regime and convective heat transport in the flow compartment of the two modules. The flow channel Reynolds numbers ranged between 283 to 770 for the flat sheet module while the Reynolds numbers ranged between 106 to 287 for the hollow fiber module. Our work also indicated that the Nusselt number Nu can be as much as 11 times higher for the flat sheet module than for the hollow fiber. This clearly

indicates that the convective heat transfer coefficient in the hot side is much greater in the flat sheet module than in the hollow fiber module. The maximum hot side convective heat transfer coefficient for the flat sheet module was estimated to be 17044 $W/m^2.h$ compared to 2163 $W/m^2.h$ for the hollow fiber module. The values of thermal coefficients obtained in this work were consistent with literature values. The observed salt rejection for all used membranes is above 99.8% thus confirming the ability of DCMD desalination to produce very pure water. This work has shown that more work needs to be done in hollow fiber module design to enhance flow turbulence and therefore improve convective thermal coefficients which will lead to higher permeate fluxes.

Table of Contents

List of Figures

List of Tables

Acknowledgment

I would not be able to finish my MSc. Thesis without the guidance, support, and help from several individuals who contribute in the preparation and accomplishing of this research and writing this thesis.

I would like to express my sincere gratitude to my supervisor **Prof. Farid Benyahia** from Qatar University for the continuous support, patient, enormous knowledge, excellent guidance, and professional advice that helped me overcome many crisis situations and finish this research. I have been amazingly fortunate to have an advisor who taught me how question thoughts and express ideas. His constructive criticisms at different stages of my research were thought-provoking and they helped me focus on my work. I could not have imagined having a better advisor and mentor for my MSc. Research.

I would also like to thank the faculty and the staff of the **Chemical Engineering Department** at Qatar University, including Dr. Ahmed El Khatat, Mr. Saeed Gad, Mr. Khaled Aljaml, and Mr. Sivaprasad for their assistant and support in performing experimental work in terms of maintenance in the laboratory and water quality analysis.

Moreover, I would like to thank Mr. Mohamed Sheldan for the arrangements to provide and deliver the necessary amount of real Arabian Gulf seawater in order to conduct the experiments.

I express my warm thanks to **ConocoPhillips Global Water Sustainability Center (GWSC)** and **Qatar University** for the financial support of this research in terms of equipment, consumables, and the graduate assistantship (GA) position.

Many **friends** have helped me stay sane through these difficult years. Their support and care helped me overcome the obstacles and stay focused on my graduate study. I greatly value their friendship and I deeply appreciate their belief in me.

Most importantly, none of this would have been possible without the love, believe, and patience of **my family** including; my parents and my young sister, that has been a constant source of love, concern, inspiration, support and strength all these years. I warmly appreciate the generosity and understanding of my beloved family.

Nomenclature

a	Coefficient ranged between (1-2)
A	Cross-sectional area of empty channel
${A_r}^m$	Membrane area ratio for heat transfer through fiber outside, fiber wall or fiber inside
b	Membrane thickness
B	Geometric pore coefficient ($B = 1$ for cylindrical pores)
C	Membrane mass transfer coefficient
C_c	Mass transfer coefficient when the transition region is dominant
C_f	Salt concentration in the feed bulk
C_m	Salt concentration on membrane surface from feed side
C_{Kn}	Mass transfer coefficient when the Knudsen diffusion is dominant
C_M	Mass transfer coefficient when the Molecular diffusion is dominant
C_p	Heat capacity
d	Main pore size of the membrane
d_o	Tube outside diameter
d_f	Diameter of spacer filament
d_h	Hydraulic diameter
di	Fiber inside diameter
d_{lm}	Log-mean radius difference of the fiber
D	Molecular diffusion coefficient
D_h	Hydraulic diameter in the spacer-filled channel
D_s	Shell inside diameter
f	Friction factor
g	Earth gravity
h	Heat transfer coefficient
h_f	Feed heat transfer coefficient
h_{mg}	Heat transfer coefficient of vapor within membrane pores
h_{ms}	Heat transfer coefficient of membrane material

h_p	Permeate heat transfer coefficient
h_{sp}	Spacer thickness
H_v	Enthalpy of water vapor
$H_{l,f}$	Enthalpy of the feed solution
J_p	Permeate flux through membrane
k	Thermal conductivity
k_{dc}	Spacer correction factor
k_B	Boltzman constant (1.381×10^{-23} JK^{-1})
k_m	Thermal conductivity of membrane
K	Coefficient depends on temperature, pressure, composition, membrane structure
K_g	Thermal conductivity of gas in membrane pores
K_m	Mass transfer coefficient
K_s	Thermal conductivity of membrane material
l	Characteristic length
l_b	Baffle spacing
l_m	Mesh size
L	Mean free path of the molecules, Channel length
m_a	Molecular weights of air
m_w	Molecular weights of water
n, N	Number of hollow fibers inside the module
P	Mean pressure within the membrane pores
P_{air}	Air pressure within the membrane pore
P_p	Hydraulic pressure on permeate side
P_f	Hydraulic pressure on feed side
P_{pore}	Gas phase pressure in pores
P_t	Tube pitch
P_1	Vapor pressure at feed side of membrane

P_2	Vapor pressure at permeate side of membrane
PD	Membrane diffusivity
Q	Volumetric flowrate
Q_c	Heat transfer by conduction through membrane material
Q_f	Heat transfer by convection through feed boundary layer
Q_m	Heat transfer through membrane
Q_p	Heat transfer by convection through permeate boundary layer
r	Pore radius
r_o	Tube outside radius
r_{max}	Maximum pore size radius
R	Gas constant
S_{vsp}	Specific spacer surface
T	Mean temperature in the pores
T_f	Feed bulk temperature
T_p	Permeate bulk temperature
T_1	Feed temperature at membrane surface
T_2	Permeate temperature at membrane surface
u	Fluid velocity
v	Gas mean molecular speed
v_s	Velocity in spacer-filled channel
Y	Salt rejection percentage

Greek Letters

α	Membrane surface area based on fiber inside diameter per unit length per fiber layer
β	Thermal expansion coefficient
γ_l	Liquid surface tension

γ_{sl}	Solid-liquid interfacial tension
γ_{sv}	Solid-vapor interfacial tension
δ_m	Membrane thickness
ε	Membrane porosity
ε_s	Spacer porosity
θ	Contact angle between solution and membrane surface
θ	Hydrodynamic angle
ϑ	Temperature polarization coefficient
μ	Fluid viscosity
ρ	Fluid density
ρ_m	Membrane density
ρ_{pol}	Density of Isopropyl alcohol
σ_a	Collision diameter for air (3.711×10^{-10} m)
σ_w	Collision diameter for water vapor (2.641×10^{-10} m)
τ	Pore tortuosity
φ	Concentration polarization coefficient
ϕ	Packing density

Chapter 1: Introduction

Saline water occupies approximately 97.5% of the total amount of water in our planet. The remaining 2.5% of water is subjected to fresh water in which 70% is located in the polar ice and glaciers. This means that less than 0.8% of water resources in the earth is fresh water that is available as rivers, lakes, air moisture, and groundwater and can be utilized by human. Figure (1) illustrated the distribution of earth surface water. All the percentages are approximated and rounded [1].

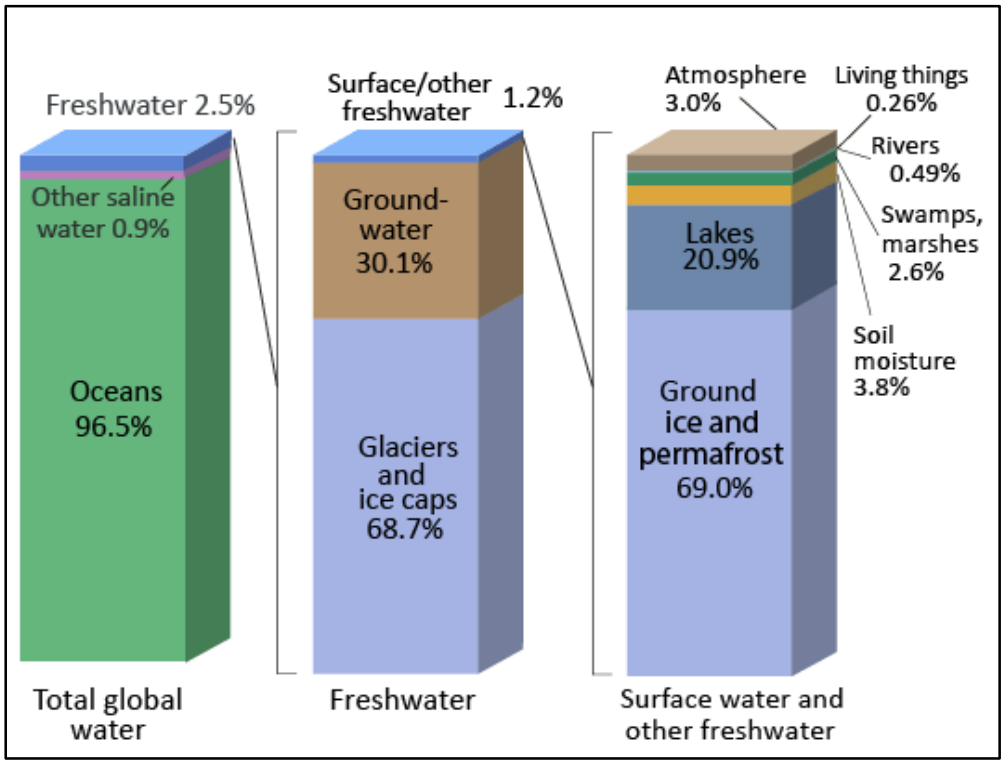

Figure 1: Water distribution on earth (Adapted from [1])

Furthermore, fresh water is not equally distributed among the all countries and with the industrial booming in the last decades, fresh water demand is increasing. Due to high population growth rate, increase of human industrial,

municipal, and agricultural activities, polluting the natural water resources, and climate change, keeping the hydrological cycle balanced became a serious issue [2]. Water Health Organization (WHO) [3] reported that the main reason of fresh water shortage is the huge consumption of 64 billion cubic meters of fresh water annually, which is beyond the natural recharge. Figure (2) represent human use of water where approximately 90% of fresh water goes to agricultural and industrial usage [3].

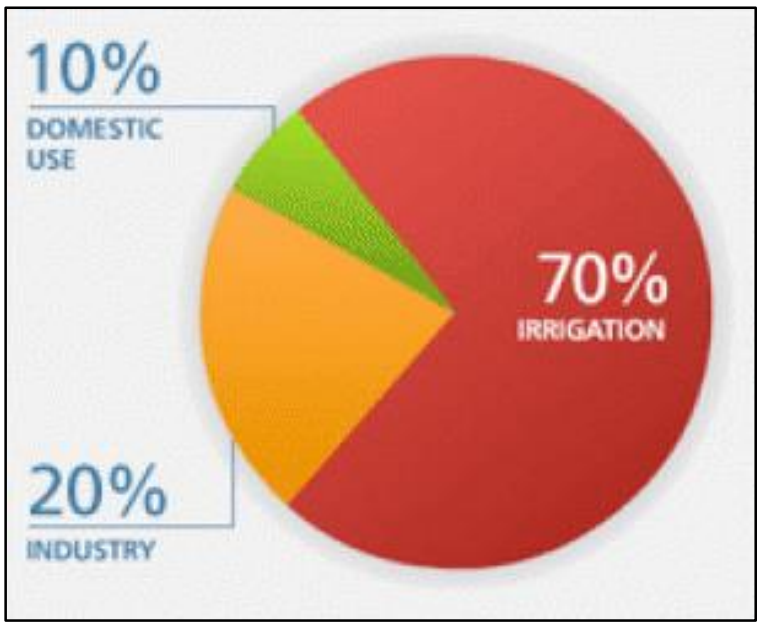

Figure 2: Human water consumption (Adapted from [3])

WHO is also reported that by year 2025, more than half of the world's population will be allocated in water-stressed areas [3]. Therefore, alternative water resources are studied and implemented to cover the shortage of fresh water, especially in countries that are classified as below the world's water-poverty line countries. Processes like desalination that traps world's main water resource [5] and wastewater treatment became the promising solutions to avoid complete depletion of fresh water and solve water-shortage problem [6], [7].

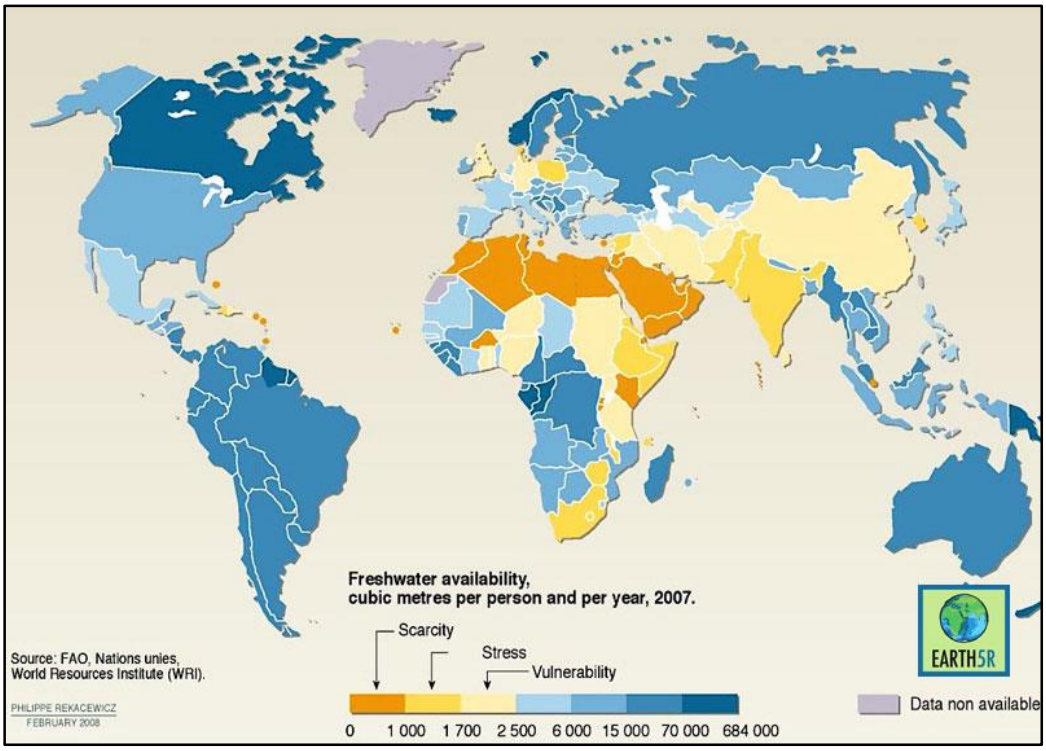

Figure 3: Fresh water availability in the world (Adapted from [4])

Figure (3) illustrated water availability in the world by year 2007 and it is clearly shown that some regions such as Middle East region and Gulf Cooperation Council (GCC) countries are facing large fresh water shortage.

1.1 Water resources and water consumption in Arabian Gulf Region

Middle East region and Gulf Cooperation Council (GCC) countries (Bahrain, Saudi Arabia, Qatar, UAE, Oman and Kuwait) are considered as very scarce regions of water resources. This is due to the lack of natural water resources, low average annual rainfall, high evaporation rate and tremendous consumption rate of water. Raouf [8] reported that the average water consumption in GCC countries is between 300–750 liters per person per day which considered the highest in the world. In order to compare water consumption rate in GCC countries to the whole world, figure (4) illustrates the average daily water usage

per person of different industrial and agricultural countries allocated in different continents such as Europe, Asia, and America.

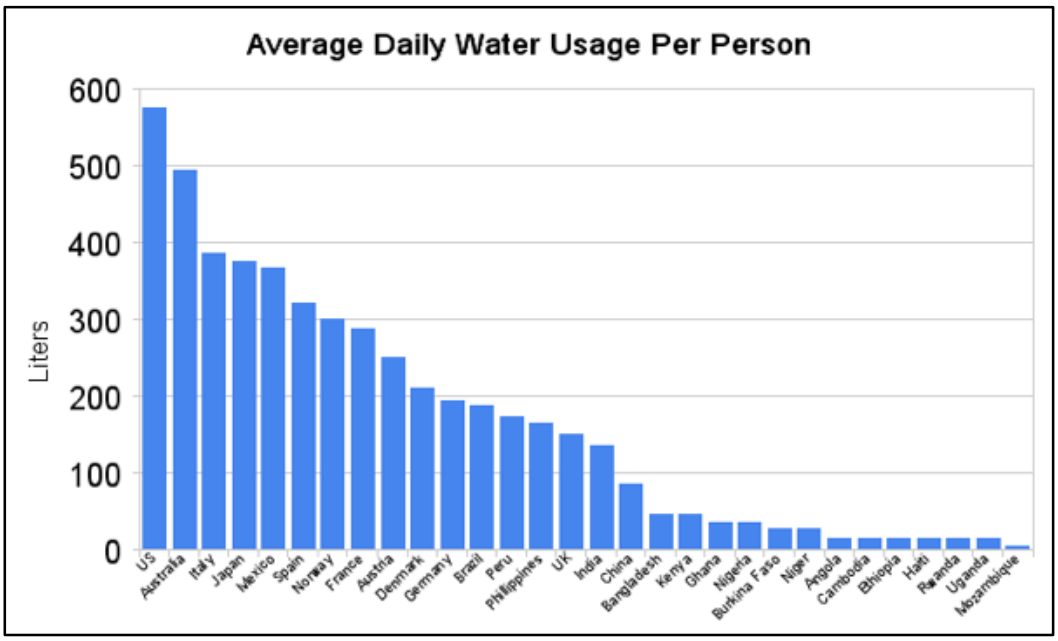

Figure 4: Water consumption rate in different countries in the world (Adapted from [9])

The lack of renewable water resources is represented in figure (5) that illustrates water consumption and renewable water resources in GCC countries in cubic meter per capita per annum and demonstrates that the consumption of fresh water is several times higher than the available renewable resources.

Even when GCC countries serve as the poorest in terms of water resources, they have one of the highest population growth rates, consequently, the highest consumption rate. With high water demand and growing population, desalination became the only solution of solving water shortage problem.

There are several desalination technologies, and mainly the selection of desalination process is based on several factors. These factors include salinity

range of the water and its temperature, plant capacity, site conditions, qualified labor, the form of available energy source, and the cost of energy [6], [11].

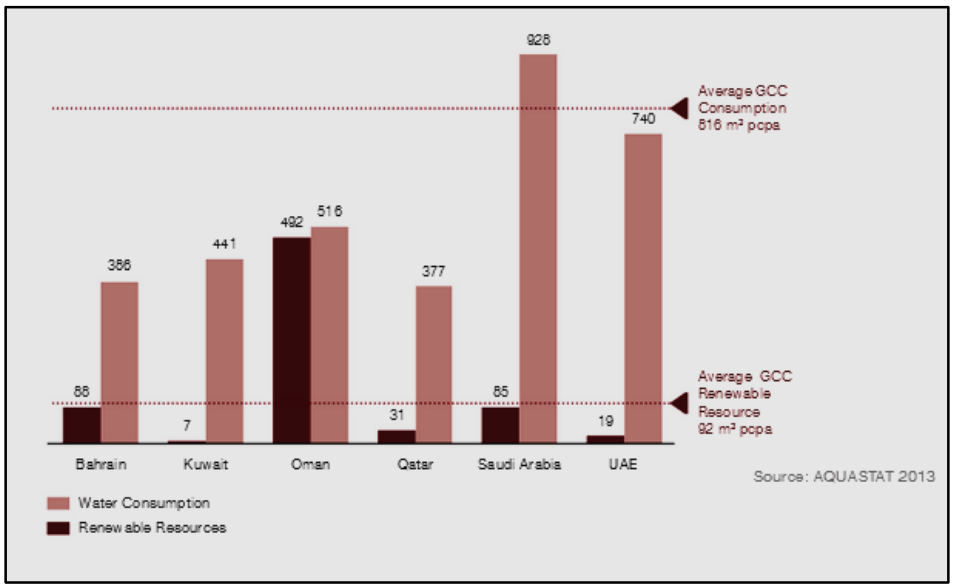

Figure 5: GCC countries water consumption and renewable water resources (Adapted from [10])

Seawater salinity and its temperature are the main factors that affect selection of desalination method. As shown in table (1), the salinity of Arabian (Persian) Gulf is the highest.

Table 1: Salinity and temperature of different seawater sources [12]

Seawater Source	Typical TDS Concentration (mg/L)	Temperature (℃)
Pacific and Atlantic Oceans	35,000	9 – 26 (avg 18)
Caribbean Sea	36,000	16 – 35 (avg 26)
Mediterranean Sea	38,000	16 – 35 (avg 26)
Gulf of Oman, Indian Ocean	40,000	22 – 35 (avg 30)
Red Sea	41,000	24 – 32 (avg 28)
Arabian Gulf	45,000	16 – 35 (avg 26)

High salinity of seawater source restricts the type of used desalination process. Process such as Reversed Osmosis (RO) is highly affected by the level of salinity as RO process is limited by 46,000 mg/L salinity level [12]. However, thermal desalination processes including Multiple effect distillation (MED) and Multiple stage flash desalination (MSF) are usually not affected by the salinity level of the sea. The measure of seawater salinity, its classifications and different salinity ranges are covered in **Chapter 2**.

1.2 Desalination History

Over the past 50 years, desalination process has made tremendous progress in some regions such as the Middle East and the Mediterranean region. Desalination plants start to be applied in Gulf region after the Second World War (WWII) with the discovery of oil and gas [13]. Nowadays, desalination plants are distributed all over the world in more than 150 countries [12]. Figure (6) illustrates the worldwide desalination capacity that produce more than 70,000 cubic meter per day.

It is clearly shown in figure (6) that more than 75% of desalination plants are allocated in the Arabian Peninsula and half of them are in Saudi Arabia.

Currently, desalination process is responsible for more than 70% of water supply in GCC countries producing more than 11 million cubic meters per day (MCM/d) as reported by year 2013 in which 6.3 MCM/d are produced by United Arab Emirates, Saudi Arabia 2.3 MCM/d, Kuwait 1.7 MCM/d, Qatar 0.9 MCM/d, Bahrain 0.4 MCM/d [12], [15]. In 2015, desalination process was responsible for approximately 86 million cubic meter of produced water per day. With Water demand that is approximately doubling every 20 years, complete relay on desalination process occurs in Gulf region [16]. In order to cover the need of high water demand, more desalination plants are planned to be built in different areas of the world especially in the Gulf countries with fresh water shortage problem. Figure (7) represents the present and the predicted demand for desalination plants in the middle east and GCC countries. According to 2011–2012 IDA

Desalination Year book [Global Water Intelligence (GWI) and International Desalination Association (IDA), 2012], approximately 16,000 desalination plants are installed worldwide with total capacity of 70 million cubic meters of produced desalinated water per day [12].

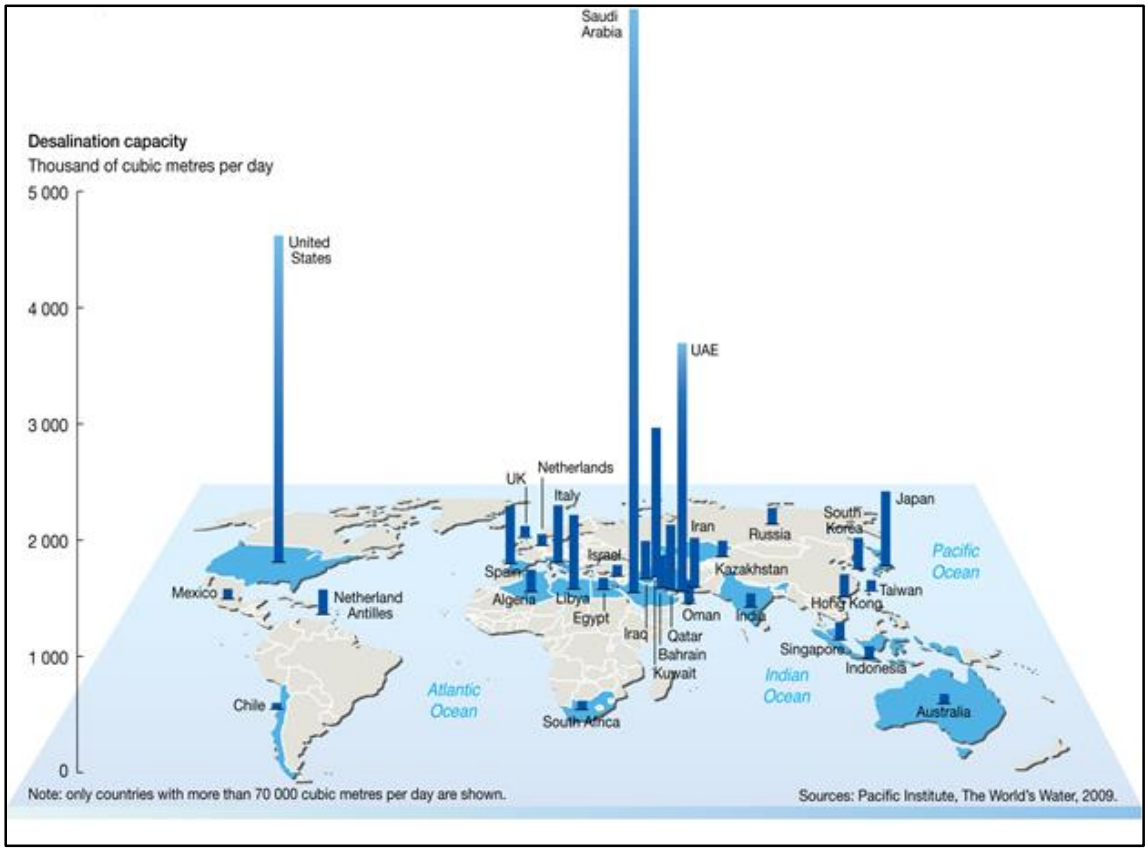

Figure 6: Desalination capacity worldwide (Adapted from [14])

Different types of desalination processes are implemented in Gulf countries such as Multiple effect distillation (MED), Multiple stage flash desalination (MSF), and Reverse Osmosis (RO). The selection of desalination process is limited by the physical characteristics of seawater. Countries like Qatar, Bahrain, and Kuwait are limited by high saline water of the Gulf. Therefore (MED) and (MSF) are dominating in these countries. On the other hand, KSA, UAE, and Oman have

the choice of other water bodies [13]. The majority of the used desalination processes are explained in details in **Chapter 2**.

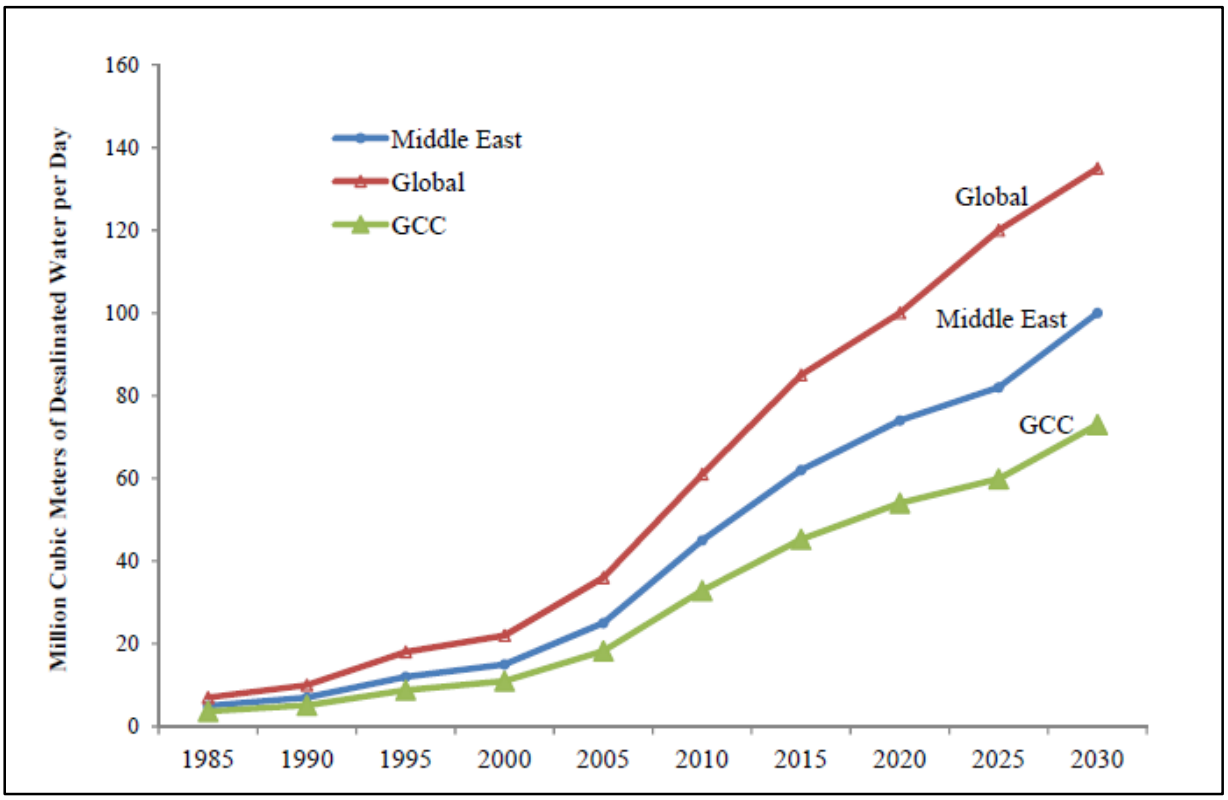

Figure 7: The demand for desalination plants Global, Middle East and GCC (Adapted from [17])

Table (2) below lists the number and the type of desalination plants in each Gulf country where it is shown that the usage of RO plants is narrowed by KSA, UAE, and Oman. Small desalination plants with very limited production capacities are not listed in table (2).

Table 2: The existing and future planed desalination plants in GCC countries [18]

Technology	UAE	Bahrain	KSA	Oman	Qatar	Kuwait	Total
MSF	20.0	1.0	20.0	3.0	6.0	7.0	57.0
RO	25.0	3.0	79.0	45.0	2.0	1.0	155.0
MED	9.0	2.0	9.0	-	2.0	-	21.0
VC	-	1.0	-	-	-	-	1.0
ED	-	-	-	-	-	-	-
RO+MSF	2.0	1.0	-	1.0	-	-	4.0
Total	55.0	7.0	108.0	49.0	10.0	8.0	237.0

Moreover, figure (8) shows the number and the location of these desalination plants on the Arabian Gulf with its corresponding technology and capacity.

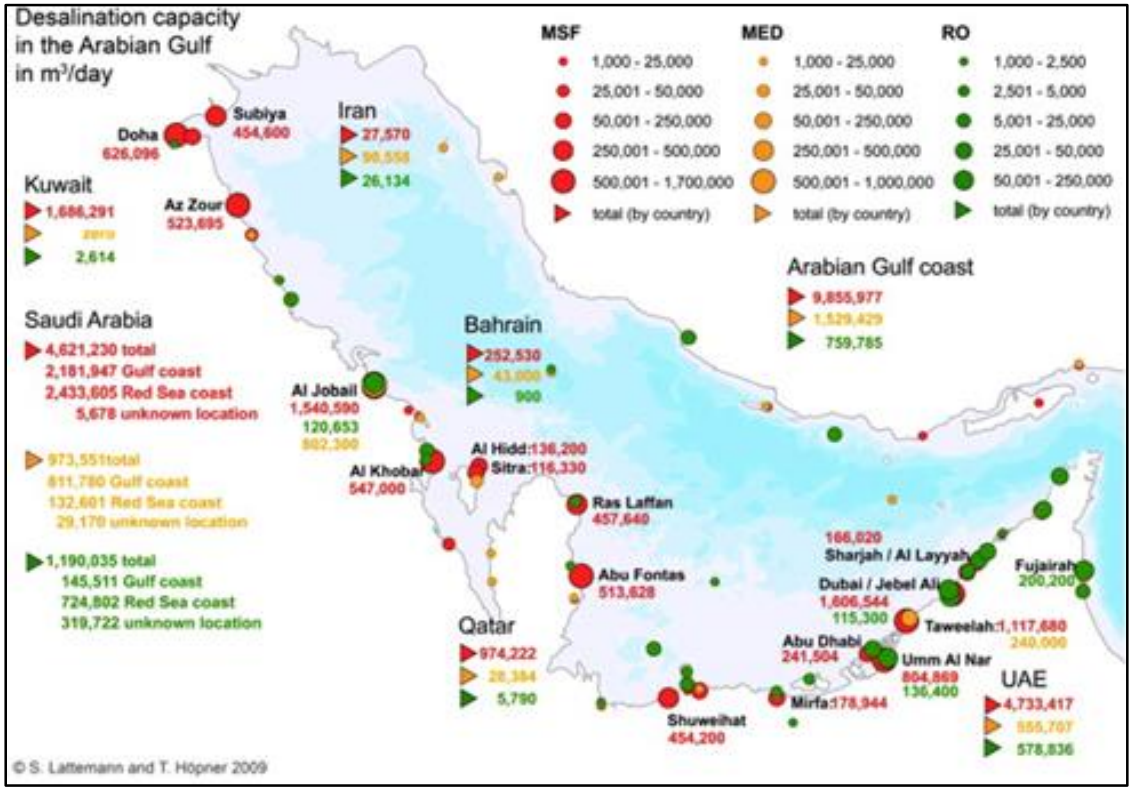

Figure 8: The number and location of desalination plants on the Arabian Gulf coastal (Adapted from [18])

Taking Qatar as an example, 974,222 m^3/day of fresh water is produced by MSF technology, 28,384 m^3/day by MED technology, and 5,790 m^3/day by RO technology as recorded by year 2009.

As it is mentioned before, due to Gulf's harsh conditions such as high temperatures, high salinity, and high turbidity [13], the implementation of RO technology shares only 30% of the total global capacity. RO technology is practiced more in Europe and USA where the turbidity and the salinity of water is much less than the Gulf seawater.

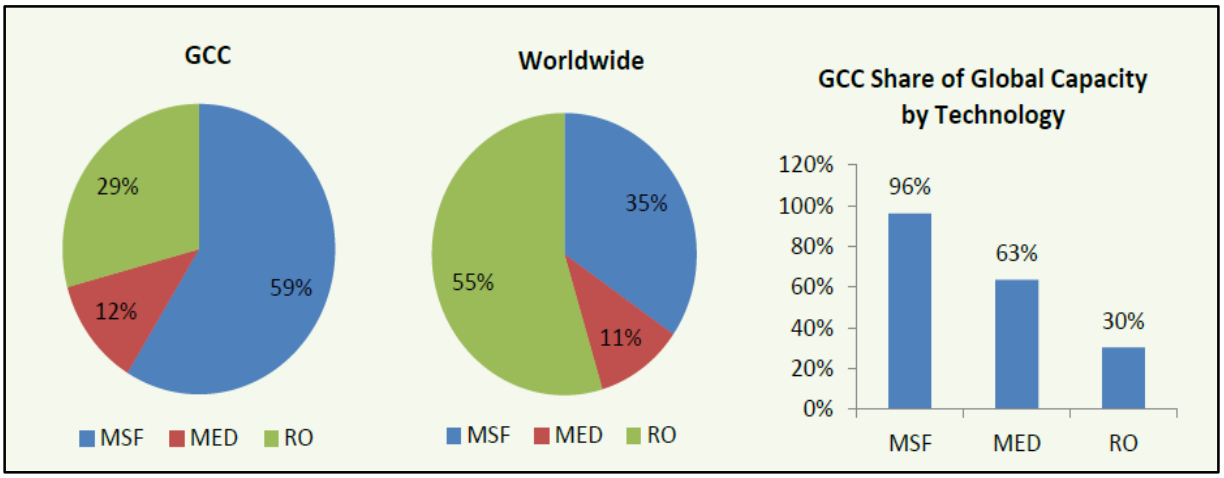

Figure 9: Desalination capacity by technology in GCC and worldwide, 2012 (Adapted from [13])

Figure (9) compares the desalination technology of GCC countries to the worldwide showing that GCC countries are responsible for the majority of thermal and especially the MSF desalination processes in the world.

1.3 Desalination in Qatar

Qatar met the fresh water demand for drinking, domastic and industral use, and irrigation mainly through desalination process. The first desalination plant in

Qatar was operated in 1962. Nowadays, several desalination plants are operating in Ras Laffan and Ras Abu Fantas. The Ras Abu Fantas desalination and power plants are corresponded for approximately 50% of fresh water supply. Desalination and power plants allocated to each other are usually practesed worldwide to provide the high temperatures from the low grade heat.

Figure (10) illustrates the location and the capacity of desalination plants in Qatar that produces more than 50,000 m^3/day of water. A small RO desalination plant was build in Dukhan city to treat high saline water and produce approximately 750 m^3/day of fresh water.

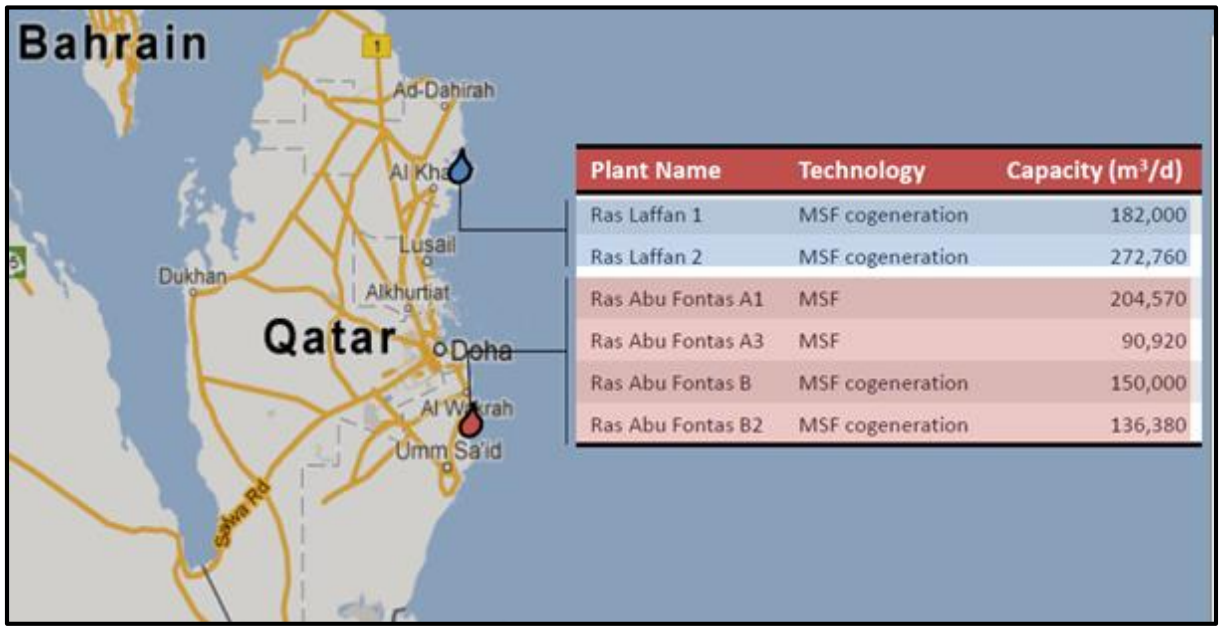

Plant Name	Technology	Capacity (m^3/d)
Ras Laffan 1	MSF cogeneration	182,000
Ras Laffan 2	MSF cogeneration	272,760
Ras Abu Fontas A1	MSF	204,570
Ras Abu Fontas A3	MSF	90,920
Ras Abu Fontas B	MSF cogeneration	150,000
Ras Abu Fontas B2	MSF cogeneration	136,380

Figure 10: Desalination Plants in Qatar (Adapted from [13])

Figure (11) illustrates the total desalination technology share only in Qatar where more than 70% of desalination processes is dominated by MSF technology.

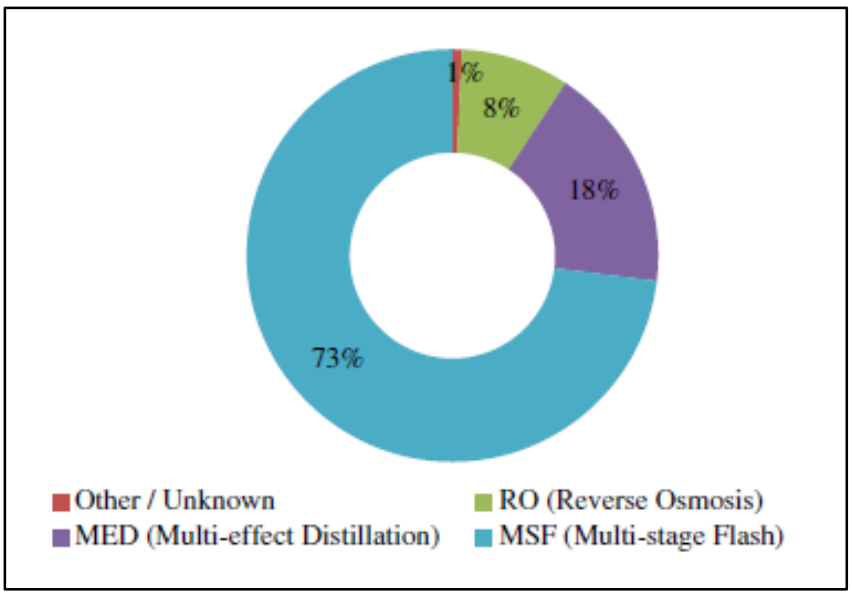

Figure 11: Technology market share in Qatar (Adapted from [19])

As mentioned before, Arabian Gulf seawater has harsh conditions; high temperature, high salinity level, and high turbidity. Therefore, RO technology is rarely used in Qatar and MSF technology is dominated as it is independent on water salinity.

1.4 Environmental Impact

As seawater desalination became the only promising solution of solving fresh water shortage in Gulf area, more desalination plants are planned in order to satisfy water need.

Most desalination plants on the Arabian Gulf costal are allocated with power generation plants and approximately, all the desalination plants are using natural gas as fuel which is more environmental friendly than petroleum, more efficient, and cheaper [15]. Even though natural gas is more efficient than petroleum, huge amount of GHG gases such as Co_x, So_x, and No_x are result as desalination products. Desalination can be sorted as serious environmental

issue that negatively affect the environment. The negative impacts of desalination plants are summarized as:

- High energy consumption
- Water pollution
- Air pollution in a form of greenhouse gasses (GHG) emissions such as Co_x, So_x, and No_x
- Seawater intake that affect the aquatic life of sea organism due to massive seawater feed consumption
- Increased temperature of the sea that affect the aquatic life
- Rejected brine that is produced from desalination plant is returned back to seawater with high temperature and increased level of salinity. Rejected brine also contains amounts of chemical byproducts and heavy metals that are also discharged to the sea [20]. The amount of discharged brine into the sea is estimated to be 33 MCM/day. Due to the weak circulation of tides in the Gulf region, low average annual rainfall, and high evaporation rates, the accumulation of salts occurs causing the rise of salinity level [15].
- Chemical discharge into the sea including biocides and chlorination [15].

Different environmental impacts on the land, water, and atmosphere from the desalination processes is covered more in details in **Chapter 2**.

1.5 Promising Solution

Due to the massive amount of negative effects of desalination process, other technologies are emerging in order to reduce some of the harmful effects and develop more environmental-friendly methods of producing water. Membrane Distillation (MD) desalination process combined with the low-grade heat is studied as an alternative solution for desalination. Renewable energy resources

such as solar, biomass, or wind energy can be used instead of fossil fuels. MD process can provide the production of fresh water with less energy consumption and lower environmental impact. High quality produced water, effective treatment of highly saline water, utilization of low-grade heat, low operating and capital cost provide more advantages of MD process over RO.

1.6 Objective and Scope of Work

Desalination is the main source of fresh drinkable water in Qatar. Currently, thermal desalination provides the bulk of fresh water production. It is well known that thermal desalination is energy intensive and has a negative environmental impact in terms of CO_2 emissions. Reverse Osmosis (RO) has not been considered a viable alternative to thermal desalination because of its sensitivity to the high salinity of the Arabian Gulf and the potential for biofouling by abundant phytoplankton. Clearly, there is a need for an alternative desalination technology that is less energy intensive and less sensitive to salinity. In that respect membrane distillation (MD) has been reported as a promising solution.

Membrane distillation can take advantage of abundant low grade heat currently dissipated by a wide range of industries and also solar energy that is abounded by abundant in the Gulf region. Since low grade heat is generated in industrial processes, integration of membrane distillation with these industries becomes important, in particular in terms of space footprint. There are currently two competing membrane configuration: flat sheet and hollow fiber, and therefore there is a need to study their performance on a comparative basis.

It is the objectives of this work to investigate:

- Flux performance by flat sheet and hollow fiber direct contact membrane distillation modules under a range of conditions and using real Arabian Gulf seawater.

- Distillate quality and salt rejection by flat sheet and hollow fiber contact membrane distillation modules using real Arabian Gulf seawater.
- The convective heat transfer in the hot side of the flat sheet and hollow fiber direct contact membrane distillation modules in order to interpret the flux performance and potentially suggest improvements.

Chapter 2: Background and Literature Survey

This chapter will mainly cover the technologies and processes used worldwide in order to produce fresh drinkable water. The main desalination technologies such as thermal desalination and main pressure-driven processes like RO will be explained in details. The schematic diagram represented in figure (12) summarized all the widely used technologies in water desalination.

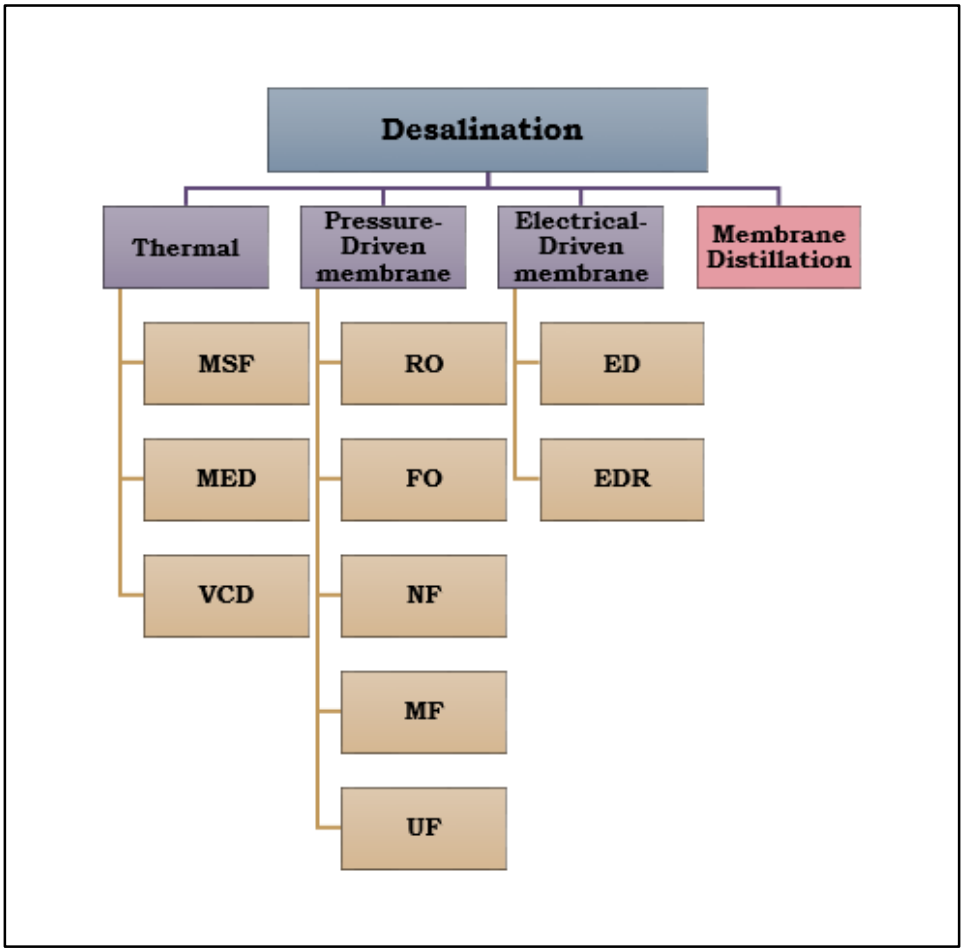

Figure 12: Schematic diagram of classification of desalination processes

In order to understand and differentiate between all types of desalination processes, the meaning of desalination should be evaluated.

2.1 Desalination

Desalination can be defined as the process of removing ions (salts) dissolved in seawater or brackish water to generate freshwater. Desalination can produce water for different applications such as drinking, domestic and industrial use, and irrigation. Desalination can be sorted into two categories; thermal desalination and using membranes. Both categories can use conventional source of energy or renewable source of energy such as wind or solar [6].

2.2 Thermal Desalination

The term distillation is used for thermal desalination as it requires phase change in order to produce freshwater from heated saline water source. The five common steams that are present in every thermal desalination process are: source water; steam that is used for evaporation; cooling water to condense evaporating steam; resulted low-saline distillate; and resulted high concentrated saline water (brine) [12]. By year 2000, thermal desalination occupies 50% of desalination processes [21]. Usually thermal desalination is used for high saline water sources (seawater, brine) as evaporation doesn't relate to salinity concentration and to desalinate low-saline water (brackish) will require high amount of energy. For the Gulf and Middle Eastern countries surrounded by the most saline water bodies on earth and lack of other water resources, thermal desalination is considered as the main source of produced drinkable fresh water. As thermal desalination requires large amount of steam and power generation can offer this steam as low-cost steam, desalination plants and power generation stations are usually combined together [12]. The waste heat is used to evaporate seawater and provide cooling requirements to the power generation plant simultaneously (co-generation plants). The most frequently used thermal desalination methods are Multistage Flash Distillation (MSF), Multiple Effect Distillation (MED) and Vapor Compression Desalination (VCD) [12], [21]. A short summary about the main processes is covered in sections below.

2.2.1 Multiple Effect Distillation (MED)

The MED process is one of the oldest desalination processes that go back to late 1950s and early 1060s [21]. Then the MED process was implemented by oil production companies to produce fresh water during first and second wars. Significant production rate using MED process occurs in 1960s with a production capacity of 5,000 m^3/day and in 2006 it reached 36,000 m^3/day [5]. However, comparing MED process to other thermal desalination technologies concludes the limitation to small production capacities that doesn't exceed 12.5% [5].

The main feature of MED process is that feed water doesn't need to be heated. Seawater at ambient temperature is sprayed over tubes with hot steam [12]. The steam can be generated as waste heat from power plants. The operating temperature of MED process doesn't exceed 70 ℃ due to the horizontal configuration of vessels which helps in reducing scale formation [5], [12]. Furthermore, easier combination with thermal and mechanical vapor compression can be achieved and thus Gained Output Ratio (kg distilled water/kg steam) is increased. Additionally, less expensive materials such as aluminum can be used for heat transfer areas. All these benefits due to lower process temperature, increase lifetime of the equipment and reduce corrosion hence less frequent cleaning is required.

The basic idea behind MED system is a series of evaporators that are gradually decreased in temperature and pressure to allow water to evaporate without introducing more heat [16]. In the first heat exchanger, the steam is recirculated back to the boiler for further usage. The evaporated steam is introduced to the next effects consequently where it is condensed and collected. The brine collected in the first effect is spayed on the tubes of collected vapor in the second effect. The same process is repeated until the last stage where distillate temperature reduced to 30-40 ℃ and the brine is discharged out of the system. Process efficiency and energy utilization increased as the number of effects increase [22]. However, 12 effects in average is the optimum number that is applied for MED

systems in industry [5], [23]. MED systems can collaborate with thermal vapor compression system (MED/TVC) where portion of the low-pressure vapor formed in the final stage is compressed to certain temperature that can help evaporation to occur in the first stage. This combination enhances thermal efficiency of the evaporator and increase GOR. Vertical tube evaporator design raises GOR from 15 to 24 (kg water/kg steam) [5], [12], [24]. Figure (13) represents the schematic diagram of MED system.

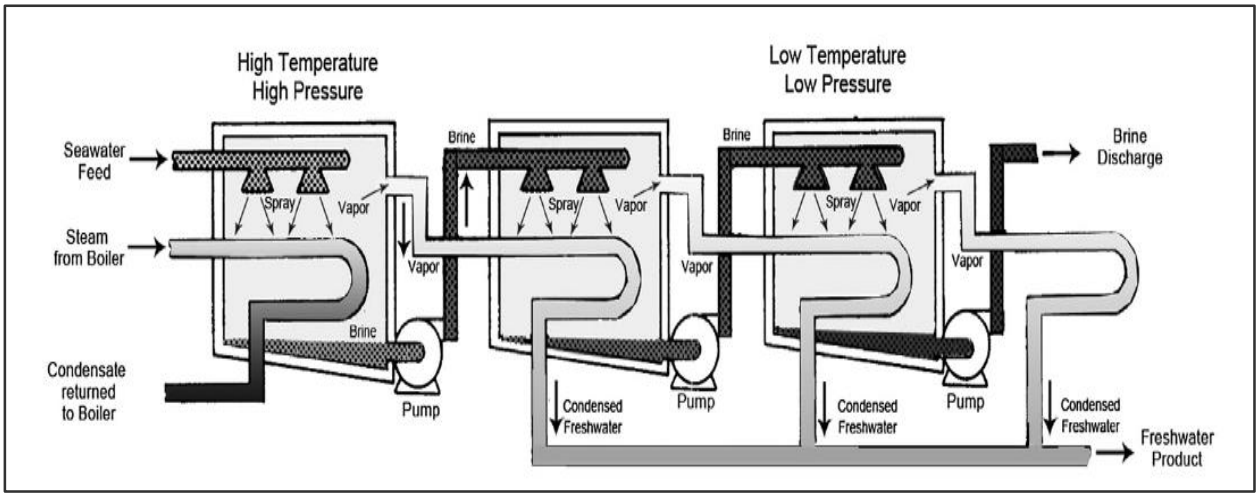

Figure 13: Schematic diagram of Multiple Effect Distillation (MED) (Adapted from [25])

The production capacity of MED system in Qatar, Saudi Arabia, and Oman together reaches 100,000 m3/day. The largest MED production capacity is found in UAE that reaches 600,000 m3/day even when it represents only 10% of (MSF) total production [5].

2.2.2 Multiple Stage Flash Distillation (MSF)

The MSF process is considered as the simplest and most common method for thermal desalination that is applying for the last 60 years. Similar to MED process, MSF technology starts to be used in the late 1950s [21]. MSF systems

are account for 40% of desalination worldwide with a production capacity more than 75,000 m^3/day and 80% for thermal desalination processes [5], [12]. The main difference between MSF and MED systems is that MED achieve evaporation through heat transfer between the steam and sprayed seawater, while MSF by flashing that happen when seawater is heated and passed through chambers with reduced pressure in evaporation chambers [12]. MSF plant requires large quantity of high-temperature steam as it operates near boiling point of water [12]. A typical MSF system consists of three major sections; heating section, flash and heat recovery section, and heat rejection section [24]. Seawater is heated to a temperature of 90℃ to 110℃ by low-grade steam in the heating section and sent to the chambers therefore the heating and the evaporation occur in two different sections [26]. When heated seawater undergoes pressure reduction in the first chamber where the pressure is below equilibrium, part of the water will flash. The same process is repeated through each chamber. At each chamber portion of seawater is evaporated due to pressure reduction. The produced vapor is passed through demister pads in each chamber to remove the entrained brine droplets from the flashed off vapor and achieve product salinity of 10 ppm only [5], [12], [23]. Then the flashed vapor condensed on the outer tube surface when comes in contact with seawater leading to raise its temperature [25]. The condensate is collected on distillate trays and conveyed to the next stage. The brine is collected at the end of each stage and sent to the next one. All highly concentrated brine is collected in the last section and part of it is recycled and mixed with feed seawater in order to regulate the temperature and the volume of the feed. The remaining brine is discharged to the sea [5], [12], [23], [24]. Usually a MSF plant has from 19 to 26 stages or effects and the maximum achieved GOR (kg distilled water/kg steam) is 10 [23]. Even though MSF is a preferable process, it has some disadvantages and the main problems are scaling and corrosion. As this method requires high temperature (~110℃), scale formation occurs in the system. Coatings are applied to reduce scaling and prevent corrosion. De-gassing of the dissolved oxygen is able to reduce scale formation [23], [25].

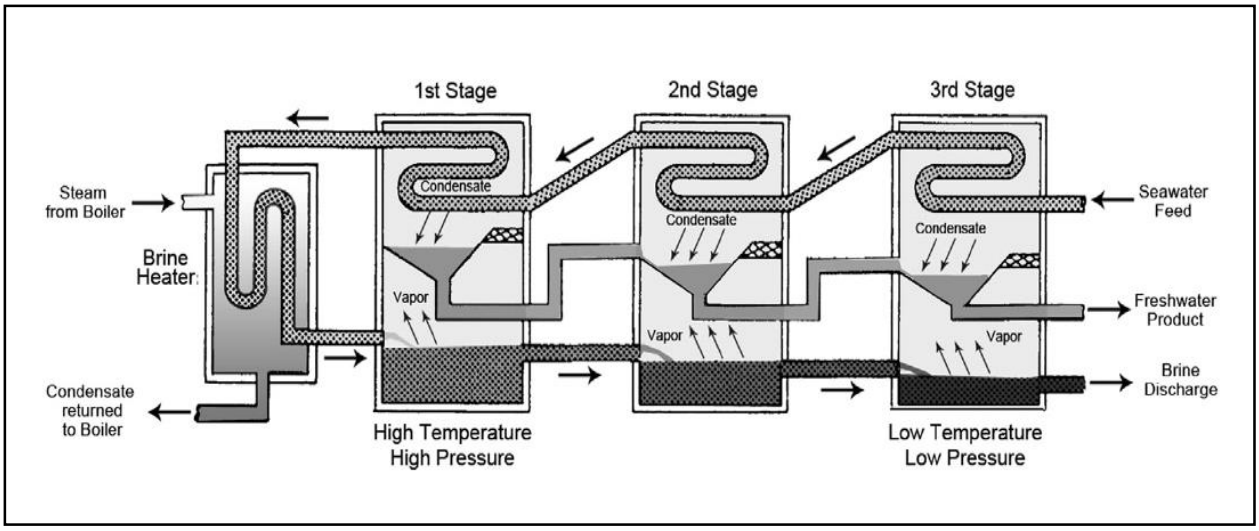

Figure 14: Schematic diagram of Multiple Stage Flash Distillation (MSF) (Adapted from [25])

Figure (14) illustrated the schematic diagram of Multiple Stage Flash Distillation (MSF) process.

Schematic diagrams of Multiple Effect Distillation (MED) and Multiple Stage Flash Distillation (MSF) processes are proposed by Reif and Alhalabi [16] in order to differentiate between the processes. These schematic diagrams could be found in **APPENDIX A**.

2.3 Membrane Desalination

Membrane separation processes use membranes in order to separate water molecules from undesirable other molecules which can be salts, bacteria, viruses, and metals. Membranes can be manufactured from different materials such as cellulose, acetate, and non-polymeric materials. However, polymeric material is the most widely used for desalination purpose [27]. Membrane technologies can be either pressure driven or electrical driven processes. Electrical-driven processes include Electrodialysis (ED) and Electrodialysis Reversal (EDR). Pressure-driven processes include Ultrafiltration (UF), Microfiltration (MF), Nanofiltration (NF), Reverse Osmosis (RO), and Forward

Osmosis (FO) [27]. Pressure driven processes are classified according to their ability to separate different-size molecules. Figure (15) illustrates some of the molecules that are separated by different membrane technologies.

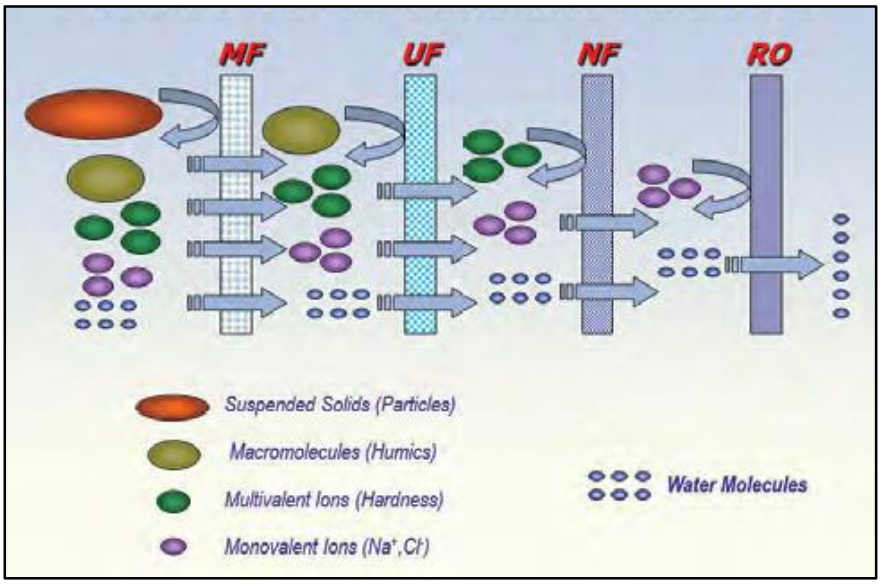

Figure 15: Pressure-Driven membrane processes (Adapted from [28])

Membrane distillation (MD) is also considered as membrane technology that combine thermal desalination process. Membrane technologies became one of the most promising technologies in the last decades due to several advantages over conventional thermal desalination which are [6]:

- Continuous separation process
- Hybrid technology with other desalination processes
- Function under mild conditions
- Relevant scaling-up
- Adjustable membrane properties

The main membrane technologies that are used for desalination will be discussed in details in the sections below.

2.3.1 Reverse Osmosis (RO)

Comparing to conventional thermal desalination processes, Reverse Osmosis (RO) is considered as a new process which implementation starts in 1970s [21]. Worldwide, RO technology is the most used one with 59% among all desalination methods [16]. The driving force in RO process is the pressure difference that is applied to overcome the osmotic pressure. The operating pressure increases with increasing water salinity. Seawater with 35 g/Kg salinity level and osmotic pressure of 25 bar is suitable for RO process [16]. RO system operates at ambient temperature (35 – 40℃) and 60 – 80 bar pressure. Higher feed temperature is recommended for high salinity desalination process to enhance membrane performance [23].

In RO, water is transported from saline side through semipermeable synthetic membrane to freshwater side by applied pressure [23], [27]. Figure (16) illustrates the principle of reverse osmosis process. The used membranes in RO are manufactured as flat sheet membranes and then rolled into spirals to provide higher surface area. The diameter of one RO spiral can reach 18 in [24]. Feed water is passing through spiral sheets and the treated water is collected through the central tube. Hollow fiber membranes can also be used for Reversed Osmosis (RO) system, but not as common as spiral [21]. Feed water pre-treatment is needed in RO systems to avoid biofouling, chemical scaling, and particulate blockade of the membrane [24].

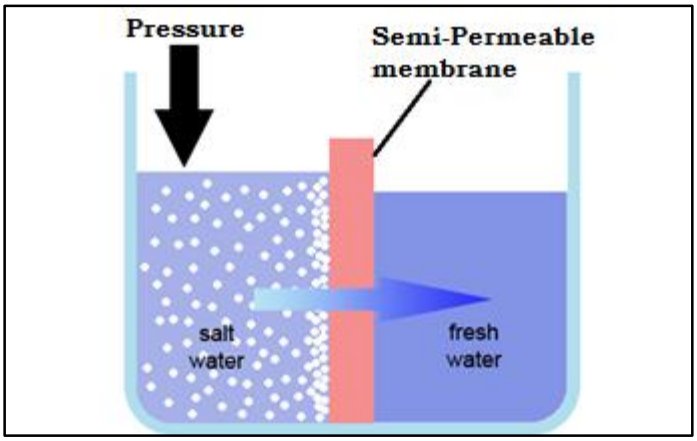

Figure 16: Reverse Osmosis principle (Adapted from [29])

Typical pre-treatment consists of cartridge, sand filtration, coagulation, softening, and flocculation to remove large particles, organic matter, suspended solids, bacteria, oil, and grease [24], [27]. Ultrafiltration (UF) and Microfiltration (MF) is also a solution to be used before RO process [23].

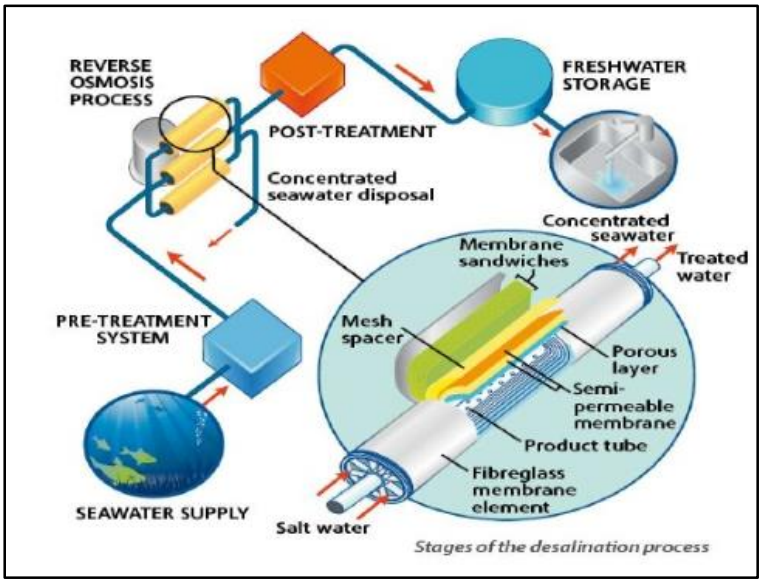

Figure 17: Schematic diagram of Reverse Osmosis (RO) desalination process (Adapted from [30])

Figure (17) illustrates the schematic diagram of Reverse Osmosis (RO) desalination process stages.

After RO section, post-treatment unit is used to treat water. pH and alkalinity adjustment is required to lower the potential of carbonate and silica scale formation [24]. Concentrated seawater from RO unit is disposed back to the sea. Recovery rate is used to evaluate RO membrane efficiency. Typical recovery rate of RO system varies between 35 – 50% depending on seawater salinity level. Low recovery rates occur in close water intakes such as Persian Gulf. Two-pass RO process is preferable for higher flux and quality. The typical achieved flux for first stage of RO system is ranged as 13 – 17 $L/m^2.h$ and 30 – 40 $L/m^2.h$ for second stage [23].

2.4 Membrane Distillation (MD)

Membrane distillation is a combination of thermal distillation and membrane desalination processes in which phase-change process occurs that allows only vapor permeation through non-wettable porous hydrophobic membrane [6]. Membrane distillation (MD) process is an encouraging desalination technology that is highly studying these days. MD has been investigated as a cheap and less energy intensive technology compering to thermal desalination [31]. The first research on membrane distillation was conducted in 1963 [32]. However, membrane distillation attracts the huge interest in the early 1980s [33].Moreover, the "research boom" about MD is noticed in the last 10 years due to attractive features and advantages over thermal desalination and reverse osmosis (RO) that MD processes have in the academic field and can be implemented in industry [34]. These features are listed below [12], [31], [33], [34], [35], [36]:

- Low operating temperature in comparison to conventional thermal desalination where the temperature requires to reach boiling point.
- Low operating pressure in comparison to pressure-driven processes (RO, NF, UF, MF, FO)

- Low environmental foot print in comparison to conventional thermal desalination [37]
- Less fouling performance comparing to pressure-driven processes (RO, NF, UF, MF, FO) [35]
- High salt rejection in desalination process (approximately 100%) [32]
- Low sensitivity to feed concentration [2], [32]
- Cost effective process where cheap materials are used
- The possibility to use renewable energy resources such as solar energy [16], [37], [38], [39], [40], [41] and low-grade heat
- Less requirements of membrane mechanical properties [32]

Membrane distillation (MD) term comes from the combination of using membranes and thermal distillation that is based on vapor pressure theory that requires heat for separation. So MD is thermal driven separation process involving the use of micro-porous membrane [42]. Hydrophobic semi-permeable membrane separates the cold distilled from hot saline feed solution. The difference of temperatures between the feed and distilled sides across the membrane creates vapor pressure gradient which is the driving force of the membrane distillation process. Due to this vapor pressure difference and the morphology of the membrane, only vapor molecules can pass the membrane through membrane pores from high pressure side (feed) to low pressure side (permeate). Bouchrit et al. [42] summarized the MD process in three steps; evaporation at feed side, vapor molecules transport through membrane, and condensation on the distilled side. Feed temperature can vary for a range of 60 to 90℃ [41].

MD process can fulfill in many applications such as desalination of seawater and brackish water, separation of different concentrations of non-volatile components, food industry, medical field [41], waste water treatment, extracting organic and heavy metals, separation of volatile components, radioactive waste treatment, and produced water treatment [32], [35], [42]. As examples of different membrane distillation, Hou et al. [43] conducted research on fluoride removal

from groundwater and Gryta et al. [44] studied the treatment of saline water using hollow fiber membranes.

MD Desalination process receives major interests and the first sweater MD plant is planned to be constructed in Maldives with production capacity of 10,000 L/day utilizing low grade heat [34]. Goh et al. [7] reported that MD process can be applicable for high saline water with electrical conductivity of 70 mS/cm. Commercial different hydrophobic membranes are used in MD process such as capillary, hollow fiber, and flat sheet membranes. [33] Fabricated membrane from (PTFE, PP, PVDF) material are also used [41].

As membrane distillation has many advantages over conventional thermal and pressure- driven processes, it also has some drawbacks that potentially can limit processing MD in large scales [31]:

- Membrane pore wetting
- Permeate flux declination in comparison to pressure-driven processes (RO, NF, UF, MF, FO)
- Trapped air in the system and heat loss due conduction cause mass transfer resistance
- Unstable economic cost [33], [35]
- High energy consumption in comparison to pressure-driven processes (RO) [32]
- Lack of commercial high performed membranes [32]

With ongoing research globally, most of the above drawbacks will be addressed to improve prospects of membrane distillation in desalination.

Membrane distillation (MD) process has basics four configurations which are: Air Gap Membrane Distillation (AGMD), Sweeping Gas Membrane Distillation (SGMD), Vacuum Membrane Distillation (VMD), and Direct Contact Membrane Distillation (DCMD). All different processes will be studied in details in the section below [33], [35], [41]. Figures (18 – 21) illustrate the schematic diagrams of the four different configurations of membrane distillation that are adapted from [31], [45].

2.4.1 Air Gap Membrane Distillation (AGMD)

Air Gap Membrane Distillation (AGMD) system consists of the membrane, thin air gap, and a polymer surface that used for condensation. The air gap is introduced between the membrane surface and cooling plate. The main purpose of having air gap is to minimize heat loss from membrane surface by conduction and this is the main advantage of the system in addition to lower energy consumption [5], [35], [36]. However, air gap performances as resistance to mass transfer that cause lower flux production [32]. In AGMD system, feed saline solution occurs in direct contact with the hot membrane surface. Vapor molecules are passing the introduced air gap through membrane to reach the polymeric surface and be condensed. Figure (18) illustrates the schematic diagram of Air Gap membrane distillation (AGMD) system.

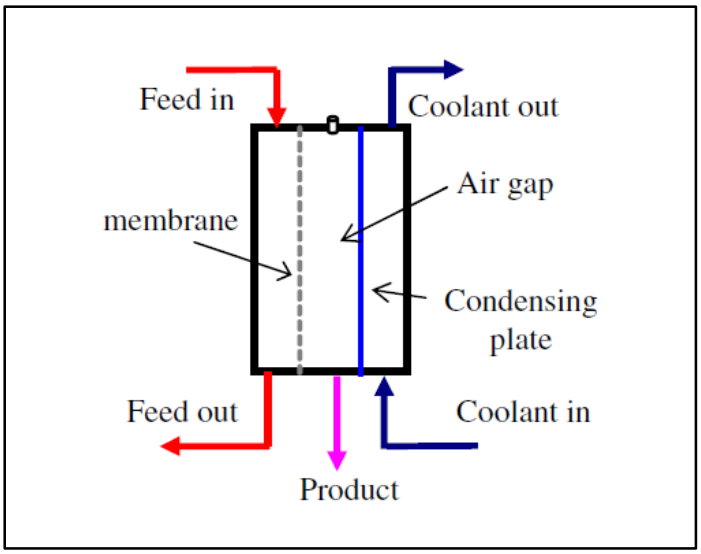

Figure 18: Schematic diagram of Air Gap membrane distillation (AGMD) system (Adapted from [45])

Khayet [33] and Lawson [41] reported that AGMD system can be applied on hollow fiber and flat sheet membranes and are applicable for desalination

process. Furthermore, as there is no direct contact of the distilled side with the membrane, membrane wetting is not considered as problem.

2.4.2 Sweeping Gas Membrane Distillation (SGMD)

Sweeping Gas Membrane Distillation (SGMD) system is very similar to direct contact membrane distillation system with additional cold inert gas that pass through the distilled side in order to carry permeate vapor. After vapor molecules are collected, they are transported by the sweeping gas to be condensed outside the system. Figure (19) represents the schematic diagram of (SGMD) system. As External condenser is used in the system, higher operational cost is required in addition to more difficult design of the system [32], [36]. Moreover, sweeping gas temperature is increased when it passes along membrane surface causing a drop in the driving force across the membrane [33]. Another disadvantage of SGMD is that the introduction of sweeping gas enlarges the total volume of permeate vapor in large sweeping gas volume that requires high condensing capacity [5].

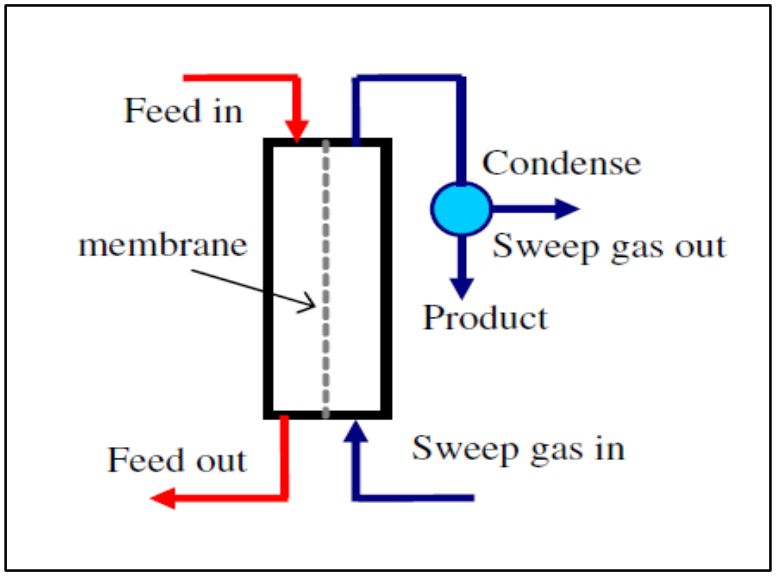

Figure 19: Schematic diagram of Sweeping Gas Membrane Distillation (SGMD) system

Due to many disadvantages, Khayet [45] concludes that SGMD configuration is the less applied MD systems in use. The only advantage of SGMD system is that higher flux than in AGMD system is produced due to mobile layer of sweeping gas that reduce mass transfer resistance [35].

2.4.3 Vacuum Membrane Distillation (VMD)

In Vacuum Membrane Distillation (VMD) system a vacuum is applied on the distillate side by installing a pump. The pump must be operated at pressure less than the liquid-vapor pressure in order to condensate the vapor outside the module [36]. There is no cooling stream in the system so external condenser is used as in SGMD system to condense the vapor. VMD and SGMD systems are similar in terms of functions also as it is recommended for Volatiles Organic Components (VOC) separation [32]. The main advantage of VMD is that heat lose is negligible in this system [35], [41].

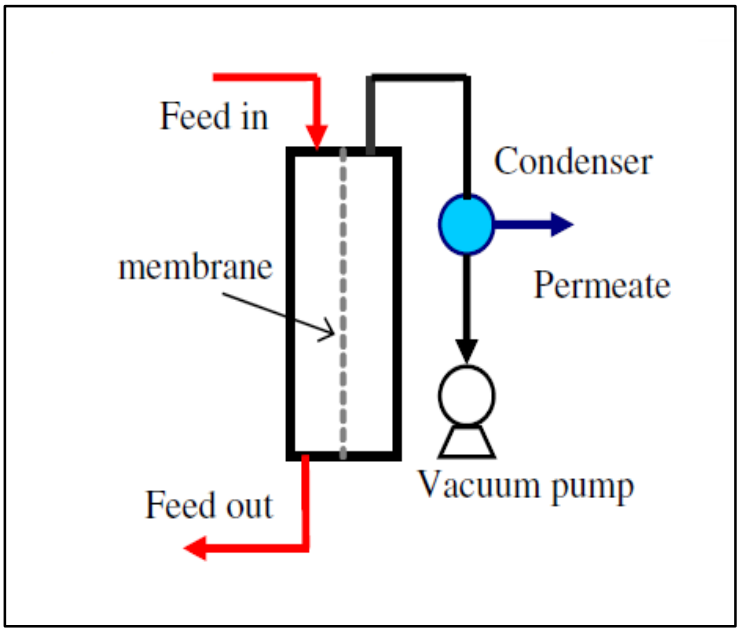

Figure 20: Schematic diagram of Vacuum Membrane Distillation (VMD) system

Figure (20) represents the schematic diagram of vacuum membrane distillation (VMD) system. Different types of membranes such as capillaries, hollow fiber, and flat sheet membranes can be used in VMD system [33].

2.4.4 Direct Contact Membrane Distillation (DCMD)

More than 60% of studies carrying membrane distillation are dealing with DCMD [33]. In Direct Contact Membrane Distillation (DCMD) system hot feed solution (seawater) is separated from the cold distilled solution by a hydrophobic porous membrane. Peristaltic pumps are used to flow the feed and distilled solutions. DCMD process starts with evaporation of feed solution on the feed membrane side. Due to pressure difference across the membrane, vapor molecules pass through the membrane to the permeate side.

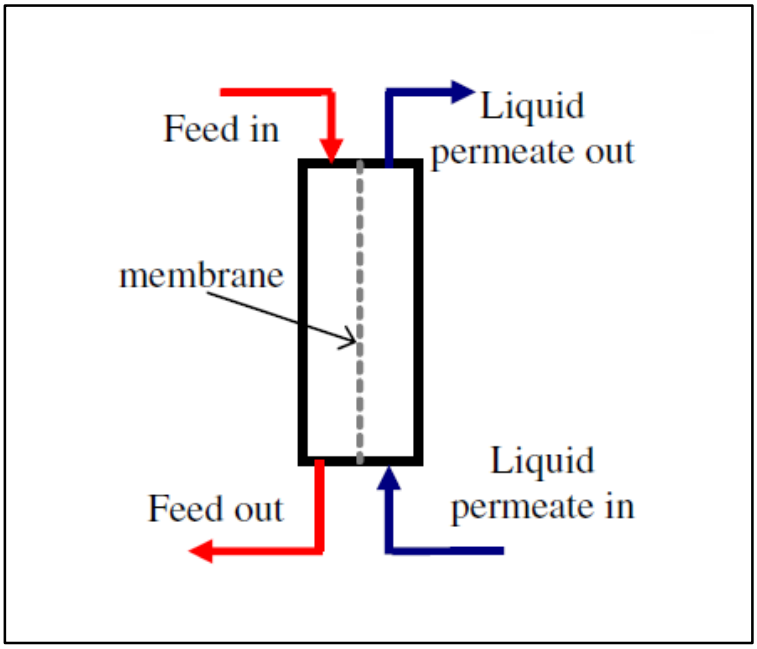

Figure 21: Schematic diagram of Direct Contact Membrane Distillation (DCMD) system

DCMD is the most applied and studied configuration of membrane distillation processes because of its simplicity without need of external condensers [7]. Alkhudhiri et al. [35] reported that this configuration is applicable for desalination process with real seawater and have been widely studied in lab-scale experiments by different researchers [38], [42], [46], [47], [48], [49], [50], [51], [52], [53]. In addition, Khayet [33] stated that flat sheet, capillary, and hollow fiber membranes can be conducted in both co-current and counter-current configurations for DCMD system.

Figure (21) illustrates the schematic diagram of Direct Contact Membrane Distillation (DCMD) system. The main drawback of DCMD is that it has the highest heat loses through conduction in the all four configurations of MD systems as the only barrier between the hot feed and cold distillate solutions is the membrane [32], [36].

2.5 Desalination Energy Consumption

Desalination technologies in general is an energy intensive process which consumes enormous amounts of energy. Energy can be generated from different resources. The main source of the energy in GCC countries is fossil fuels. The combustion process of fossil fuels has a negative effect on environment in terms of GHG emissions. However, some variation of energy consumption occurs based on desalination technology. For example, thermal desalination consumes much more energy than reverse osmosis (RO) process.

Table 3 represents the energy use for the most common desalination technologies. Thermal energy use can be calculated as (1 $kW\,h$ is equal to 3.6 MJ) with power generation efficiency of 0.33. Therefore, for 1 $kW\,h$ energy, 10.9 MJ fuel equivalent is required [24].

Table 3 Desalination technologies energy use (Adapted from [24])

Technology	Electrical Energy ($kW\ h\ m^{-3}$)	Thermal Energy ($MJ\ m^{-3}$)
Multiple-stage flash distillation (MSF)	3.6 – 4.4	200 – 380
Multiple-effect distillation (MED)	2.3	200 – 300
Seawater Reverse Osmosis (RO)	2.0	–
Membrane distillation (MD)	0.75	100 – 200

Clearly, thermal desalination requires more energy than other desalination processes. The salinity of seawater and the capacity of desalination plant are also considered as important factors in evaluating the amount of required energy. The energy used for RO desalination process is reported by other researcher [5], [32] as (2.0 – 5.5 kW/m^3) approximately. Alternatively, the energy used for MED desalination process is (6.5 – 11 kW/m^3), and the energy used for MSF desalination process is (13.5 – 25.5 kW/m^3) [16]. A huge difference between RO and thermal desalination energy requirements is noticed. Even though, the consistency and huge field implementation in thermal desalination technologies keeps its production cost reasonable compared to the RO process. As technology works to improve and enhance thermal desalination processes, less energy is required to process desalination. Reif et al. [16] reported that, nowadays thermal desalination requires only (0.86 kW/m^3) amount of energy in order to desalinate seawater at 34,500 ppm salinity level and 25℃ temperature. This process will cost approximately (0.5 – 1.0 $) per cubic meter of produced water.

2.6 Seawater Salinity

Salinity is a measure of the total dissolved solids (TDS) in seawater, usually expressed in parts per thousand (ppt) by weight. It is also can measured as parts per million (ppm) by weight and milligram per liter (mg/L). Seawater salinity is considered as a key parameter for classification of desalination technology. Table (4) represents salinity range of different water resources. According to Water Health Organization (WHO), [3] the salinity of drinking water should be less than

5000 ppm while the salinity of water bodies in the Gulf regions ranges between (35,000 – 45,000 ppm). In the coastal areas, the salinity of Arabian Gulf seawater is even higher.

Table 4: Salinity range for different water bodies [16]

Water source	Salinity Range (TDS)	Water Class
Fresh water	< 500 mg/L (< 0.5 ppt)	Non-saline
Irrigation water	500-1500 mg/L (0.5 – 1.5 ppt)	Slightly saline
Groundwater	1500-7000 mg/L (1.5 – 7.0 ppt)	Moderately saline
Drainage water	7000-15000 mg/L (7.0 – 15.0 ppt)	Saline
Seawater	30,000-50,000 mg/L (30 – 50 ppt)	Very highly saline
Brine	> 50,000 mg/L (> 50 ppt)	Extremely saline

Membrane desalination technology such as reverse osmosis (RO) is capable for seawater salinity level less than (35,000 ppm) only, therefore other desalination technologies should be applied for high saline water bodies such as thermal desalination and membrane distillation.

2.7 Environmental Impact

Desalination process accounts for production of fresh water in many countries especially Middle east and Gulf countries. Moreover, desalination is increasing rapidly in Gulf countries, doubling the installed capacity in the last 15 years [54]. Seawater desalination in GCC region is responsible for 45% of worldwide production of fresh water and it is increasing each year. However, concerns are raised due the negative environmental impacts of desalination [18]. Negative environmental effects are classified by effluent discharge to the air, nearby land, sea, marine, and environment [23]. As shown in figure (22), the sea and atmosphere are the main affected regions of the environment due to GHG emissions and concentrated brine discharge.

Figure 22: Schematic diagram of desalination process

As desalination outputs affect the environment from different aspects and all types of environmental effects are connected together. The effect of GHG emissions and concentrated brine are studied in details in the sections below.

2.7.1 Gas discharge to Atmosphere

Air pollution and emissions contribute with type of energy used for desalination process. Most desalination plants on the Arabian Gulf are allocated to power generation plants. Therefore, Environmental Impact Assessment (EIA) should consider gaseous emissions from power generation and desalination plants [15]. The main source of energy in the Gulf is fossil-fuel that generates greenhouse gasses (GHG). The major GHG are carbon dioxide (CO_2), methane (CH_4), nitrous oxide (N_2O), and other gasses like NO_x, SO_2, and volatile components [23]. Nowadays, emissions as NO_x are reduced as new technologies are implemented and SO_2 is emitted if crude oil is used instead of natural gas as fuel resource. The main GHG emission left is carbon dioxide (CO_2) which can be reduced only if renewable source of provided energy is used such as solar, biomass, and wind energy rather than fossil-fuels [18]. Table (5) represents the amount of CO_2 as GHG emissions in million metric tons in GCC countries.

Table 5: CO_2 GHG emissions for the GCC (million metric tons) Adapted from [18])

Year	Bahrain	KSA	UAE	Kuwait	Qatar	Oman
1996	15.6	248.9	103	49.1	30.9	14.5
1997	18.3	254.0	111	52.0	32.0	17.8
1998	19.1	256.8	116	56.0	33.2	21.7
1999	20.2	262.7	117	60.0	31.0	20.4
2000	20.3	289.3	109.0	59.0	34.5	21.6
2001	20.7	299.9	118.0	60.0	27.4	22.1
2002	21.6	309.6	125.0	55.0	29.1	22.8
2003	22.3	344.7	126.0	63.0	32.4	22.5
2004	23.0	385.7	132.0	67.0	38.5	24.2
2005	25.2	415.4	137.8	76.7	53.5	29.7
2006	26.0	433.0	141.0	79.0	56.0	31.0
2007	27.1	452.0	145.0	82.0	58.0	33.0
2008	28.0	470.0	149.0	85.0	61.0	34.0
2009	29.0	489.0	153.0	88.0	63.0	36.0
2010	30.0	507.0	157.0	92.0	66.0	38.0

Air emissions produced by using RO technology are lower than the emissions associated with the thermal desalination technologies [24]. Therefore, countries such as KSA, UAE, and Oman that have alternative water bodies than the Arabian Gulf seawater, are implementing RO technologies to reduce the amount of GHG emissions.

2.7.2 Effluent discharge to Sea

Brine from thermal desalination and concentrate from RO process are discharged to the sea. The concentration of the brine is double the concentration of seawater [23]. As it mentioned in the introduction, the amount of brine discharges to the Arabian Gulf daily is 33 million cubic meters. It is not a huge amount comparing to the total amount of water in the Gulf, nevertheless, it causes localized hypersaline coastal water. It is estimated that for every cubic meter of fresh water, two cubic meters of brine is produce [18]. The Gulf is considered as semi-enclosed water body so weak water circulation is provided causing water salinity build-up [15]. Low capacity production desalination plants

don't show significant negative effects. However, large-scale production plants cause serious damage to the aquatic life. It is reported that enormous damage of coral, loss of plankton, and fish take place in the Hurghada sea coastal, Egypt, on Red sea due to desalination activities and brine discharge [20].

Various chemicals such as anti-scalants, inorganic salts, chlorine, surfactants, and acids at low concentration levels are also discharged to the sea [18], [23]. The main sources of these chemicals are pre-treatment, disinfection, and post-treatment units of seawater. Some heavy metals are found in the discharged brine such as iron, copper, nickel, chromium, and molybdenum that came with the cooling water. However, the concentration of heavy metal in the brine does not exceed their range in the oceans (0.1 – 100 μg/L) [18]. In absent of mixing, denser brine plume than seawater sank to the bottom of the sea, affecting the organisms there [20], [24].

Another effect of discharging the brine to the sea is localized temperature rising. When the hot brine is discharged to the sea, the average temperature is increased. This causes dissolved oxygen depletion, salinity, and alkalinity increasing that affect the aquatic life in the discharged area [18]. It is reported that (MSF) is discharging brine into sea with (10 – 15 ℃) higher than ambient temperature of the sea [20].

2.8 Mitigation Methods

In order to reduce the harmful effects of desalination processes, different mitigation methods are applied. Nowadays, different techniques are practiced in desalination plants to reduce the effects of discharging brine to the sea. Several techniques are reported by different researchers [18], [23], [24] such as:

- Diluting the brine to make it close to seawater concentration
- Mixing the concentrate with cooling water of large plants before discharging it to the sea
- Discharging the brine to surface water
- Discharging the brine to wastewater treatment plants

- Deep well injections
- Evaporation ponds
- Land disposal
- The use of diffusers

Every mitigation method has its advantages. However, the chemicals and toxic materials present in the brine can affect the soil and groundwater while land disposal method. Chemicals in the brine can be treated before discharging or replaced with other substances that are less hazardous. For example, to minimize the effect of chlorine in brine, sodium bisulfite is added [18]. The simplest, cheapest, and the most popular way is discharging brine to surface water. Discharging the brine to sever or wastewater treatment plants is capable only if the plant is applicable for brine treatment, and won't reduce its efficiency. Evaporating ponds depends on the evaporating rates, land cost, and are not used with high volumes of rejected brine [24].

It is expected that brine discharge became more serious problem in the future because of several factors [24]:

- The increase of regional salinity of desalination intakes
- The decrease of seawater quality lead to produce more brine with time

Several methods are applied to desalination technologies to reduce energy use in order to minimize GHG emissions. These methods are:

- Using energy recovery equipment or variable frequency pumps for RO technology
- Renewable energy sources desalination (e.g. solar, biomass, wind, geothermal, etc.)

Renewable energy source such as solar energy is started to be applied for desalination. In Abu Dhabi, UAE, 30 small RO desalination units are constructed to desalinate brackish water and groundwater with salinity range of (5,000 – 20,000 ppm) using photovoltaic solar cells. Each unit is designed to produce 5 m^3/hr. Another solar powered desalination plant; the biggest in the world is

building in Al-Khafji city, KSA. The plant is designed to produce 30,000 m^3/day of fresh water [18].

Table 6: Main environmental impacts and mitigation methods of desalination process

Problem	Environmental Impacts	Mitigation Methods
Brine discharge	Salinity rise	Brine dilution Brine harvesting
	Temperature increase	Brine dilution
Air pollution	NO_x, SO_2, CO_2 emissions	Natural gas as fuel source Renewable energy
Noise	Increase in noise level	---
Land Use	High land coast value	Proper selection of desalination site

Even though, brine discharge and the atmospheric pollution are considered as the main problems of desalination processes. There are other less important factors that affect the environment in negative way such as noise pollution and land usage. Dawoud et al. [18] summarized different negative effects, their impacts, and some mitigation methods in table (6) for desalination technologies. Another novel possible technique to reduce brine discharge is Zero Liquid Discharge (ZLD) that convert liquid concentrate into dry solid. Solid waste can be disposed into appropriate liner based landfills to avoid land contamination. (ZLD) technique replaces the dealing with liquid discharge into solid waste disposal [55].

2.9 Membrane Characterization Techniques

Membrane characterization is one of the essential components of membrane study. It used to evaluate membrane structure and morphology. The main

purpose of membrane characterization is to evaluate membrane ability to proceed assigned separation process.

There are several methods to identify the membrane morphology. The traditional way of membrane characterizing is to estimate pore size and pore size distribution of the membrane.

Table 7: Main characterization tests (Adapted from [57])

Method	Characteristic
Bubble pressure	Maximum pore size
Mercury Porosimetry (MP)	Pore size distribution
Scanning Electron Microscopy (SEM)	Top layer thickness Surface porosity Pore size distribution
Atomic force microscopy (AFM)	Surface porosity
Gas adsorption/desorption (GAD)	Pore size distribution
Contact angle measurement	Surface studies (hydrophobicity)

Another important step in membrane characterization is to study membrane surface. The estimation of membrane pore size, maximum pore size, pore distribution, smoothness of membrane surface, membrane porosity, membrane layer thickness, and permeability all undergo membrane characterization techniques [56], [57].

Table (7) below summarizes main membrane characteristics such as membrane pore size distribution and membrane surface studies and the commonly used methods in order to evaluate these characteristics.

However, physical characterization and the separation application of the membrane evaluate the type of the required test. In addition to the methods

mentioned in table (7), different other tests and methods are discussed below for different membrane characterization:

- To evaluate membrane pore size and pore distribution, Gas and liquid displacement methods, Permporometry, Liquid Solid Equilibrium Method, Gas Permeability Method, and mass transportation [56], [57].
- To evaluate membrane surface studies, sessile drop method [58], Spectroscopic Method, and Microscopic Method [56], [57].

2.10 Desalination Water Quality

Seawater is a mixture of different salts and particles. Salt concentration is different at each water body. It can vary from 0.5% salt concentration at Baltic Sea to 4.2% at the Arabian Gulf [23].

Table (8) compares seawater salt concentration of the Arabian Gulf to the global distribution. Bromide at low concentration is also contained in the seawater. Alkaline earth metal cations calcium and magnesium and the polyatomic anions sulfate and bicarbonate are responsible for scaling in membrane technologies [25]. Bromide concentration in seawater is reported to be 0.007%. Bromide is responsible for taste and odor of the permeate. Therefore, disinfection of permeate water by using ozonation is preferable especially in RO technology [23].

Rather than dissolved salt, seawater has other impurities such as turbidity, metals, pathogens, organic components, suspended matter, microorganisms, and algal blooms. Organic contamination comes from the aquatic life including molecules, colloids, viruses, and bacteria that should be removed in the earlier stages of RO desalination. These organic components are the main cause of biofouling in membrane technologies. Another cause of rapid membrane biofouling is algal blooms that increase water turbidity and act like food for other microorganisms [23].

Table 8: Seawater salt composition (Adapted from [25], [23])

Component	Global distribution concentration (%)	Arabian Gulf concentration (%)
Calcium	0.042	0.044
Magnesium	0.13	0.158
Sodium	1.07	1.295
Potassium	0.04	---
Bicarbonate	0.015	0.012
Sulfate	0.27	0.32
Chloride	1.94	2.39
Total Dissolved Solids (TDS)	3.5	4.37

The quality of water is measured by its purity. In order to purify seawater, all salts and particles should be removed.

2.11 State of the Art in Membrane Distillation

Membrane distillation is receiving high attention in theoretical studies and research. As it was mentioned before, 60% of the research papers about desalination are targeting membrane distillation due to the advantages this process has. The historical timeline and the membrane developments in the recent studies are present in this section below.

One of first patents in membrane distillation is received by Dah Y. Cheng in 1981 [59] on examining composite microporous membrane with a thin hydrophobic and hydrophilic layers to separate salty water from distillate fresh water. Hydrophobic layer helps the evaporation and condensation processes to occur and the hydrophilic layer prevents membrane wetting.

Jonsson et al. [60] were the first group who investigated heat and mass transfer in air gap membrane distillation (AGMD) system theoretically. Heat and mass transfer equations were studied without including the effect of temperature polarization.

Drioli et al. [61], [62], [63] had investigated the effect of feed temperature and concentration on distillate, concluding that membrane distillation is capable to produce very pure water from saline and sugar solutions using different flat sheet and capillary membranes with different materials such as PP, PTFE, and PVDF and with different porosities. A non-linear relationship was found between generated flux and temperature gradient. Moreover, Calabro et al. [64] studied the implementation of membrane distillation in textile wastewater treatment processes and the results indicated that membrane distillation is capable of pure water production in wastewater treatment plants.

Sarti et al. [65] and other researchers [66], [67] studied the mass and heat transfer theoretically and experimentally on different membrane configurations (DCMD, AGMD) in order to produce fresh water from saline water. Different simulated models were developed that predict the experimental results.

One of the earlier studies that introduced temperature polarization to the heat and mass transfer in membrane distillation was conducted by Schofield et al. [68], [69] A theoretical model was evaluated to incorporate temperature polarization with heat transfer in terms of Knudsen-Poiseuille transition flow. Moreover, hollow fiber membranes offer the most effective performance with least temperature polarization.

Schneider et al. [70] were one of the first researchers who studied capillary membrane configurations in counter-current flow. Bundles with twisted or braided capillaries performed the best results. Moreover, different membrane morphology such as membrane pore size, diameter, and porosity were tested to generate high permeate fluxes.

Costello et al. [71] studied fluid flow dynamics and mass transfer in (PP) hollow fiber membrane bundles with different packing densities (32 – 76%). It was found that mass transfer increases with increasing packing densities in counter-current MD system until reaching the optimal one.

Gryta et al. [72] studied capillary modules and developed Nusselt number correlations for heat transfer in heat exchangers and the experimental work proved the validity and applicability of the model.

Phattaranawik et al. [73], [74], [75], [76] examined the effect of spacers in enhancing flux performance in flat sheet DCMD systems. The presence of spacer increased permeate flux by (26 – 56%) and enhanced heat transfer coefficients by 2.5 times. Moreover, temperature polarization decreased in spacer-filled channels. A model was predicted for spacer-filled channels that gives reliable results compared to experiments.

Hsu et al. [77] were one of the first who examined synthetic and real seawater as feed solution into DCMD system. Results showed that permeate flux decreased to the half when real seawater is used instead of NaCl solution. The measured conductivities of the permeate were ranged between (7 – 12 μm/cm) and indicated good quality water. However, fouling was observed after one week only using the real seawater.

Wirth and Cabassud [78] were the first who examine hollow fiber membrane configurations in terms of placing the feed water (lumen side or shell side) in PE and PVDF membranes. Results shown that no difference occurs for PVDF membrane. However, more flux achieved for PE membrane when feed water is used in the lumen side. Moreover, the effect of salinity is studied on the generated flux. A decrease of 30% for the flux is reported when the salinity of feed water is raised from 15 g/L to 300 g/L.

Li and Sirkar [79] were one of the first researchers who studied PP hollow fiber membranes in DCMD for desalination. In this study, rectangular modules were used with different fibers diameters and thickness. The operating temperature of the brine ranged between (60 – 90 ℃). Permeate flux achieved was (41 – 79 kg/m^2.h) where the highest flux generated at maximum feed temperature and high brine velocity of (150 μm) wall thickness and (330 μm) inner diameter

membrane. The calculated Reynolds number (Re) for the highest permeate flux was 70.

Cath et al. [80] had investigated DCMD performance using vacuum enhancement on three different configurations: traditional DCMD, vacuum enhancement on permeate side, and vacuum enhancement on two sides of the membrane. The results showed that less temperature polarization and higher mass transfer performed with vacuum enhancement. Almost 99.9% salt rejection is obtained for NaCl synthetic seawater.

On of the first studies on mass transfer in DCMD systems was conducted by Srisurichan et al. [81] on flat sheet membrane. Mass transfer model was proposed based on Dusty gas model concluding that molecular diffusion is dominated and most suitable describing the flux. Fouling was investigated using humic solution that contains natural salts. The results indicate that fouling layer cake occur on membrane surface.

Criscuoli et al. [82] had studied three different PP flat sheet modules with 0.2 μm pore size that are fabricated in the lab: longitudinal, transversal and cross-counter membranes for testing DCMD and VMD experiments. The results compared in term of achieved flux, membrane configuration, and energy consumption. Highest flux (56.2 kg/m^2.h) was generated by cross-counter configuration comparing to the other two configurations that performed similar flux results. Also, in this study, DCMD had lower flux performance than VMD system.

M. Gryta [83] investigated the demineralization of lake surface water using hydrophobic capillary PP membranes in DCMD configuration. The electrical conductivity of the used raw water was found to be in the range of (620 to 650 μS/cm). Permeate flux was declined with time due to bicarbonate decompositions on membrane surface. Mainly calcium carbonate is accumulated and causes membrane fouling. Results indicated that high feed temperature enhances the decompositions.

Teoh et al. [84] and Yang et al. [85] investigated novel configuration on hollow fiber membrane modules. These configurations included spaces, baffles, and modified hollow fiber geometries such as curly and braided fibers. Results showed that flax enhancement from 53% to 92% occur when the novel modified configurations were used. The highest flux enhancement achieved when curly and braided fibers were used. Moreover, heat transfer coefficients were calculated for the membranes before and after the modifications. Heat transfer coefficient increased from 2600 W/m^2. k to 3150 W/m^2. K when baffles are introduced.

Hou et al. [43] used PVDF hollow fiber membranes in DCMD for fluoride removal from brackish groundwater. The highest achieved permeate flux was (35.6 $kg/m^2.h$) with 80℃ feed and 20℃ distilled temperatures. Results showed that high rejection of fluoride salt.

Chen and Ho [6] studied the combination of DCMD system with a solar absorber used for desalination of seawater. The operating hot feed temperature ranged between (35 – 50 ℃) and PTFE flat sheet membrane was used. The absorber was integrated within membrane module. The highest permeate flux achieved by the system (4.1 $kg/m^2.h$) with high purity.

He et al. [52] examined nine different commercial membranes for DCMD system. Different operating settings were examined such as flow mode, feed and permeate flowrate, feed and permeate temperature, and feed salinity. Three membrane materials were tested and PTFE membranes represented the best performance in terms of flux and conductivity. Examining membrane pore sizes showed that 0.22 μm PTFE membranes generated the highest flux (25.6 $kg/m^2.h$) at 60℃ feed and 20℃ distilled temperatures and synthetic seawater. The flux dropped to (14.4 $kg/m^2.h$) approximately when real seawater is used as feed solution.

Nghiem et al. [53] investigated the effect of seawater, RO concentrate, and synthetic solution of containing 2000 mg/L of $CaSO_4$ on the permeate flux in DCMD system using flat sheet membranes. A graduate decline in the flux

occurred when seawater and RO concentrate were used for the first 1200 min, then dramatic decrease of the flux happened to reach zero. However, a dramatic decrease of the flux after 300 min only occurred using $CaSO_4$ solution.

Ibrahim and Alsalhy [86] were able to come out with a new heat and mass transfer simulated model for hollow fiber membranes in DCMD system. Various membrane characteristics and operating conditions were taken into account to evaluate the new model. Feed and permeate temperature and concentration, flow regime, membrane characteristics like membrane material, membrane pore size, and length, in addition to module characteristics are considered to present this model. The proposed simulated model showed high agreement with various experimental results found in literature.

Bahmanyar et al. [87] had simulated and studied the effect of operating conditions such as feed flowrate, temperature, and salinity concentration in DCMD system on temperature and concentration polarization. The simulated model on heat and mass transfer used MATLAB in solving. The model showed acceptable agreement with different experimental results. Moreover, the study found that membrane thickness of (30 – 60 μm) is the optimal choice to overcome temperature and concentration polarization.

Adham et al. [88] investigated the performance of different flat sheet membranes under various operating conditions used for DCMD desalination of Arabian Gulf brine. High permeate flux of 25 LMH is achieved at 80℃ feed temperature. Moreover, high salt rejection of 99.99% and high quality of distilled (conductivity less than 10 μm is accomplished.

Maab et al. [51] were the first to investigate the performance of fabricated Polyazole PVDF hollow fiber membranes for DCMD desalination of real Red sea water. Polyazole hollow fiber membranes includes fluorinated polyoxadiazole and polytriazole hollow fiber membranes. The enhanced Polyazole PVDF membranes achieved high permeate flux of (35 and 41 kg/m^2.h) at 80℃ feed temperature and 20℃ distilled water which is approximately (13 – 32%) higher flux than using normal PVDF hollow fiber membranes. High salt rejection of 99.95% is achieved.

Macedonio et al. [89] tested DCMD system for the treatment of oilfield produced water. Several commercial hollow fiber membranes were examined (PVDF and PP) under various thermal and hydrodynamics conditions. Results indicated that hollow fiber membranes showed reliable and stable performance with 99% salt rejection and 90% carbon rejection.

Ho et al. [90] conducted one of the latest studies on enhancing flux production in counter-current DCMD systems using artificial roughness surface. PTFE membranes were investigated in this study under various feed temperatures and flowrates. Both theoretical and experimental studies were conducted and the results showed that flux production increased by approximately 42% when rough surface was used.

Bouchrit et al. [42] examined the capability of PVDF hollow fiber membranes to treat hyper-saline water. The flux was predicted by Knudsen-molecular mechanism model. The results showed a noticeable decline of the flux from 8.43 to 4.06 $kg/m^2.h$ when concentration factor of RO concentrate increased four times. Membrane wetting was noticed at 90% of the operated time when crystallization phenomena occurred.

Zhu et al. [2] studied new design of dual-layer composite hollow fiber membranes used for DCMD systems. The outer layer of the membrane consists of polyvinylidene fluoride (PVDF) and polyvinylpyrolidone (PVP) and the inner layer of the membrane consists of polyvinylidene fluoride (PVDF) and polyvinyl alcohol (PVA). The new composite is used to enhance the hydrophility of inner layer and the pore forming agents in the outer layer. Results indicated high permeate flux approximately (7.5 $kg/m^2.h$) for more than seven days. High salt rejection of more than 99% is observed.

Ho et al. [91] conducted one of the latest studies on the flux performance of hollow fiber membrane at laminar flow in DCMD system. Theoretical and experimental work was evaluated under co-current and counter-current flow configurations. The experimental work showed close agreement with the theoretical estimates with small error of (2 – 6%). Average and local Nusselt number were calculated that fall in the range of (3.5 – 7.5).

Zuo et al. [92] exanimated polyethylene (PE) flat sheet membrane with synthetic (3.5 wt% sodium chloride) feed solution. Different pore size and porosity were examined. The permeate flux reached (123 L/m^2.h) at feed temperature of 80℃ with pore size of 0.2 μm and approximately 66% porosity. The achieved flux exceeded the majority of the reported fluxes of flat sheet and hollow fiber membranes in the literature. Stable permeate flux was observed for 100 hours of operating period.

One of the latest mathematical dynamic model was proposed by Eleiwi et al. [93] that used 2D Advection-Diffusion Equation (ADE) that describe mass and heat transfer in DCMD system. In order to conduct the experimental part, PTFE flat sheet membrane was used with Red seawater as feed solution. Time variation phase was examined experimentally in temperature range of (30 – 75℃) with and increment of 0.1℃ every 2 min and through the proposed model with an error less than 5.0 %.

Chapter 3: Direct Contact Membrane Distillation Theory

The performance of direct contact membrane distillation (DCMD) in terms of flux production, membrane life time and environmental impacts depends on many factors but three factors have major impact on DCMD performance and water quality produced. These factors are:

- Membrane configuration: DCMD, VMD, AGMD, SGMD
- Membrane physical properties and morphology
- Module configuration and flow arrangement
- The operation conditions: temperature and flowrate

Each parameter that affect the flux will be discussed in details in this chapter.

3.1 Membrane Distillation Configuration

As explained before in **Chapter 2**, membrane distillation has four different configurations that are classified according to permeate flux configuration and collecting techniques [7], [94]. The feed side remains the same for the four systems. These four configurations are:

- Air Gap Membrane Distillation (AGMD)
- Sweeping Gas Membrane Distillation (SGMD)
- Vacuum Membrane Distillation (VMD)
- Direct Contact Membrane Distillation (DCMD)

DCMD is the easiest configuration to be conducted where cold and hot sides are in direct contact, separated only by the membrane. However, VMD is used for high permeate production even when additional complexity occurs due to vacuum pump. SGMD and AGMD have the advantage of minimizing heat lose. Drioli et al. [34] and other researchers [32] proposed Several novel configurations of membrane distillation which are under research: Multi-effect membrane

distillation (MEMD), Vacuum Multi-effect membrane distillation (V-MEMD), Material Gap membrane distillation (MGMD), and Permeate Gap membrane distillation (PGMD).

The Direct Contact Membrane Distillation (DCMD) is the most studied configuration among the four systems due to the simplicity of installation in the laboratories. Nearly 64% of published research papers up to December 2010 were on DCMD [5].

Moreover, it is the oldest technology and most commonly used [95]. As explained in **Chapter 2**, the mechanism of DCMD is divided into several steps. First of all, hot feed water is evaporated at the feed side of the membrane (reach 90℃). Due to vapor pressure difference across the membrane and its morphology, only vapor molecules can transport through membrane pore to the distilled side to be condensed. As an effect of this process, the hot feed stream decreases in temperature and the cold stream increases. Therefore, a cooler and a heater are used to recover the heat lose. DCMD system is operating at consistently low operating pressure. Therefore, it is important to monitor pressure across the membrane to avoid membrane wetting. Membrane wetting can be easily determined by measuring the permeate electrical conductivity [5]. Another main advantage of DCMD is that permeate water can be produced at low temperature (40 – 80℃) [38] and no need to reach the boiling point of water. Last but not least, DCMD comparing to conventional thermal processes result low vapor space [6], [41].

DCMD can use waste heat to operate in a widespread range of different applications in which water flux is the major component. These applications include treatment of oilfield produced water, desalination of seawater and brackish water, and removal of small molecule contaminants.

Macedonio et al. [89] conducted an experimental research on oilfield produced water using two different membrane materials (PP and PVDF) in DCMD system. A flux of 9 kg/m^2.h of clean treated water can be reached in this system. The removal of small molecule contaminants is studied by treatment of the produced

water. A study on simulated produced water was conducted by Singh and Sirkar [96] using compressible PTFE membranes in DCMD process. Maximum permeate flux of 195 kg/m^2.h was achieved. Lawson [41] reported that the first DCMD desalination system was established in 1964 with a production of 1 kg/m^2.h permeate flux. With time, DCMD operating conditions are developed and permeate flux of 75 kg/m^2.h can be reached for desalination. Almost complete salt rejection is observed in DCMD desalination system. Brackish water desalination is also attracting research projects and industrial implementation [32]. Potential DCMD experimental researches in lab bench scale that involved real saline feed water achieved consistently good results.

DCMD desalination research with hollow fiber membranes [51] and flat sheet membranes [48] achieved high permeate flux. Permeate flux can reach as high as 41 kg/m^2.h and 88.8 kg/m^2.h for hollow fiber and flat sheet membranes, respectively.

Furthermore, desalination is studied in wide range with modifications such as additional renewable source of energy, hybrid configurations, optimum operating conditions, and new materials for membranes [6].

As mentioned before, the main problem of DCMD is heat lose through conduction. Alkhudhiri et al. [35] explained that this heat lose occurs through three types of mechanisms. First type is heat lose through membrane conduction, second type is heat loss due the trapped air in the membrane, and finally heat lose because of temperature polarization. Temperature polarization is explained in details in **section (3.5)** further in this chapter.

Table 9: Advantages and disadvantages of different membrane distillation configurations

Configuration	Advantages	Disadvantages
DCMD	Easiest and simplest configuration, More stable flux than VMD, Most appropriate for removal of volatile components. Operated at low pressure, Low feed pre-treatment is needed. Flexible scale-up [97], 100% salt rejection, low vapor space [6]	Lower flux than VMD, Highest temperature polarization, Permeate quality is dependable on membrane wetting, Appropriate for aqueous solutions, Mass transfer resistance due to air trapped within the membrane, Huge heat lose through conduction
VMD	High flux, Permeate quality is stable even with membrane wetting, Impossible wetting from distillate side, Temperature polarization is low.	Higher possibility of pore wetting, High fouling, Vacuum pump and external condenser are required.
AGMD	Low thermal loss, Impossible wetting on distillate side, Less fouling.	Air gap resistance to mass transfer, Complex module designing, Modeling difficulties, Lowest gained output ratio
SGMD	Low temperature polarization, Impossible wetting from permeate side, Permeate quality independent of membrane wetting.	Complexity due to extra equipment, difficult heat recovery, low flux, pretreatment of sweep gas might be needed

As conclusion, each configuration has its benefits and drawbacks in different applications that have been discussed in details in **Chapter 2**. Table (9) summarizes the main advantages and disadvantages of each system.

3.2 Membrane Modules

There are a large diversity of membrane arrangements and modules that depend on the application of the membrane. Flat sheet membranes including plate-and-frame and spiral wound and tubular membranes that include capillary and hollow fibers are the most common types of membranes [12], [36]. Two types of these (flat sheet and hollow fiber) membranes are explained in details in the sections below as this study focuses on them. Zhang et al. [98] mentioned two different researches involved hollow fiber and flat sheet membranes to study the permeate flux at (40 – 60℃) feed temperature. The generated fluxes were (1 – 4) $L/m^2.h$ and (20 – 30) $L/m^2.h$ for hollow fiber and flat sheet membranes, responsivity. Figure (23) illustrates the schematic diagrams of hollow fiber and flat sheet membranes.

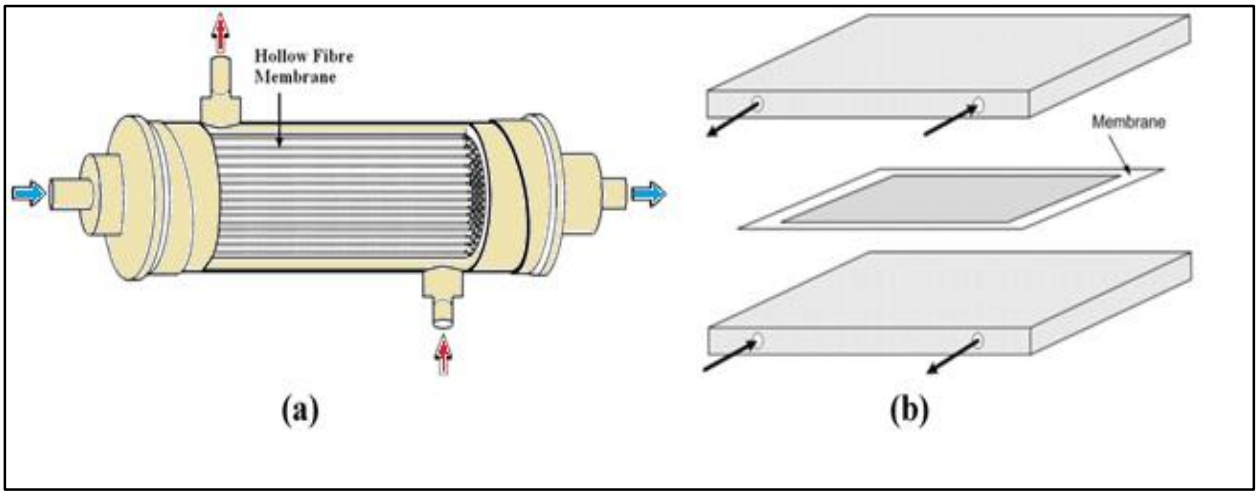

Figure 23: Schematic diagram of a) hollow fiber membrane b) flat sheet membrane

A detailed evaluation between flat sheet and hollow fiber membranes is represented in the sections below including the modified designs on the hollow fiber membrane module.

3.2.1 Flat Sheet membrane

Flat sheet membranes are usually manufactured as sheets that could be placed with spacers between two rectangular cells. Figure (23b) illustrates the schematic diagram of flat sheet membrane. Flat sheet membranes are chosen over hollow fiber membranes due to simple preparation, cleaning and handling [12], [36]. They can be easily removed and replaced [41]. However, the packing density and effective surface area per unit volume are very low. Moreover, membrane support is required in flat sheet membranes. Desalination and water treatment researches are the preferable fields for flat sheet membrane applications [35]. Earlier mentioned in this chapter that many researchers studied saline water treatment using flat sheet membranes. Some of these experimental researches include real seawater, synthetic seawater, and thermal brine are covered in these papers [38], [47], [50], [52].

3.2.2 Hollow fiber membrane

Hollow fiber membranes are consisting of many membrane tubes that are placed in a shell and tube type housing. Figure (23a) illustrates the schematic diagram of hollow fiber membrane. Membrane tubes are glued and permanently fixed inside the bundle and can not be replaced. Therefore, cleaning is hardly controlled in hollow fiber membranes and high tendency of fouling occur [99]. Also, replacing hollow fiber membranes is more expensive than flat sheet. Nevertheless, these membranes have the highest packing density and effective surface area per unit volume so from industrial perspective these membranes are more attractive [5], [36], [99]. Furthermore, membrane support is not required in hollow fiber membranes resulting low boundary layer resistance [41]. Feed solution can be placed either in the tube side or shell side in co-current or counter-current configuration [100]. Flow arrangements applied for hollow fiber membranes that can be also applicable for flat sheet membranes are explained in details in **section (3.8)**. Similar to flat sheet membrane, many researchers

studied saline water treatment using hollow fiber membranes. Some of these experimental researches include real seawater, synthetic seawater, and thermal brine are covered in these papers [46], [49].

3.3 Novel Designs of Hollow Fiber membrane

Modified fiber geometrics, spacers and baffles can improve the hydrodynamics of hollow fiber membrane process. All these novel designs are made to modify the commercial membranes. Spacers enhance permeate flux by preventing the membranes from sticking to each other by increasing the effective membrane surface area. Baffles enhance permeate flux by increasing heat transfer coefficients of the hot feed stream. Yang et al. [85] reported that an enhancement of 300% permeate flux can be reached when the fibers are modified inside the hollow fiber module.

3.3.1 Structured-Straight module

The Structured-Straight module is arranged by placing all the hollow fibers into a fiber sheet and then rolling them together to produce a bundle that could be placed into the module house. The main objective of this module is to spread hollow fibers from others leading to uniform flow distribution in the shell-side of the module [85].

3.3.2 Central-tubing module

Central-Tubing module is prepared by arranging hollow fibers in a wavy way around a central tube. In this design, the central tube represents the shell side of the module and has two drawtubes that are allocated for the feed inlet and outlet. Thus the hot feed water will pass through the central tube to be collected as permeate from fiber lumen. All the space between the fibers, central tube, and module housing is sealed using epoxy (Araldite®). As the main objective of this

design is to create more turbulence flow pattern and more uniform fiber arrangement in a module, designing the central tube is the major challenge. It includes the hole interval, distribution, and shape in addition to size, material, and wall thickness of the tube [85].

3.3.3 Modified fiber geometrics

Modified fiber geometrics include two types of fibers: the braided fibers and the twisted fibers. Teoh et al. [84] reported that an enhancement of 36% of permeate flux occurs when braided and twisted configurations are introduced to the system. The increase in flux happen for un-straight membrane configurations due to the increase of heat transfer coefficients.

3.3.3.1 Braided (curly-fiber geometry) module

The modified fiber geometrics membranes include braided (curly-fiber geometry) and twisted modules. The fabrication of curly-fiber geometry requires proper temperature and specific winding angle. The fibers are wrapped around stainless steel rods with certain diameters that indicate the winding angles. Then the fibers are placed in oven for certain temperature and period of time until the curly shape occur. This configuration with wavy membrane surface is aimed to increase the turbulence and improve hydrodynamics under laminar flow conditions [85]. Teoh et al. [84] reported that permanent braided hollow fibers could be created by placing the fibers in a wryer net for half an hour in an oven of 80 ℃. Gryta et al. [101], [102] reported that the enhancement of permeate flux occurs with braided fibers as they are performed as static mixers that increase heat transfer coefficients.

3.3.3.2 Twisted modules

The fabrication of twisted modules can be completed in two easy steps. First step is to twist the hollow fibers in one direction and tie them with a rope or a sting

with uniform intervals. The other step is to untwist the hollow fibers in the other direction to return to its previous position. Repeating these actions is creating an outward "bow" configuration of the hollow fibers [84].

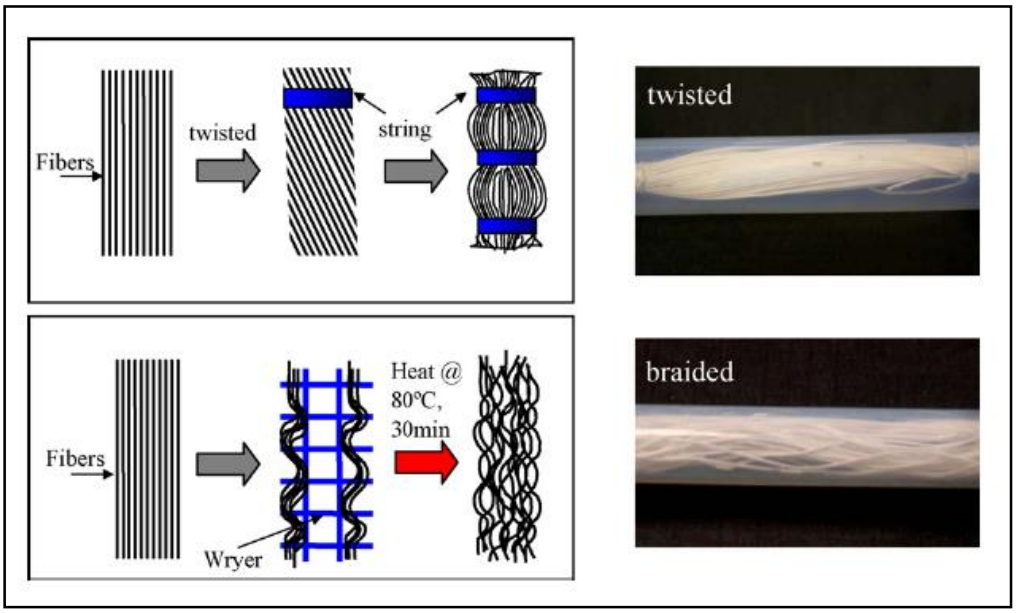

Figure 24: Schematic Diagrams of braided and twisted fibers preparation. Adapted from Ref. [84]

The schematic diagram of preparing braided and twisted modules is illustrated by Teoh et al. [84] in figure (24) above.

3.3.4 Spacers

Hollow fiber membranes stick together when become wet and lower membrane effective surface area. Spacers are used in hollow fiber modules to separate fibers from each other in order to enhance the effective surface area of the membranes [84]. Therefore, two configurations with spacer which are spacer-wrapped and spacer-knitted modules are explained below. Teoh et al. [84] reported that an enhancement of 30% of effective membrane surface area occurs when spacers are introduced to the system. Chen et al. [103] mentioned that the

implementation of spacer not only increasing the flux, also reducing scaling deposition.

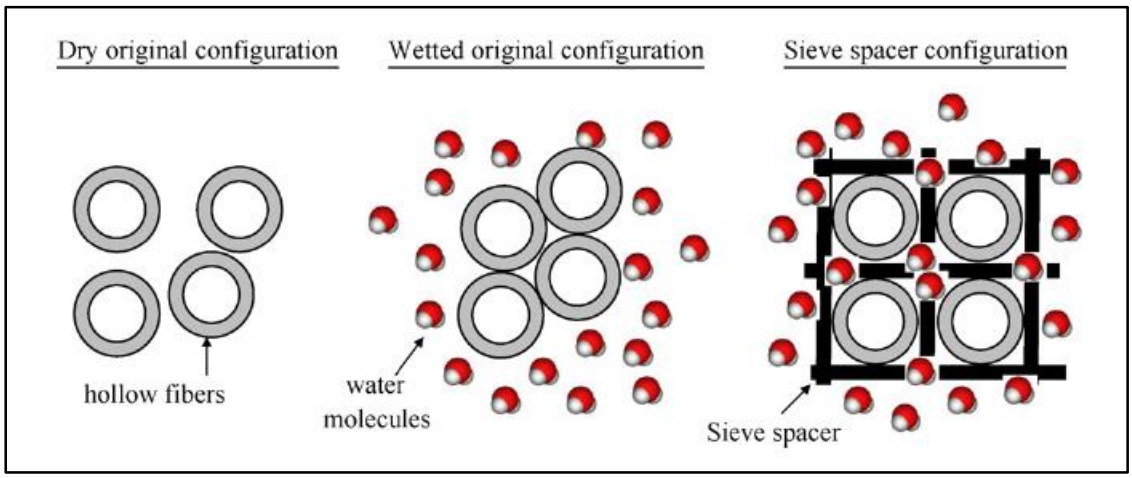

Figure 25: schematic diagram of hollow fiber tubes with in/out spacer

Figure (25) illustrates the water contact and effective surface area of wet membrane and the effective membrane surface area with spacer.
The spacer in hollow fiber membrane can be either wrapped or knitted with the fibers.

3.3.4.1 Spacer-wrapped module

Yang et al. [85] suggested spacer-wrapped configuration in which the fibers are wrapped by woven fabric sheet (spacer) and rolled up inside the module. Turbulent flow occurs when the water flow between membrane and spacer layers. This configuration is very sensitive as the incorrect placement of the spacer across the fibers can cause fluid immobilization inside the module that inversely affect the hydrodynamic conditions.

3.3.4.2 Spacer- knitted module

In spacer-knitted configuration, membrane fibers are woven into the mesh sheet of the spacer. Similar to the spacer-wrapped module, turbulent flow occurs when the water flow between membrane and spacer layers. However, the incorrect way of knitting the spacer could cause over-packing of the membranes in the module. Therefore, fluid immobilization occurs inside the module that inversely affect the hydrodynamic conditions [85].

3.3.5 Baffles

Baffles avoid the formation of the dead zones inside the hollow fiber module. However, lower enhancement of flux is reached when baffles are used instead of spacers. This can be explained as the baffles occupy more volume in the module than the spacers that cause high compactness of the fibers.

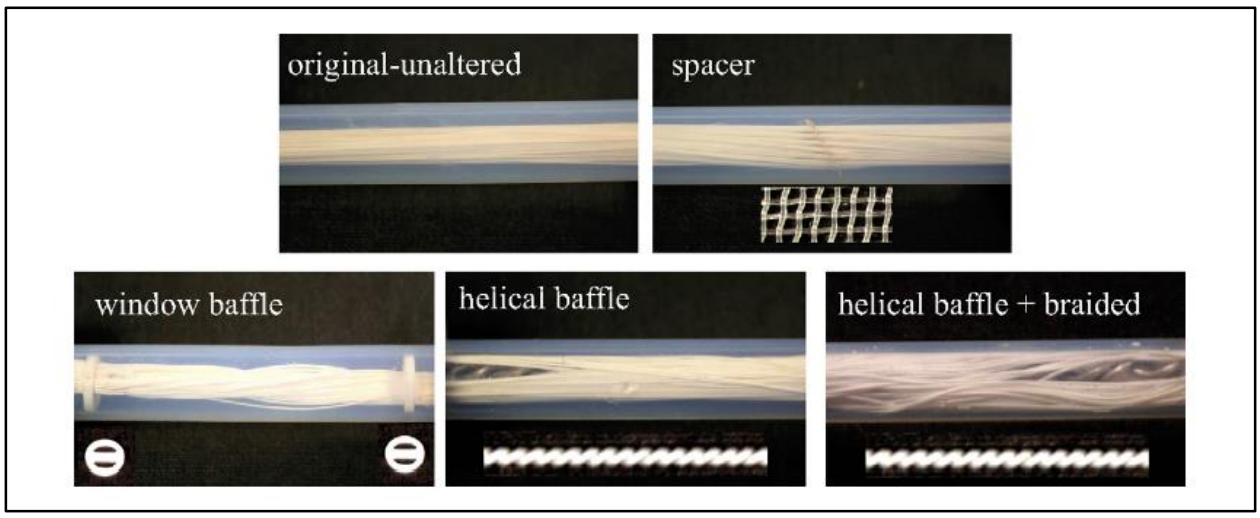

Figure 26: Original hollow fiber module and the introduction of spacers and baffles (Adapted from [84])

Teoh et al. [84] reported that enhancement of 20 - 28% of permeate flux occurs when baffles are introduced to the system. Flux enhancement occur in baffled

configurations due to increasing thermal coefficients that reduce temperature polarization in the module and overcome boundary layer resistance [34].
Figure (26) represents the introduction of baffles into the original hollow fiber membrane. Baffles in hollow fiber membrane can be either helical or window.

3.3.5.1 Helical baffle

Helical baffles are placed in the middle of hollow fiber modules and the fiber tubes are surrounding and covering the baffle across the module. Teoh et al. [84] reported that combining more than one design like the usage of braided membranes in helical baffled designs leads to additional 11% increase of the flux.

3.3.5.2 Window baffle

Window baffles are placed along the membranes with specific spacing between them (usually 5 cm). The effect of window baffled configuration is achieved at high feed temperature.
High permeate fluxes are achieved when these novel designs of hollow fiber modules were introduced. The highest permeate flux is related to the knitted fibers with spacer due to the transverse flow across the curved fibers that don't appear with straight parallel fibers [104].

Teoh et al. [84] reported that permeate flux enhancement of approximately 50% is achieved at 75℃ feed temperature when hollow fiber module modifications are applied. The highest permeate flux of approximately (8 kg/m^2.h) is achieved for helical baffled with spacer module configuration when feed temperature reached 75℃. At 50℃ feed temperature, very low permeate flux enhancement of less than 15% is achieved only. However, Yang et al. [85] reported that the highest permeate flux of approximately (12 kg/m^2.h) at 50℃ feed temperature is achieved at spacer knitted fibers. Moreover, heat transfer coefficients at the hot side were calculated by Teoh et al. [84] for the original and baffled hollow fiber modules. It

was found that heat transfer coefficients increased from (2600 W/m^2.K) for the original configuration to (3150 W/m^2.K) and (3750 W/m^2.K) for window baffled and helical baffles, respectively .

3.4 Heat and Mass Transfer in MD

Heat transfer and Mass transfer are combined together to represent the most important concepts in membrane distillation (MD). Same direction is taken for heat and mass flow in MD system. Heat and mass transfer would be explained in details for flat sheet and hollow fiber membranes.

3.4.1 Heat Transfer

The mechanism and the theory of heat transfer in both flat sheet and flat sheet membranes is covered in details in these sections below.

3.4.1.1 Heat Transfer (Flat Sheet membrane)

Heat transfer occurs in Membrane Distillation (MD) as it is a thermal driven process. The main mechanisms that are responsible for heat transfer from the hot feed side to the cold permeate side are latent heat of vaporization, and conductive heat transfer [35], [45]. Heat Transfer in MD follow 3 steps as illustrated schematically in figure (27) and explained later in details:

i. Heat Transfer by convection through feed boundary layer, Q_f

ii. Heat Transfer through membrane, Q_m

iii. Heat Transfer by convection through permeate boundary layer, Q_p

Different experimental researches on flat sheet DCMD evaluate the equations of calculating heat transfer and thermal coefficients [98], [105], [106], [107], [108].

The method of evaluating heat transfer in flat sheet membrane [7], [100], [109] is explained in details in the section below.

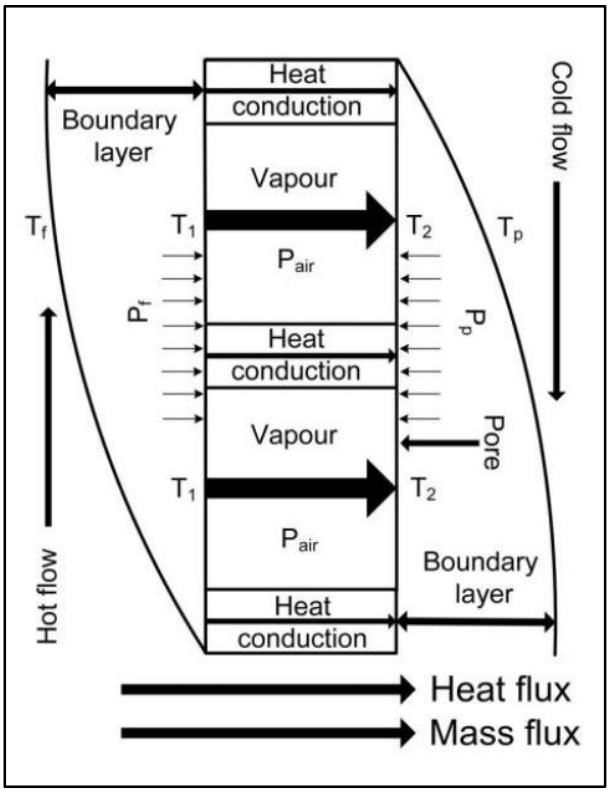

Figure 27: Heat and Mass Transfer through membrane in DCMD system (Adapted from [12])

Starting with the heat transfer in the feed boundary layer Q_f, the temperature of hot feed T_f is decreased until it reaches membrane side temperature T_1. The heat is transferred by convection due to this temperature difference. Maximizing this heat transfer by turbulent flow pattern can avoid temperature polarization [5]. Heat transfer is calculated by equation (1):

$$\boldsymbol{Q_f = h_f\,(\,T_f - T_1\,)} \qquad \textbf{(1)}$$

where h_f is feed heat transfer coefficient and $(T_f - T_1)$ is the temperature difference between the feed and hot membrane surface. Next, the heat is transferred through the membrane. This heat transfer is a summation of latent heat of vaporization Q_v and conductive heat transfer through membrane material and pores Q_c [110]. Equation (2) represents the energy balance across the membrane.

$$\boldsymbol{Q_m = Q_v + Q_c} \quad \textbf{(2)}$$

Water vapor is created when water is evaporated in the interference of hot feed water and membrane pores. Then water vapor is condensed at the interference of membrane pores and permeate side. This heat is transported with the permeate flux through the membrane J_p. Equation (3) is used to calculate the heat transfer of latent heat of vaporization Q_v:

$$\boldsymbol{Q_v = J_p\ \Delta H_v} \quad (3)$$

where ΔH_v is the enthalpy of vapor water that is a function of absolute temperature (K) and can be calculated using equation (4)

$$\boldsymbol{H_v(T) = 1850.7 + 2.8273T - 1.6 \times 10^{-3}\ T^2} \quad \textbf{(4)}$$

The second part is conductive heat transfer through membrane material and pores Q_c. It can be evaluated by the following equation (5)

$$\boldsymbol{Q_c = \frac{k_m}{\delta_m}\ (T_1 - T_2)} \quad \textbf{(5)}$$

where δ_m is membrane thickness and k_m is thermal conductivity that can be calculated using equation (6)

$$\boldsymbol{k_m = (1 - \varepsilon)K_s + \varepsilon K_g} \quad \textbf{(6)}$$

where ε is porosity of the membrane, K_s is thermal conductivity of membrane material and K_g is thermal conductivity of the gas in membrane pores.

Therefore, following equation (2), the resulted heat across the membrane is summarized by equation (7)

$$\boldsymbol{Q_m = \frac{k_m}{\delta_m} (T_1 - T_2) + J_p \, \Delta H_v} \quad \textbf{(7)}$$

This part of heat transfer across the membrane should be lowered as possible as it is considered as heat loss which doesn't take part in evaporation. Air Gap Membrane Distillation (AGMD) is the best solution to decrease conductive heat loss as the air gab provides thermal insulation. However, this air gap limits the mass transfer. In order to enhance mass transfer, air gap is replaced with stripping gas (SGMD). In Vacuum Membrane Distillation (VMD), the heat transferred through membrane can be negligible. For DCMD systems, using multi-layer membranes can also reduce heat loss [5], [33], [111]. Latent heat Q_v is responsible for 50% - 80% of vapor production and the remaining is achieved by conductive heat transfer through membrane Q_c. At higher operating conditions, conductive heat Q_c effect become less significant [45].

The last part is heat transfer in the permeate boundary layer Q_p that can be evaluated by equation (8)

$$\boldsymbol{Q_p = h_p (T_2 - T_p)} \quad \textbf{(8)}$$

where h_p is permeate heat transfer coefficient and $(T_2 - T_p)$ is the temperature difference between membrane surface and the permeate. In order to enhance mass transfer (permeate flux), heat boundary layers that work as resistance should be minimized. To minimize temperature polarization, as in feed boundary layer, turbulent flow is recommended [45].

At steady state conditions, heat transfer equations are equated as shown in equation (9) in order to evaluate the temperature at the hot and cold surfaces of the membrane that can't be measured experimentally or calculated. The resulted equations of temperature are expressed in equations (10) and (11).

$$Q_f = Q_m = Q_p \tag{9}$$

$$T_1 = T_f - \frac{J_p}{h_f} \Delta H_v \left[\frac{T_1 - T_2}{2}\right] \tag{10}$$

$$T_2 = T_p - \frac{J_p}{h_p} \Delta H_v \left[\frac{T_1 - T_2}{2}\right] \tag{11}$$

Temperatures across the membrane T_1, T_2 are essential terms of evaluating temperature polarization coefficient (θ) that will be covered in Temperature Polarization in **Section (3.5)**.

The convective heat transfer coefficients in the feed and permeate boundary layers represented in equation (13) can be estimated by Nusselt correlations that has an empirical formula expressed in equation (12):

$$Nu = Constant\ Re^a\ Pr^b \tag{12}$$

$$h = \frac{k}{d_h} Nu \tag{13}$$

where a, b, are constants and d_h is hydraulic diameter. Reynolds (Re), Prandtl (Pr), and Grashoff (G_r) numbers that are required to evaluate Nusselt correlations are represented in equations (14), (15), and (16).

$$Re = \frac{v\, d\, \rho}{\mu} \tag{14}$$

$$Pr = \frac{C_p\, \mu}{k} \tag{15}$$

$$G_r = \frac{g\, \beta\, \Delta T\, l^3\, \rho^2}{\mu^3} \tag{16}$$

where $v, d, \rho, \mu, k, C_p, g, \beta, \Delta T$ and l are fluid velocity, diameter, density, viscosity, thermal conductivity, heat capacity, gravity, thermal expansion coefficient, temperature difference and characteristic length, respectively [35].

Different Nusselt number corrections generated experimentally for various operating conditions, flow patterns, and membrane configurations in flat sheet membrane DCMD process are present in **APPENDIX B**.

The boundary layers of heat transfer coefficients are found using the heat transfer empirical correlations which take into consideration some dimensionless numbers such as Reynolds Prandtl and Nusselt. These correlations were used by some researchers to model the heat transfer in MD using the heat transfer correlations for rigid non-porous heat exchangers. However, the heat transfer in MD is associated with mass transfer and involves non-rigid and porous surface. This study will take into consideration all these factors in order to study the convective heat transfer taking place inside MD systems by starting with the basic heat balance equation described above.

3.4.1.2 Heat Transfer (Hollow Fiber membrane)

Similar procedure to flat sheet membrane distillation occurs for hollow fiber Heat transfer occurs in MD systems as thermal driven process. The main mechanisms that are responsible for heat transfer from the hot feed side to the cold permeate side in hollow fiber membrane are latent heat of vaporization, and conductive heat transfer. [35], [45] Heat Transfer in Hollow fiber membrane follow 3 steps as illustrated schematically in figure (28) and explained later in details:

i. Heat Transfer within tube feed boundary layer, Q_f

ii. Heat Transfer across membrane, Q_m

iii. Heat Transfer within shell permeate boundary layer, Q_p

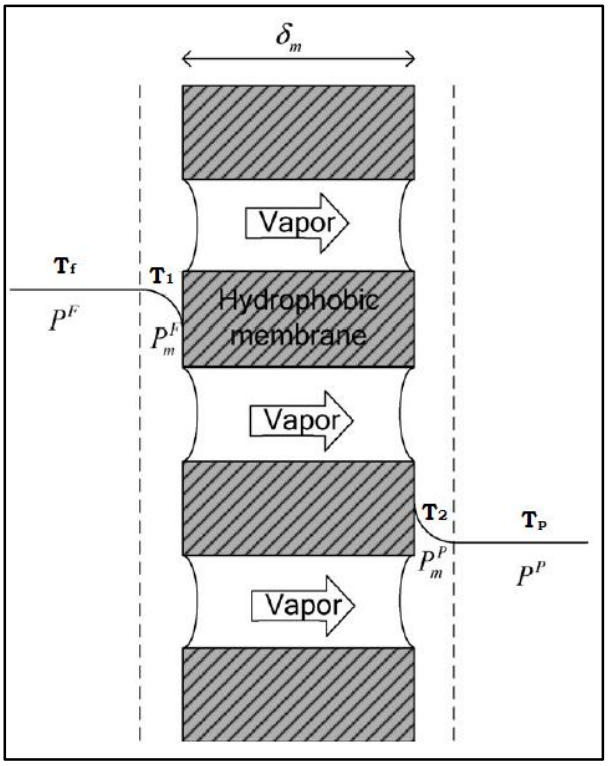

Figure 28: Heat and mass transfer in hollow fiber DCMD system

Different experimental researches on hollow fiber DCMD evaluate the equations of calculating heat transfer and thermal coefficients [98], [105], [106], [107], [108]. The method of evaluating heat transfer in hollow fiber membrane is explained in details in the section below [86], [100], [109].

Starting with the heat transfer within tube feed boundary layer Q_f, the temperature of hot feed T_f is decreased until it reaches membrane side temperature T_1. The heat is transferred by convection due to this temperature difference. Maximizing this heat transfer by turbulent flow pattern can avoid temperature polarization [5]. Heat transfer is calculated in hollow fiber membranes by equation (17):

$$\boldsymbol{Q_f = h_f\, A_r{}^f\, \alpha\, (T_f - T_1)} \qquad \textbf{(17)}$$

where h_f is heat transfer coefficient at membrane feed side and ($T_f - T_1$) is the temperature difference between the feed and membrane surface, $\alpha = \pi N d$ and ${A_r}^f = 1$ [100], [109].

Next step is the heat transferred through the membrane. This heat transfer is a summation of latent heat of vaporization Q_v and conductive heat transfer through membrane material and pores Q_c. Previously mentioned, equation (2) represents the energy balance across hollow fiber membrane also.

Water vapor is created when water is evaporated in the interference of hot feed water and membrane pores. Then water vapor is condensed at the interference of membrane pores and permeate side. This heat is transported with the permeate flux through the membrane J_p. Equation (18) is used to calculate the heat transfer of latent heat of vaporization Q_v in hollow fiber membrane:

$$\boldsymbol{Q_v = {A_r}^m \alpha J_p \Delta H_v} \qquad \textbf{(18)}$$

Where $\alpha = \pi N d$, ${A_r}^m = {d_{lm}}/{d_i}$ where d_{lm} is the log-mean radius difference of the fiber, and ΔH_v is the enthalpy of vapor water that is a function of absolute temperature (K) [100] and can be evaluated using equation (4) mentioned by Ibrahim and Alsalhy [86].

The next part is the conductive heat transfer through membrane material and pores Q_c. It can be evaluated by the following equation (19)

$$\boldsymbol{Q_c = {A_r}^m \alpha \frac{k_m}{\delta_m} (T_1 - T_2)} \qquad \textbf{(19)}$$

where δ_m is membrane thickness and k_m is thermal conductivity that can be calculated using equation (6)

Therefore, combining equations (18) and (19), resulted heat transfer across the membrane that is represent by equation (20)

$$\boldsymbol{Q_m = {A_r}^m \alpha \left[\frac{k_m}{\delta_m} (T_1 - T_2) + J_p \Delta H_v\right]} \qquad \textbf{(20)}$$

The last part is heat transfer in the tube permeate boundary layer Q_p that can be evaluated by equation (21)

$$\boldsymbol{Q_p = A_r{}^p\, \alpha\, h_p\, (T_2 - T_p)} \qquad \textbf{(21)}$$

Where $\alpha = \pi N d$, $A_r{}^p = {}^{d_o}/_{di}$ where d_o is the outside diameter of the fiber, and h_p is permeate heat transfer coefficient and $(T_2 - T_p)$ is the temperature difference between membrane surface and the permeate [100]. To minimize temperature polarization, as in feed boundary layer, turbulent flow is recommended [5].

Similar to heat transfer with flat sheet membranes, at steady state conditions, heat transfer equations are equated as was shown in equation (9) in order to evaluate the temperature at the hot and cold surfaces of the membrane that can't be measured experimentally or calculated.

The convective heat transfer coefficients in hollow fiber membranes are evaluated similar to flat sheet membrane mentioned in the previous section using equations (12 – 16).
Different Nusselt corrections generated experimentally for various operating conditions, flow patterns, and membrane configurations in Hollow fiber membrane DCMD process are present in **APPENDIX B**.

3.4.2 Mass Transfer

Mass transfer in DCMD process can be defined as the vapor molecules collected in the permeate side after been transferred through the membrane. Since the DCMD process is a thermal driven process, mass and heat transfer is occurring together. The main objective of studying mass transfer in DCMD process is to identify and quantify the effect of concentration and temperature polarization in mass and heat transfer analysis to achieve maximum permeate flux.

Starting with the mass transfer that occurs based on three stages:

1. The water molecules vaporize and transfer from liquid to vapor phase.

2. The vapor molecules from hot side transport through membrane pores to the cold side where the driving force is vapor pressure difference across the membrane.

3. The vapor molecules condense and transfer from vapor phase to liquid phase [42].

Consequently, the main factors that control the mass transfer in DCMD process are the vapor pressure difference across the membrane and the permeability of the membrane itself [33]. Figure (27) mentioned before in heat transfer section, explains heat and mass transfer in DCMD system. Feed temperature (T_f) drops down to reach temperature at feed side of the membrane (T_1). This temperature evaporates water at feed membrane layer and the vapor transport through the pores to reach the permeate side where it condenses. Permeate temperature at membrane side (T_2) decreases toward the permeate side (T_p). Vapor Pressure difference across the membrane at ($T_2 - T_1$) is less than feed and permeate vapor pressures at ($T_f - T_p$) which create the driving force of mass transfer [98].

Generally, the mass transfer mechanism in the membrane pores is occurring due to four well-known mechanisms known as Knudsen-diffusion (K), Poiseuille-flow (P) and Molecular-diffusion (M) and a combination between Knudsen-diffusion and Molecular-diffusion known as the Transition Mechanism [73], [98]. These mechanisms indicate the collision process of the molecules between each other and the membrane [35]. These mechanisms are explained as:

Knudsen-diffusion (K): takes place with small membrane pore size with the dominant collusion is occur between the molecules and membrane wall while the collision of molecules with each other can be ignored [35].

Molecular-diffusion (M): takes place when the molecules undertake the concentration gradient [35].

Poiseuille-flow (P): takes place in viscous media when the molecules undertake the pressure gradient [35].

Transition-Mechanism: is a combination of the three previous methods [73].

Phattaranawik et al. [73] and other researchers [68] mentioned that transition-mechanism is the most relevant with the experimental results. The Knudsen number (Kn) is used to show the leading mass transfer mechanism in the membrane pores according to specifications in table (10) below:

Table 10: Dominant mass transfer mechanism in membrane pore [98]

$Kn < 0.01$	$0.01 < Kn < 1$	$Kn > 1$
Molecular diffusion	Knudsen-molecular diffusion transition mechanism	Knudsen mechanism

The Knudsen number (Kn) is expressed in equation (22):

$$Kn = \frac{L}{d} \tag{22}$$

where d is the main pore size of the membrane and L is the mean free path of the molecules. The transport mechanism in MD system is changed according to the mean free path of the molecules.

Phattaranawik et al. [73] and Andrjesdottri et al. [112] evaluate the mean free path (L) as a binary mixture of air and water as shown in equation (23)

$$L = \frac{k_B T}{\pi \left(\frac{\sigma_w + \sigma_a}{2}\right)^2 P_{pore}} \frac{1}{\sqrt{1 + \frac{m_w}{m_a}}} \tag{23}$$

where

k_B: Boltzman constant (1.381×10^{-23} JK^{-1})

T: mean temperature in the pores

P_{pore}: gas phase pressure in pores

σ_w: collision diameter for water vapor (2.641×10^{-10} m)

σ_a: collision diameter for air (3.711×10^{-10} m) [15]

m_w : Molecular weights of water

m_a : Molecular weights of air

As an example, at a temperature of 60℃ membrane distillation, the mean free path of water vapor molecules (L) in the membrane pores is calculated to be $0.11\mu m$ [33], [35]. As the usual pore size used for membrane distillation varies from 0.2 to 1.0 μm, this results of a Knudsen number (Kn) that occur in the range of 0.1 to 0.5. Referring to table (10), this proves that the dominant mass transfer mechanism in DCMD is Knudsen-molecular diffusion transition mechanism.

Khayet et al. [113] reported the mean free path of water vapor molecules (L) in different expression as shown in equation (6) below

$$\boldsymbol{L_i = \frac{k_B\, T}{\sqrt{2}\,\pi\,\sigma_i^2 P}} \qquad \textbf{(24)}$$

where σ_i is collision diameter for water vapor (2.641×10^{-10} m), and P mean pressure within the membrane pores [33], [114].

For Knudsen mechanism($Kn > 1$), Khayet at al. [113] reported that membrane transfer coefficient can be estimated using equation (25)

$$\boldsymbol{C_{Kn} = \frac{2\,\pi}{3}\,\frac{1}{RT}\left(\frac{8\,RT}{\pi\,M_w}\right)^{0.5}\frac{r^3}{\tau\,\delta}} \qquad \textbf{(25)}$$

where $\tau, \delta, r,$ and M_w are pore tortuosity, membrane thickness, pore radius, and

water vapor molecular weight, respectively. Bouchrit et al. [42] suggested a correlation to evaluate the tortuosity by equation (9).

$$\boldsymbol{\tau = \frac{(2 - \varepsilon)^2}{\varepsilon}} \quad \textbf{(26)}$$

where ε is membrane porosity. For Molecular mechanism($Kn < 0.01$), Alkhudhiri at al. [35] reported that membrane transfer coefficient can be estimated using equation (27).

$$\boldsymbol{C_M = \frac{\pi}{RT}\left(\frac{PD}{P_{air}}\right)^{0.5}\frac{r^2}{\tau\,\delta}} \quad \textbf{(27)}$$

where P, D and P_{air} are the total pressure inside the pore which is equal to the partial pressure of air and water vapor, diffusion coefficient, and the air pressure within the membrane pore, respectively. Phattaranawik et al. [73] reported that the diffusivity of water vapor through the stagnant air inside the pores can be evaluated using equation (28).

$$\boldsymbol{PD = 1.895 \times 10^{-5}\, T^{2.072}} \quad \textbf{(28)}$$

For Transition mechanism($0.01 < Kn < 1$), Khayet at al. [113] reported that membrane transfer coefficient can be estimated using equation (29)

$$\boldsymbol{C_c = \frac{\pi}{RT}\frac{1}{\tau\,\delta}\left[\left(\frac{2}{3}\left(\frac{8\,RT}{\pi\,M_w}\right)^{0.5} r^3\right)^{-1} + \left(\frac{\pi}{RT}\,r^2\right)^{-1}\right]^{-1}} \quad \textbf{(29)}$$

After evaluating membrane transfer coefficient, mass transfer flux (J) can be evaluated according to Darcy's law represented by equation (30). The simplified mass transfer model through porous media is mentioned by Alkhudhiri at al. [35] in equation (31) below. A linear relation between mass transfer flux and membrane transfer coefficient is shown in equation (31).

$$\boldsymbol{J = K\,\Delta P^o} \quad \textbf{(30)}$$

$$J = C_m \Delta P = C_m [P_1 - P_2] \quad (31)$$

where C_m is membrane transfer coefficient, P_1 is the vapor pressure at feed side of membrane and P_2 is the vapor pressure at permeate side of membrane [34], [35], [42], [115]. K is a coefficient that depends on temperature, pressure, composition with the membrane in addition to membrane structure. Vapor pressure at membrane feed and permeate surfaces can be evaluating using Antoine equation (32) [112]. Therefore equation (31) can be rewrite as equation (33) and Clausius-Clapeyron equation (34) can be used to evaluate vapor and temperature relationship [35], [63], [116].

$$p_i = exp\left(23.1964 - \frac{3816.44}{T_{m,i} - 46.13}\right) \quad (32)$$

$$J = C_m \frac{dP}{dT}\left(T_{f,m} - T_{p,m}\right) \quad (33)$$

$$\frac{dP}{dT} = \left[\frac{\Delta H_v}{RT^2}\right] P_o(T) \quad (34)$$

This relation is applicable for temperature difference of 10℃ across the membrane [35], [113], [117]. As ΔP^o is a complex function of temperature at membrane surface, not the bulk solutions. Therefore, iterative process has to be applied in order to evaluate the variables. Several assumptions are proposed by Lawson [41] to provide an analytical solution. The limitation allows this method for very dilute ideal aqueous solutions (e.g. desalination).

Gryta [101] reported that permeate flux in membrane distillation (MD) process as it is shown in equations (25, 27, 29) above, is very sensitive to membrane porosity, pore size, and membrane thickness. Zhang et al. [98] summarizes membrane characteristics that affect mass transfer coefficient in equation (35) below

$$C_{membrane} \propto \frac{r^a \varepsilon}{b \tau} \quad (35)$$

where r, ε, τ, a and b are nominal membrane pore size, membrane porosity, pore

tortuosity, coefficient in a range of (1-2), and membrane thickness.

Other models can be used to determine mass transfer in MD systems. Hitsov et al. [114] reported several models for mass transfer inside the membrane evaluation. These models include: Fick's law model, Dusty gas model, Simplified Dusty gas model, Pore size distribution model, Schofield's model, and other models.

As an example, the Dusty gas model that describes mass transfer across the membrane is evaluated by many researchers [81], [114]. It consists of four mechanisms: viscous flow, Knudsen diffusion, molecular diffusion, and surface diffusion. For DCMD viscous flow and surface diffusion are neglected. Equation (36) demonstrates the general flux in Dusty gas model [111].

$$J = \frac{M_w}{RT}\left[\left(K_o\, v + \frac{B_o\, P_{pore}}{\mu}\right)\frac{P_1 - P_2}{\delta}\right] \quad (36)$$

where v is gas mean molecular speed, K_o and B_o can be evaluated using equations (37,38)

$$K_o = \frac{2\,\varepsilon\, r}{3\,\tau} \quad (37)$$

$$B_o = \frac{\varepsilon\, r^2}{8\,\tau} \quad (38)$$

where r is membrane pore radius [114].

3.5 Temperature Polarization

Temperature Polarization is a significant phenomenon that affects MD performance. As it was mentioned before, the driving force for membrane distillation is temperature difference between the hot feed and cold permeate sides. The temperature polarization phenomena occur when the water evaporate from the hot side through the membrane pores absorbing the heat and leading to cool down the region corresponded to the membrane. As a consequence, a

thermal boundary layer occurs next to the membrane [72] and causes vapor pressure decrease across the membrane [101]. Therefore, permeate flux production is reduced. Figure (29) represents the thermal boundary layer that cause temperature polarization.

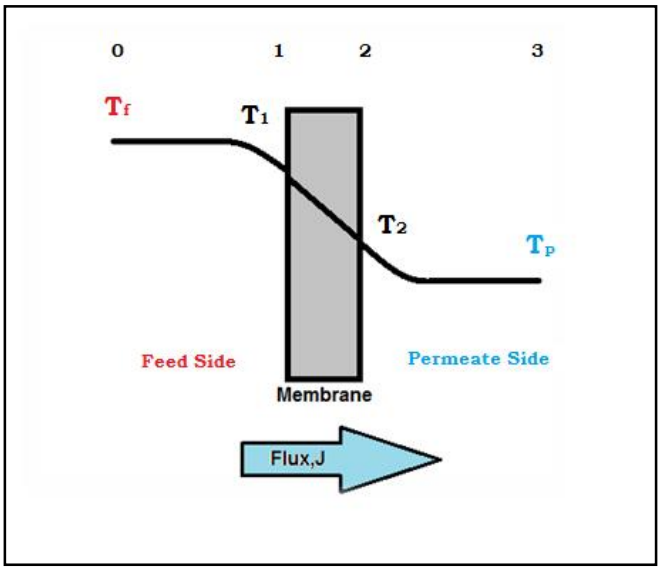

Figure 29: Schematic diagram of temperature polarization

Mathematically, temperature polarization can be quantified as the ratio of the difference of hot and cold bulk temperatures over the difference of hot and cold temperatures close to the membrane. This can be expressed as temperature polarization coefficient (TPC) shown in equation (39). Temperature polarization is also used to describe heat loss effect on MD process efficiency [31].

$$\vartheta = \frac{T_1 - T_2}{T_f - T_p} \tag{39}$$

where ϑ is temperature polarization coefficient, T_1 and T_2 are the hot feed temperature and cold permeate temperature and membrane surface,

respectively. Similar, T_f and T_p are bulk feed temperature and bulk permeate temperature, respectively.

In figure (29), temperature at point **1** is lower than temperature at point **0** from the feed side. Moreover, temperature at point **2** is greater than temperature at point **3**. Therefore, temperature difference across the membrane is reduced causing less vapor pressure difference to occur. As the driving force reduced, less mass transfer (permeate flux) is generated [118]. Temperature polarization coefficient can vary from 0.2 to 0.9 but to achieve higher flux, it should be as close as possible to one [47], [80]. For DCMD, TPC is reported as a value between 0.4 – 0.7 [35], [76]. Ignoring temperature polarization leads to overestimating the mass transfer. Schofield et al. [68] reported that temperature polarization coefficient is found to be 0.6 at 60℃ feed temperature that cause 40% mass transfer overestimation if TPC is not taking into account. Termpiyakul et al. [119] ensured that temperature polarization is more noticeable at high feed concentration, salinity, and low feed flowrate. Bouchrit et al. [42] studied the effects of feed and permeate temperature and flowrate on temperature polarization coefficient. Maintaining feed temperature as high as possible and permeate temperature as low as possible helps to overcome temperature polarization [80]. Different techniques are applied to increase the coefficient such as changing membrane properties and morphology, enhancing flow pattern, increase mixing and operating at high feed velocities [120]. Gryta et al. [102] and other researches [34], [101] mentioned that module design in hollow fiber membrane highly affect temperature polarization coefficient. All these techniques are required to operate in the turbulent system and therefore increase feed heat transfer coefficient. Promoters like mesh spacers are most common used to overcome temperature polarization [68], [90], [99].

3.6 Concentration Polarization

The term of concentration polarization is defined by Alkhudhiri et al. [35] as the rise of solute concentration across membrane surface comparing to bulk solution concentration. As hydrophobic porous membrane is used in DCMD system that permit only water vapor molecules to pass, an accumulation of non-volatile particles near feed membrane surface occurs [36], [99].

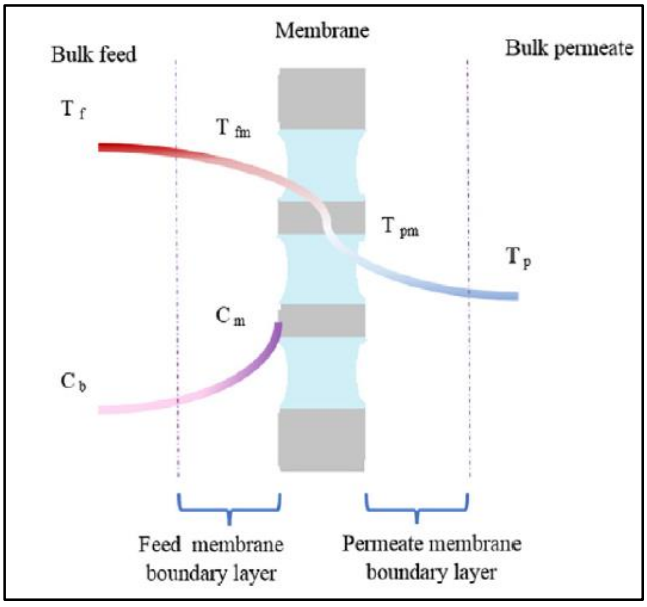

Figure 30: Concentration and Temperature boundary layers in DCMD system (Adapted from [42])

Figure (30) illustrates concentration polarization boundary layer in DCMD system. Concentration polarization coefficient (φ) can be evaluated using equation (40).

$$\varphi = \frac{C_m}{C_f} \tag{40}$$

where C_m is salt concentration on the membrane surface from feed side and C_f is salt concentration in the feed bulk [118]. Martinez-Diez et al. [121] evaluated

a correlation to calculate salt concentration on the feed membrane surface using equation (41).

$$C_m = C_f \, exp\left(\frac{J}{\rho \, K_m}\right) \quad (41)$$

where J is mass flux through membrane, ρ is fluid density, and K is mass transfer coefficient that can be evaluated by equation (42) [42].

$$K_m = \frac{D}{\delta} \quad (42)$$

where D is the molecular diffusion and δ is membrane thickness. Bouchrit et al. [42] reported several methods and correlations to evaluate molecular diffusion thus concentration polarization coefficient. The effect of concentration polarization is studied by different researches [116], [122]. Banat and Simandl [116] conducted in the research that increasing feed concentration from (1 – 10 wt%) cause permeate flux decline by 6%. However, concentration polarization can be ignored when comparing to temperature polarization effect [36], [42], [45]. The main effect of concentration polarization is that it stimulates scaling formation and fouling of the membrane [35], [99].

3.7 Membrane Characteristics

In addition to mass transfer, wetting phenomena, and module configuration, membrane characteristics are highly affecting membrane selection [36]. Membrane distillation was poorly studied in the late 1960 and never commercially employed due to low performance. However, after membrane characteristics were improved, the research about MD started again. Nowadays, MD research is booming to find optimum membrane characteristics that provide highest flux with least drawbacks [58], [123].

Common membrane characteristics [58] that are preferable to be available in MD processes are listed below:

- Low membrane thickness
- Low pore tortuosity

- Low membrane thermal conductivity to minimize conductive heat loss
- Large pore size
- High membrane porosity to maximize water vapor transport
- High membrane hydrophobicity or low surface energy
- High thermal stability that can tolerate as high temperature as 100℃ [33]
- High permeability [45]
- High chemical resistance to feed solutions if other applications than desalination is performed and membrane has to be cleaned [45]

All these characteristics would be explained in details in the section below.

3.7.1 Membrane Porosity

Membrane porosity is identified as the volume of pores divided by the total volume of the membrane [124]. Membrane porosity represents the void fraction of the membrane that indirectly expresses vapor permeability [33]. Membranes with high porosity provide higher flux as evaporation surface is increased and more space is occupied by the vapor in the membrane [33], [36], [125]. Therefore, it was agreed that membranes with high porosity provide high permeate flux [35], [36]. Alkhudhiri et al. [35] mentioned that membrane porosity can be evaluated using Smolder-Franken equation (43). Membrane porosity (ε) is simply determined by measuring membrane material density (ρ_{pol}) using isopropyl alcohol (IPA) that can penetrate membrane pores and measuring membrane density (ρ_m) using pure water that can not penetrate through the pores. This method is applicable for different membranes such flat sheet and hollow fiber membranes [45], [126]. Another process of measuring membrane porosity is proposed by Zhang et al. [58] and Francis et al. [48]. For hollow fiber membrane porosity calculation, a method reported by Hou et al. [125] can be used.

$$\boldsymbol{\varepsilon = 1 - \frac{\rho_m}{\rho_{pol}}} \quad (43)$$

Membrane porosity is also important in term of evaluating heat loss through membrane conduction (h_m) as was represented in equation (44).

$$\boldsymbol{h_m = \varepsilon\, h_{mg} + (1-\varepsilon) h_{ms}} \quad (44)$$

where h_{mg} and h_{ms} are heat transfer coefficients of vapor within membrane pores and membrane material, respectively [36], [41]. Al-Obaidani et al. [105] reported that increasing membrane porosity increases permeate flux production and decreases thermal conductivity of the membrane. Commercial membranes that are used in MD system are having porosity of 75% for PVDF membranes, 70% for PP membranes, and 60% for PTFE membranes [36], [41], [105].

3.7.2 Membrane Pore Size

Membrane pore sizes are ranged from 100 nm to 1 μm according to different MD applications [41], [127]. As pore sizes increase, more permeate flux is produced [128]. However, large membrane pore sizes cause membrane wettability [33], [35], [36], [41]. The optimum membrane pore size as reported by different researchers [52], [129] is between 0.2 and 0.5 μm. Lawson et al. [41] reported that permeate flux (N) is directly affected by pore size according to equation (45).

$$\boldsymbol{N\ \alpha\ \frac{r^{a}\varepsilon}{\delta\,\tau}} \quad \textbf{(45)}$$

where r is mean pore radius of membrane pores, δ is membrane thickness, ε is membrane porosity, τ is membrane tortuosity, and a is a constant (1 for Knudsen diffusion or 2 for viscus flux) [41], [86]. Therefore, mass transfer mechanism is chosen according to membrane pore size. Knudsen diffusion mechanism is applied with small pore size and Knudsen viscous mechanism is applied with large pore size [41], [73].

3.7.3 Pore Size Distribution

The membranes used for MD processes have non-uniform pore size distribution. Therefore, different mass transfer mechanisms are occurring at once [73]. Standard test method is used to determine pore size distribution [124]. Uniform pore size and as narrow as possible distribution is preferable to avoid membrane wetting through maximum pore size [45].

3.7.4 Membrane Material

Membrane material is considered as one of the most important membrane characteristics. Polymeric, hydrophobic, and microporous membranes are encouraged for MD processes [36], [41]. Single-layer or multi-layers hydrophobic membranes can be used [33]. Polytetrafluoroethylene (PTFE), polypropylene (PP), polyethylene (PE), and polyvinylidenedifluoride (PVDF) materials are the most common commercial membranes used for MD processes. [32], [45]. These polymers are preferable due to their low surface tension values and each material is selected based on MD applications. Different methods are used for membrane fabrication such as traditional phase inversion, thermal induced phase separation, and stretching of dense films [41]. MD membranes can be fabricated in laboratories with specific membrane characteristics. Composite membranes that consist of a hydrophobic and a hydrophilic layers or a hydrophobic layer placed between two hydrophilic layers are receiving interest recently [41]. Khayet and Matsuura [45] summarized all the commercial flat sheet and hollow fiber membranes commonly used for MD. Desalination is one of the most studied fields of MD process where plenty of researches are conducted in order to examine different membrane materials. Francis et al. [46] tested four different membrane materials fabricated in the lab to conclude that PVDF membranes generate highest flux.

3.7.5 Membrane thickness

Membrane thickness is significant membrane characteristic that determine flux amount. Permeate flux is inversely proportional with membrane thickness [35], [36]. The thicker the membrane, the less flux is achieved as membrane thickness provides more resistance to mass transfer. However, heat loss through conduction decreases as membrane thickness increases [35]. Therefore, optimum membrane thickness should be chosen. In this case, multi-layered membranes provide high permeate flux by applying hydrophobic layer as thin as possible and low heat transfer by making the overall membrane thickness (hydrophobic and hydrophilic layers) as thick as possible [35]. The optimum membrane thickness is estimated to be 30 – 60 μm [35], [36].

3.7.6 Pore Tortuosity

Pore tortuosity is defined as the actual pores length divided by membrane thickness. Pore tortuosity is measured due to fact that molecules travel larger distance than membrane actual thickness. [49] Therefore, high pore tortuosity leads to low permeate flux [33], [36]. As pore tortuosity is hardly measured, a constant value of ($\tau = 2$) is assumed for water vapor in MD processes [33], [49], [127]. Different correlations are suggested in order to evaluate pore tortuosity (equation 26, 46).

$$\tau = \frac{1}{\varepsilon} \tag{46}$$

where ε is membrane porosity [35], [49], [96].

3.7.7 Thermal Conductivity

Heat conduction through membrane occurs by heat transfer through membrane material and vapor in pores. Conductive heat loss through membrane material is a major drawback in MD system, especially in DCMD. Therefore, membrane material with low thermal conductivity should be chosen. Thermal conductivity of polymer membranes used in MD fall in the same region, approximately with

slight difference. Khayet [33] and other researchers [74], [130], [131] evaluate thermal conductivity for commercial membranes between ($0.04 - 0.06\ Wm^{-1}K^{-1}$). However, thermal conductivity of membrane materials differs according to temperature, degree of crystallinity, and shape of crystals [35], [41] Table (11) summarized thermal conductivities of most common membranes used in MD process. Al-Obaidani et al. [105] reported that (PP) membranes have the lowest thermal conductivity, while (PTFE) is the highest.

Table 11: Thermal conductivity of different materials [35], [36], [86]

Membrane Material	Thermal Conductivity ($Wm^{-1}K^{-1}$)
PP	0.11 – 0.16 (at 23℃), 0.20 (at 75℃)
PVDF	0.17 – 0.19 (at 23℃), 0.21 (at 75℃)
PTFE	0.25 – 0.27 (at 23℃), 0.29 (at 75℃)
Air	0.020 (at 25℃), 0.029 (at 60℃)
Water vapor	0.026 (at 25℃), 0.022 (at 60℃)

Thermal conductivity for PP, PTFE, and PVDF membranes can be estimated using equation (6) mentioned before. [35], [41], [86]

The thermal conductivity of polymeric materials can be calculated using equations (47 – 51) that are valid at temperature range of (0 - 100℃).

$$k^{G}_{water}(T) = 2.72 \times 10^{-3} + 5.71 \times 10^{-5}\, T \quad \textbf{(47)}$$

$$k^{G}_{air}(T) = 2.72 \times 10^{-3} + 7.77 \times 10^{-5}\, T \quad \textbf{(48)}$$

$$k^{M}_{PVDF}(T) = 9.2308 \times 10^{-3} + 5.77 \times 10^{-4}\, T \quad \textbf{(49)}$$

$$k^{M}_{PTFE}(T) = 0.087 + 6 \times 10^{-4}\, T \quad \textbf{(50)}$$

$$k^{M}_{PP}(T) = -0.248 \times 10^{-3} + 1.3 \times 10^{-3} \quad \textbf{(51)}$$

The substituted temperature in equations (47 – 51) should be in K. From the above equation (42), it is shown that thermal conductivity is a function of membrane porosity.

Lawson and Lloyd [41] also reported that PP membranes have the lower thermal conductivity of (0.15 – 0.20 $Wm^{-1}K^{-1}$) while PVDF and PTFE membranes have thermal conductivities of (0.22 – 0.45 $Wm^{-1}K^{-1}$).

In order to reduce heat loss through conduction, several methods are applied rather than using materials with low thermal conductivity. Khayet et al. [33] suggested using high porosity and thicker membranes. High porous membranes have more air trapped in the pores and therefore lower thermal conductivity [35], [36]. Another possible technique to lower thermal conductivity is to use multi-layered membranes. As mentioned before, very thin layer of hydrophobic material and thicker layer of hydrophilic material is suggested. The purpose of using hydrophilic layer is to resist conductive heat, [33] while the hydrophobic is to resist liquid penetration [35].

3.8 Membrane Flow Arrangement

Different membrane flow configurations are studied in order to enhance flux production and reduce fouling phenomena. Counter-current flow, cross-current flow, and co-current flow arrangement can be used in both hollow fiber and flat sheet membranes.

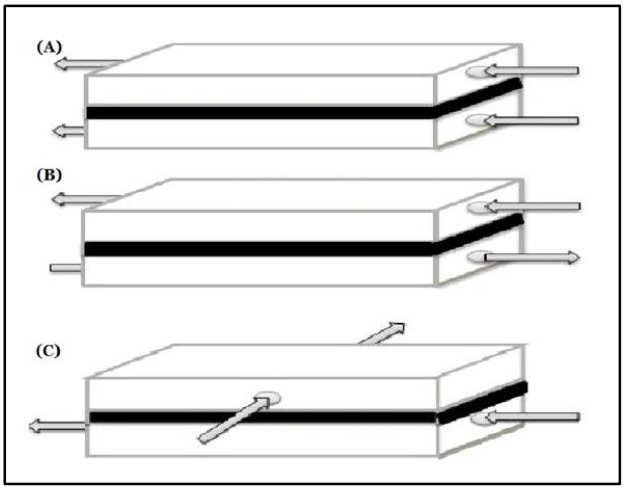

Figure 31: Flow arrangements (A) co-current, (B) counter-current, and (C) cross-current (Adapted from [129])

Figure (31) illustrates different flow arrangements. Different studies [52], [120], [129] conclude the counter-current flow provide slightly high performance in term of flux than co-current flow due to higher turbulence. Manawi et al. [47] showed that counter-current flow result higher flux comparing to co-current flow by approximately 3%. Cross-current flow produces the highest flux among the three arrangements.

More arrangements are applied for hollow fiber membrane in order to enhance the flux and increase membrane life as hollow fiber membranes have higher tendency for fouling [99], [130]. In addition to novel hollow fibers arrangements discussed in **section (3.8)**, placing feed water in the shell side instead of lumen side is recommended to reduce membrane fouling [99], [132]. Gas bubbling is a novel method that is used to control fouling. Chen et al. [103] investigated gas bubbling method through four different arrangements. Figure (32) illustrated these flow arrangements which are 45° inclined, horizontal, upflow vertical, and downflow vertical. According to Chen et al. [103], 45° inclined module produced highest permeate flux.

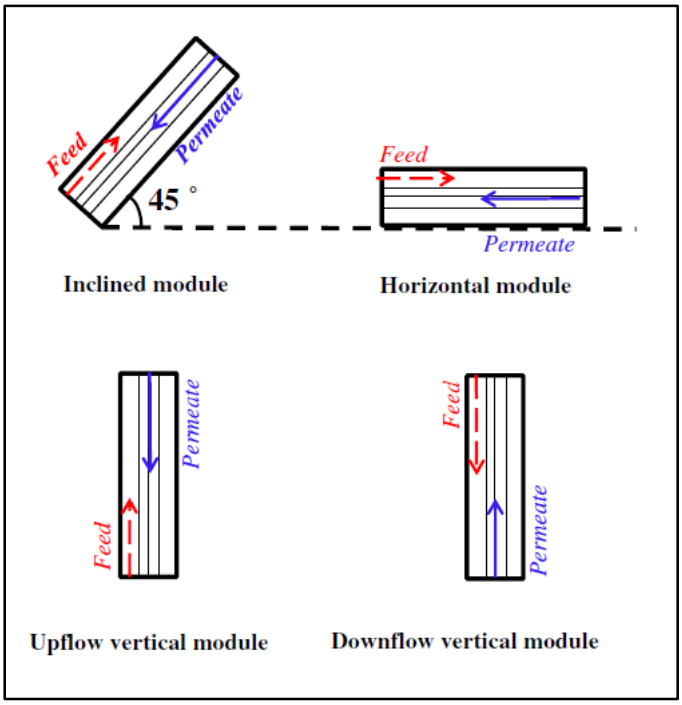

Figure 32: Hollow fiber flow arrangements investigated by Chen et al. [103]

Moreover, different hollow fiber modules such as cylindrical, rectangular, helical, and shell-and-tube bundles are studied by Wickramasinghe et al. [132] showing that better results are achieved through flow outside the fibers.

3.9 Liquid Entry Pressure (LEP)

In membrane distillation (MD) processes, porous hydrophobic membranes are used. Hydrophobic membranes allow vapor molecules to penetrate and prevent liquid from passing through the membrane. Liquid entry pressure (LEP) is particular characteristic of membrane that is defined as minimum pressure that allow feed vapor molecules to penetrate through the membrane. Sometimes LEP is defined as wetting pressure [124]. Overcoming LEP will lead to membrane wetting thus, lowering permeate water quality and declining permeate production [33]. When membrane pores are wetted, saline feed water can penetrate through membrane contaminating permeate side. To overcome

penetration, permeate hydrostatic pressure should be kept higher than feed hydrostatic pressure [41]. LEP can be determined using Laplace-Young (Cantor) equation [35], [36], [41], [58], [80]. represented by equation (52).

$$\Delta \boldsymbol{P} = \boldsymbol{P_f} - \boldsymbol{P_p} = \frac{-2\, \boldsymbol{B\gamma_l} \cos \boldsymbol{\theta}}{\boldsymbol{r_{max}}} \quad \textbf{(52)}$$

where P_f is hydraulic pressure on feed side and P_p is hydraulic pressure on permeate side. B, γ_l, θ and r_{max} are geometric pore coefficient ($B = 1$ for cylindrical pores), liquid surface tension, contact angle between solution and membrane surface, and maximum pore size radius, respectively. According to equation (52), LEP depends on membrane hydrophobicity and pore size. [35], [42] LEP should be maintained as high as possible by choosing highly hydrophobic membranes (large contact angle between solution and membrane surface), small maximum pore size, low surface energy, and high liquid surface tension [33], [35], [36]. However, small pore size decreases membrane permeability [33].

Table 12: Liquid Entry Pressure at different mean pore size

Material	Mean pore size (μm)	LEP (kPa)
PTFE/PP	0.20	282
	0.45	138
	1.00	48

Banat et al. [116] suggested membrane pore size of (0.1 – 0.6 μm) to prevent pore wetting. Alkhudhiri et al. [35] mentioned that for same membrane material (PTFE/PP), LEP is affected by membrane pore size. Table (12) listed Liquid Entry Pressure (LEP) at different mean pore size.

3.10 Contact angle (θ)

Contact angle is used to describe membrane hydrophobicity. Liquid entry pressure (LEP) and Contact angle ($\boldsymbol{\theta}$) are related to each other. Low contact angle (low membrane hydrophobicity) decreases LEP, hence membrane wetting occur. Therefore, membrane wetting can be directly measured by contact angle.

The contact angle of water droplet on different membrane surfaces is listed by Alkhudhiri et al. [35] in table (13) below.

Table 13: Contact angle ($\boldsymbol{\theta}$) of different membrane materials [27]

Membrane material	Contact angle (θ)
PTFE (Teflon)	$108^{\circ} – 115^{\circ}$
PVDF	107°
PP	120°
Fabricated Ceramic membrane	$177^{\circ} – 179^{\circ}$

Figure (33) explains the relation between the contact angle and the hydrophobicity of the membrane. If a drop of liquid is spread on membrane surface and the contact angle is given between (0° - 90°), that's mean that the membrane is hydrophilic and the liquid can pass the membrane. Wetting happen when contact angle is close to 0° [36].

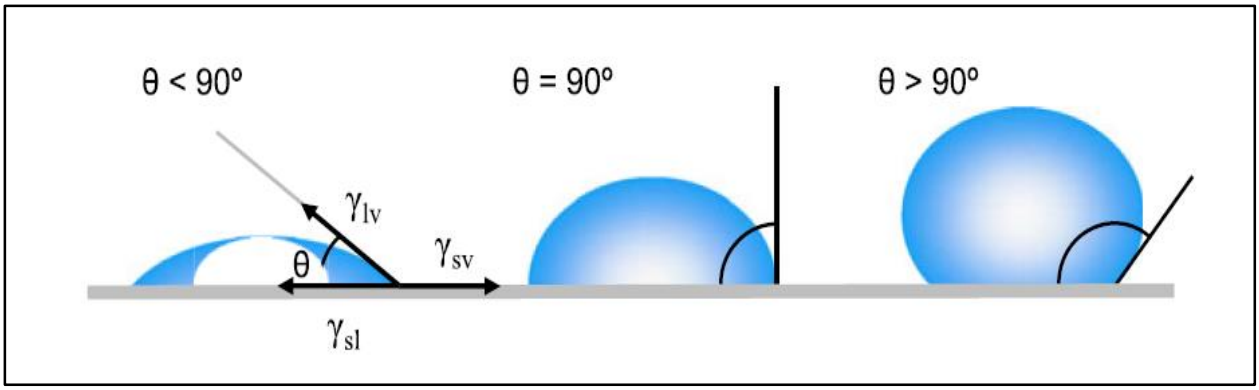

Figure 33: Contact angle identification of membrane hydrophobicity

If the contact angle is given between (90° - 180°), that's mean that the membrane is hydrophobic and the droplet can not penetrate the membrane [36]. Contact angle can be estimated by Young's equation (53) below:

$$\gamma_{lv} \cos\theta = \gamma_{sv} - \gamma_{sl} \tag{53}$$

where γ_{sv} is solid-vapor interfacial tension, γ_{sl} is solid-liquid interfacial tension, and γ_{lv} is liquid-vapor interfacial tension.

3.11 Pressure Drop (ΔP)

Pressure drop (ΔP) and liquid entry pressure (LEP) are two important concepts in MD process. Pressure drop along the module is a natural phenomenon that occurs in flow channels. It can be defined as the minimum pressure that is maintained at channel entrance to ensure fluid flow. [80] Cath et al. [80] expressed the pressure drop in equation (54).

$$\Delta P = f \frac{L}{d} \rho \frac{u^2}{2} \tag{54}$$

where $f, L, d, u,$ and ρ are friction factor, channel length, hydraulic diameter of flow channel, fluid velocity, and fluid density, respectively.

Pressure drop should always maintain a value lower than liquid entry pressure to avoid membrane wetting. Hitsov et al. [114] reported that the best performance of permeate flux is achieved at lowest pressure drop.

3.12 Flow Turbulence and Flow Distribution

Flow turbulence is an important parameter in MD system that improve membrane characteristics. It can enhance permeate flux production by increasing the vapor pressure across the membrane [75], [133]. Increasing thermal coefficients is directly affecting permeate flux production. Phattaranawik et al. [75] mentioned that heat transferred from hot feed solution across the thermal boundary layer to the membrane surface at a rate of $q_f{}^m + q_f$ can be evaluated using equation (55, 56).

$$\boldsymbol{q_f = h_f\left(T_f - T_1\right)} \quad \textbf{(55)}$$

$$\boldsymbol{q_f{}^m = J\, H_{l,f}\left(\frac{1}{2}\left(T_f - T_1\right)\right)} \quad \textbf{(56)}$$

where $H_{l,f}$ is the enthalpy of the feed solution, J is mass flux, h_f is heat transfer coefficient of feed solution, T_f is feed bulk temperature, and T_1 is temperature at membrane surface of feed.

In order to enhance the heat transfer coefficient of feed solution, the thickness of boundary layer should be reduced. This can be achieved by enhancing flow turbulence in feed side and permeate sides. Several techniques can be applied such as improving flow configuration, changing membrane arrangement, and the usage of turbulent promoters (spacers) to increase turbulence of the flow. As explained before in **section (3.3**), spacers, baffles, and membrane arrangements showed significant improvements of heat transfer coefficient by lowering temperature polarization. Tamburini et al. [134] mentioned that temperature polarization coefficient is ranging between 0.57 – 0.76 for channels without spacers, while temperature polarization coefficient is ranging between 0.90 – 0.97 for spacer-filled channels. Additionally, placing the spacer on hot feed side

shows more effect than placing it on the cold permeate side. Phattaranawik et al. [76] by (30 – 40 %). Moreover, turbulence and better mixing can be achieved by finding the optimum operating conditions. Lawson et al. [41] and other researchers [2], [36], [40], [105], [135], [136] reported that increasing process flowrates improve the mixing, hence decrease temperature boundary layers. High flowrates decrease temperature difference between bulk and near the membrane, hence temperature boundary layer decreases [86]. However, very high feed and permeate flowrates decrease the amount of resulted permeate flux [100], [109] and consume pumping energy [136].

3.13 Drinking Water Quality

The quality of water depends on the characteristics and purity of water. As mentioned before in **Chapter 2**, the quality of water is measured by its salinity level. Salinity level and other characterizations of seawater were discussed before in details in **Chapter 2**. Standards of safe drinking water and its quality are established by several agencies such as Environmental Protection Agency (EPA) in USA and European Drinking Water Directive. The World Health Organization (WHO) is limited the drinking water by 0.5 ppt [3]. The quality of drinking water in Qatar is established by KAHRAMA and the main parameters are listed in the table (14). Water Quality of Rayyan production company of drinking water in Qatar is also represented in table (14) showing high quality of water.

Table 14: The quality of drinking water in Qatar [137]

Composition	Guide level (mg/L)	Maximum level (mg/L)	Concentration level (mg/L)
TDS	200 – 600	1,000	104
Alkalinity	30	---	---
Total Hardness	60	500	52
Chloride	25	250	32
Chloride Residuals	0.2	0.5	---
Fluoride	0.7	1.5	< 1
Sulphate	25	250	7
Calcium	100	---	13
Copper	1	2	---
Sodium	20	200	6
Iron	0.3	2	---
Manganese	0.1	0.5	---
Magnesium	30	50	5
Aluminum	0.05	0.2	---
Nitrate	25	50	---
pH	6.5 – 8.5	9.5	7.2

In order to evaluate the quality of desalinated water in MD systems, several analyses are conducted such as the measure of anions and cations, electrical conductivity, and salt rejection percentage.

3.13.1 Membrane Salt Rejection

Salt rejection percentage is a relative measure of the amount of salts that was initially present in the water and retained by the membrane. Salt rejection percentage ($\boldsymbol{Y}$) can be evaluated through equation (57) reported by Khayet [33].

$$\boldsymbol{Y = \frac{C_f - C_p}{C_f} \times 100} \qquad \textbf{(57)}$$

where C_f and C_p are salt concentration or TDS, initially in the feed and in the permeate, respectively.

Salt rejection is important parameter in RO membranes. However, not all the ions are rejected equally. The higher the ion, the better the rejection is. It is also

important to note that RO membranes don't reject gases. Therefore, gasses such as ammonia, chlorine gas, carbon dioxide, and oxygen can be present in permeate water. Some of these gasses can be rejected after pH adjustments [45].
In membrane desalination technologies, Nanofiltration membranes usually reject less than 30% of TDS comparing to Reverse Osmosis membranes that reject more than 90% of TDS. Most commercial RO membranes achieve high salt rejection percentage in the range of (99.60 – 99.85%) [45].
Singh and Sirkar [138] evaluated salt rejection for different hollow fiber membrane materials (PP, PVDF) finding that PP membranes provide higher salt rejection percentage than PVDF membranes.
Zhang et al. [98] reported that the implementation of hollow fiber membranes in DCMD systems provide high salt rejection that is higher than 99%. Similar results are achieved by Macedonio et al. [89] investigating PVDF and PP hollow fiber membranes in DCMD systems in oilfield produced water treatment. Moreover, carbon rejection more than 90% is accomplished.

Even higher salt rejection of 99.8% is achieved by Tang et al. [139] who investigated PVDF hollow fiber membranes in VMD system using aqueous NaCl solution as hot feed inlet. Alike results of 99.9% of salt rejection are reported by Cath et al. [80] using three different PTFE and PP hydrophobic flat sheet membranes with synthetic seawater at feed solution of 40℃. Vacuum enhanced DCMD system is responsible for high performance of permeate flux and salt rejection. As high as 99.95% salt rejection is performed by Maab et al. [51] and Khayet et al. [140] for hollow fiber and flat sheet membranes, respectively.
The highest salt rejection is achieved by Francis et al. [46] who studied the performance of PVDF, PP, PTFE, and PVC hollow fiber membranes in DCMD system. Salt rejection of 99.99% was achieved. Similar results performed by Francis et al. [48] for the desalination of Red sea water by using PTFE and PP flat sheet membranes in DCMD system. Additionally, boron rejection of 99.41% is achieved at extreme operating conditions.

Chapter 4: Approach and Methodology

This chapter discusses the methodology of conducting Direct Contact Membrane Distillation (DCMD) system in a Lab scale for hollow fiber and flat sheet membranes. In the experimental section, all the used equipment and devices are described in details representing their main functions. After completing the experimental part and evaluating the permeate flux for both membranes, a comparison of performance between the membranes is conducted according to different thermal coefficients. The used approach of calculating these thermal coefficients is presented in the last section of this chapter.

4.1 Experimental Part (Methodology)

In this section, the experimental procedure and set-up will be explained in details including the explanation and the function of each equipment. The specifications of the used membranes are presented in addition to the algorithm of conducting DCMD experiments. The methodology of DCMD process is followed by the experimental procedure and end up with water quality tests of the resulted permeate water.

4.1.1 Qatar University Laboratory

This research work was processed in the chemical engineering research laboratory (I 216) in Qatar University. Figure (34) pictured the Lab (I 216) from inside at Qatar University where all the experiments were conducted.

Figure 34: Chemical Engineering Laboratory (I 216) Qatar University

All the experiments are performed in a lab scale using Direct Contact Membrane Distillation (DCMD) apparatus.

4.1.2 Experimental Set-up

The experimental set-up of the DCMD system will be will be summarized and explained in three main sections which are:

- DCMD bench scale system
- The used membranes (Flat sheet and Hollow fiber)
- Flat Sheet Membrane Compartment
- The Auxiliary equipment

A brief introduction and a short description of each equipment and device will be present, illustrating the devices in a figure and listing the most important specifications.

4.2 DCMD Bench Scale System

Direct Contact Membrane Distillation (DCMD) apparatus is a combination of different parts and devices that together represent a DCMD system. The schematic diagram of DCMD system in figure (35) represents all the instruments that involve in DCMD system. These instruments are:

- Membrane cell (flat sheet and hollow fiber)
- Heating and cooling circulators
- Feed and distillate tanks
- Feed and distillate balances
- Pumps
- Temperature probes and display
- Pressure transducers and display
- Flow meters and display
- Data Acquisition System

The process of DCMD Bench Scale System is explained through figure (35) and figure (36). Figure (36) represents DCMD Bench Scale set-up in Qatar University Laboratory (I 216).

The process of DCMD systems starts with adjusting the peristaltic pumps to the required flowrates and setting-up the temperatures of cooling and heating circulators. Feed tank is filled with 5 Liters of seawater and the distilled tank is filled with 2.5 Liters of Deionized water. After the temperatures reached the set-points, the valves of the distilled and feed tanks are opened to let the water circulate through pumps. Hot feed seawater is pumped from feed tank to the heating circulator by pump. The water is passed through flexible polymeric tubing. Temperature sensor is measuring the temperature of feed water just before MD cell. When the water reaches the desired temperature, feed flow is entering membrane compartment to face the membrane. After the MD process in the compartment, feed water with the rejected brine is recycled to feed tank. Permeate water is added to the distilled flow. Similar path of feed water, distilled water is taken. Distilled water is flowing through flexible tubing by another pump

from distilled tank to cooling circulator. Temperature sensor is measuring the temperature of distilled water just before MD cell. When the water reaches the desired temperature, distilled flow is entering membrane compartment to face the membrane. Distilled water is combined with the permeate and recirculated back to the distilled tank. Therefore, the weight of distilled tank is increasing and the weight of feed tank is decreasing. Each experiment runs for 4 hours approximately in stable operating conditions. After that, two sample bottles are filled with permeate water to undergo water quality tests. Conductivity of the brine is measured. The system is shut down and refills with distilled water as feed and permeate solutions. The system nearly runs for an hour at same operating conditions to rinse and flush the membrane from deposited particles. This process is called flushing and it is done at the end of each experiment.

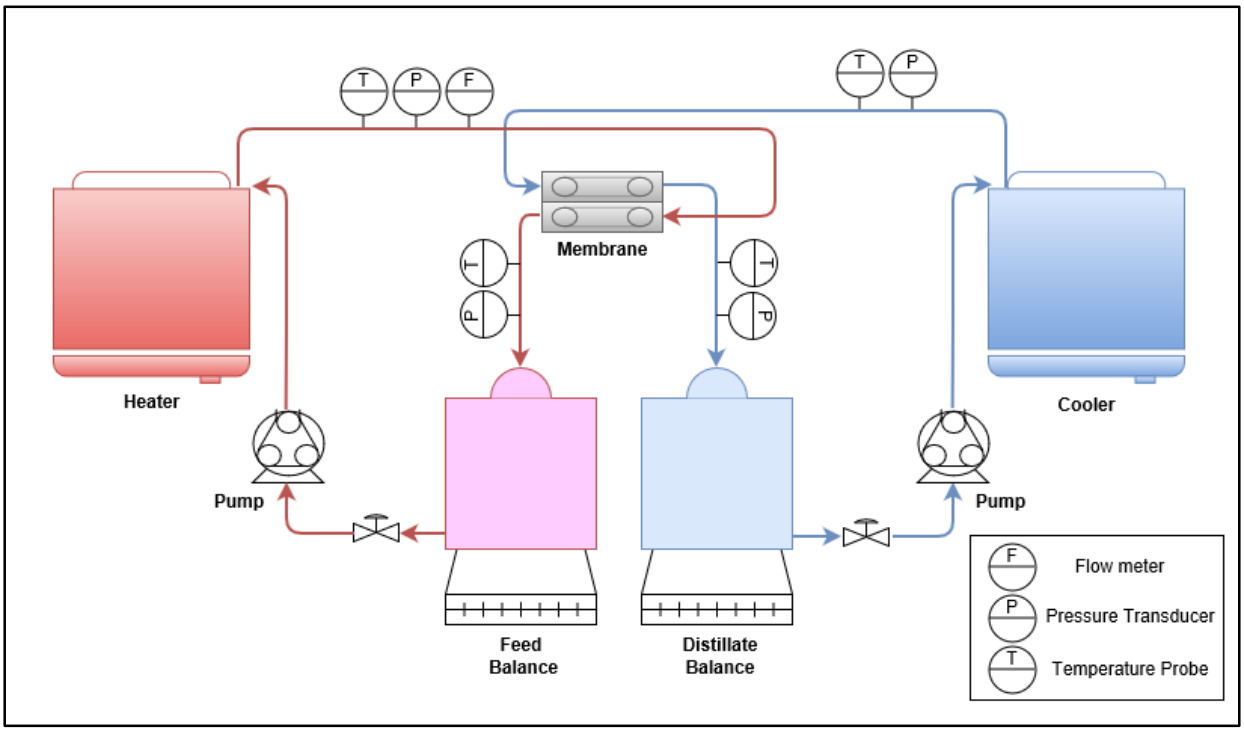

Figure 35: Schematic Diagram of DCMD Bench Scale System

The weight of permeate is continuously measured using permeate balance that hold the distilled tank. As distillation process carry on, more permeate is collected thus, distilled weight is increased. At the beginning, the initial weight of distilled tank with deionized water is measured. After that, the weight of distilled with the added permeate is recorded every 30 seconds with the help of Data Acquisition system (DAQ). DAQ analyzes the signals that collected from the sensors and sent them to the computer. Distilled weight data is saved as text files and processed in the Microsoft Excel program in order to generate permeate flux graphs.

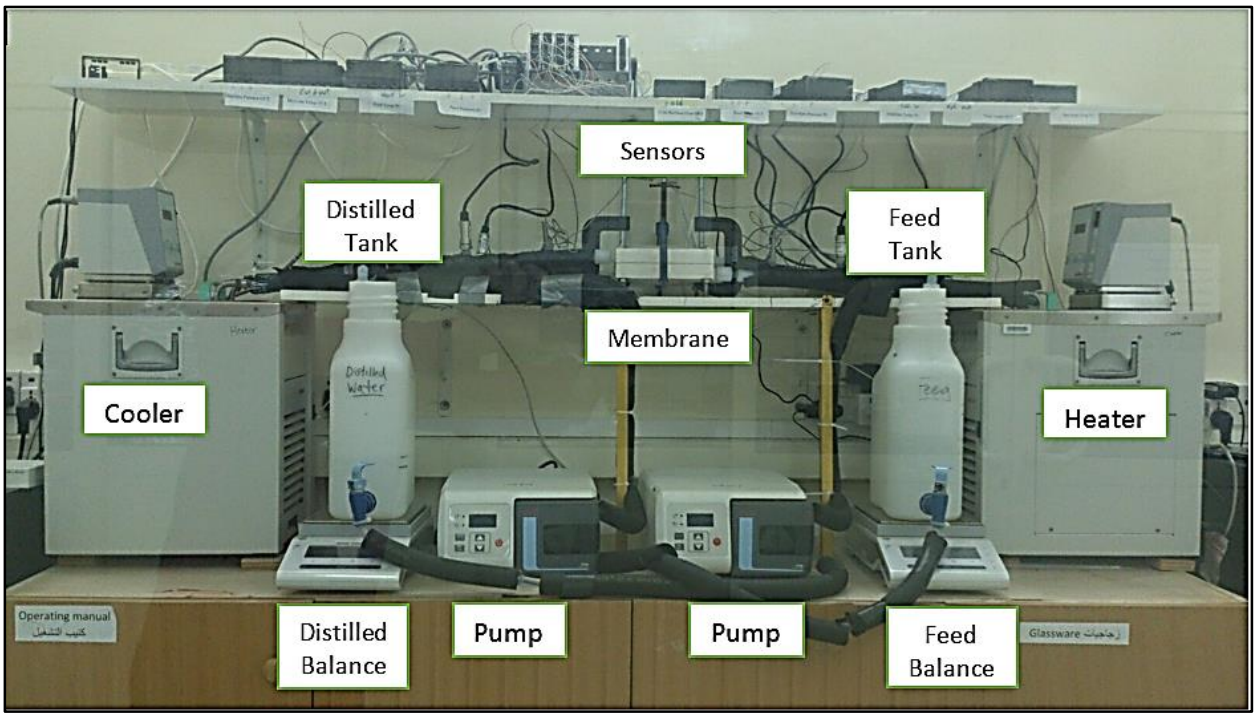

Figure 36: DCMD Bench Scale System in Qatar University Laboratory

Temperature, pressure, and the flowrate of feed and distilled streams are contentiously measured during the whole experiment. The sensors are placed on

the streams before entering the membrane compartment and after exiting the compartment. They are measured to ensure experimental stable mode. Temperature profile of feed and distilled inlet and outlet streams to MD cell is studied. Continues measurement of feed and permeate temperatures is very important for hollow fiber membrane case as it was noticed that the permeate temperature is highly affected by membrane configuration. Conductivity and pH of feed water and permeate are measured to study the quality of water and to calculate salt rejection. Total Dissolved Solids (TDS) of resulted permeate is also measured.

4.3 Feed Solution

In this research, real saline water is used for Direct Contact Membrane Distillation (DCMD) system. Seawater is collected from open intake of Arabian Gulf from Al-Wakraa coastline.

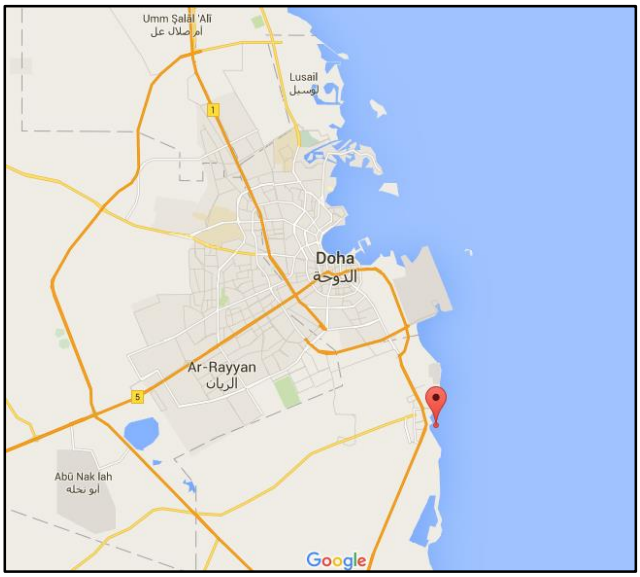

Figure 37: Location of seawater collecting on Al-Wakraa coastline

Gulf seawater is characterized as high saline water with an electrical conductivity of 65 $\mu S/cm$ approximately. pH of the used seawater is around 8. Figure (37) identifies the location of used seawater collection.

4.4 Membrane

Two different types of membranes are used in this study to compare their performance at similar operating conditions. These membranes are Polypropylene (PP) flat sheet membrane and Polypropylene (PP) hollow fiber membrane. These types of membrane materials were chosen according to their availability in the market, low cost, and popularity in the literature. Characteristics and properties of each membrane will be explained in details in the sections below.

4.4.1 Flat Sheet Membrane

In these experiments, flat sheet membranes (Accurel PP 2E HF (R/P)) that are purchased from MEMBRANA Company in Germany and used. The hydrophobic (water resistant) flat sheet membranes are made of Polypropylene (PP) and have intended use in microfiltration. An advantage of (PP) membranes is having lower thermal conductivity (k) that lies between (0.15 – 0.25 W/m.K) comparing to other commercial membranes that have higher thermal conductivities [32], [33]. This will reduce heat lost through membrane by conduction. The porosity of used flat sheet membrane is ranged between 73% to 75% and the average pore size is 0.2 μm. The thickness of one membrane sheet is 170 μm.

The used flat sheet membrane was 19.2 cm in length and 14.1 cm in width with an active membrane area of 0.014 m^2. A hammer and a special steel-rule die are used to cut the membrane with the specific dimensions that will fit in the comportment.

Figure (38) represents two flat sheet membranes used in the experiments. Cutting instruments are also purchased from Sterlitech to avoid membrane surface roughness occur while using basic cutting instruments.

Figure (38) represents two flat sheet membranes used in the experiments. Cutting instruments are also purchased from Sterlitech to avoid membrane surface roughness occur while using basic cutting instruments.

Figure 38: Two sheets of PP flat sheet membranes

Figure (39) represents these instruments that used to cut the membrane. After cutting the membrane, it has to be fitted in between two special membrane compartments (cells) for flat sheet membrane distillation in order to process the experiment.

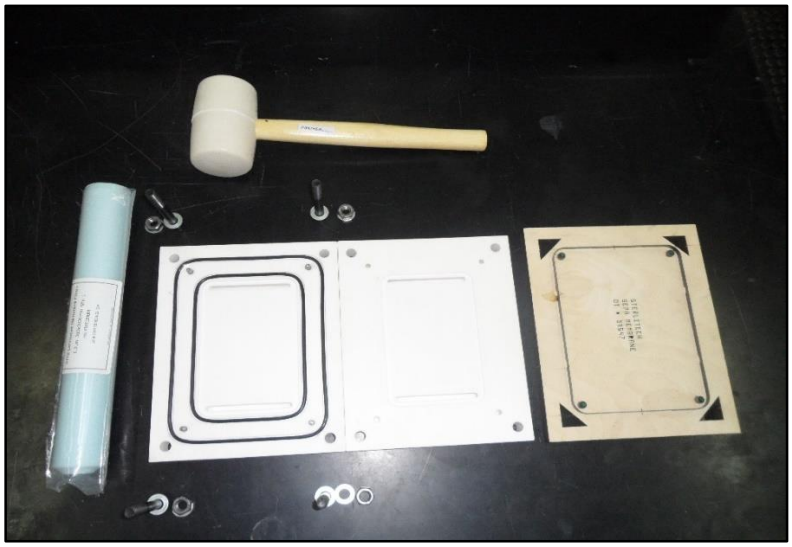

Figure 39: Cutting instruments used to cut flat sheet membrane

The characteristics of flat sheet membrane are summarized in table (15) below.

Table 15: PP Flat Sheet Membrane Characteristics

PP Flat Sheet Membrane	
Manufacture	MEMBRANA
Material	Polypropylene (PP)
Membrane Thickness (μm)	170
Membrane Length (cm)	19.2
Membrane Width (cm)	14.1
Average Pore Size (μm)	0.2
Porosity (%)	73 – 75
Membrane Active Area (m^2)	0.014
Contact Angle (°)	134.8

The measurement of contact angle of PP flat sheet membrane is adapted from Mashael Al-Obaidli [141] thesis project research measured in the same laboratory using drop shape analyzer (DSA25, KRUSS, Germany). The measured

contact angle of PP membrane with 0.2 μm pore size ranged between 131.1° and 137.8 ° with an average contact angle of 134.8°.

4.4.2 Membrane Compartment

In order to process membrane distillation process with flat sheet membrane, the membrane has to be placed between two compartments. the compartments were designed at Qatar University in association with ConocoPhillips GWSC and machined in a workshop in Hong Kong. The compartments are manufactured according to the design from solid Polytetrafluoroethylene PTFE (Teflon). Teflon material for the blocks was chosen in order to minimize heat loss through the blocks by conduction as it has low thermal conductivity. Teflon material is also corrosion resistance as seawater is used at high temperature.

The MD compartment consists from two rectangular blocks (upper and lower plates), feed and permeate channels and O-rings.

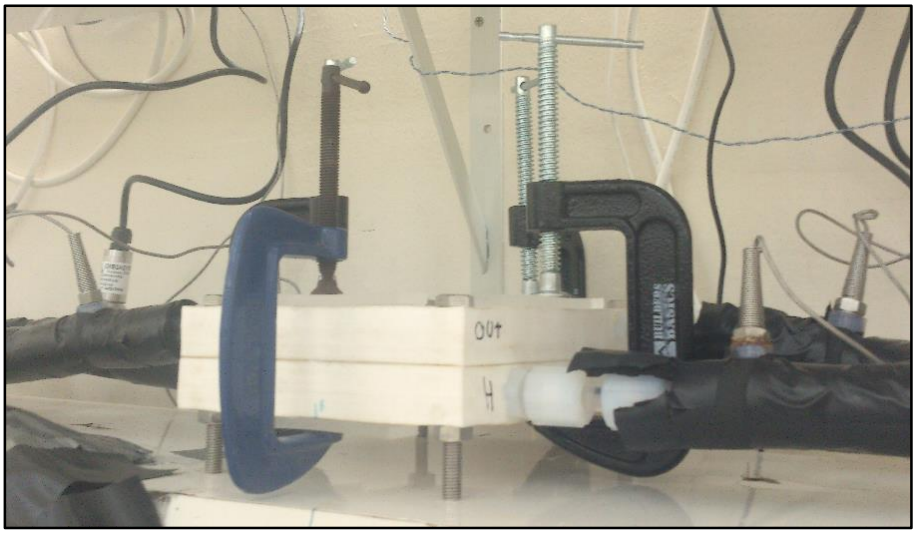

Figure 40: Membrane Compartment with C-Clamps used in DCMD system

Figure (40) represents the used membrane cell in DCMD system with the C-Clamps holders along the cell membrane.

4.4.3 Dimensions

One cell compartment has overall dimensions of 233 x 182.8 x 30 mm. For the whole compartment (two plates together), the dimensions are 233 x 182.8 x 60 mm. Figure (41) illustrates the upper and lower blocks of the compartment with the dimensions in mm.

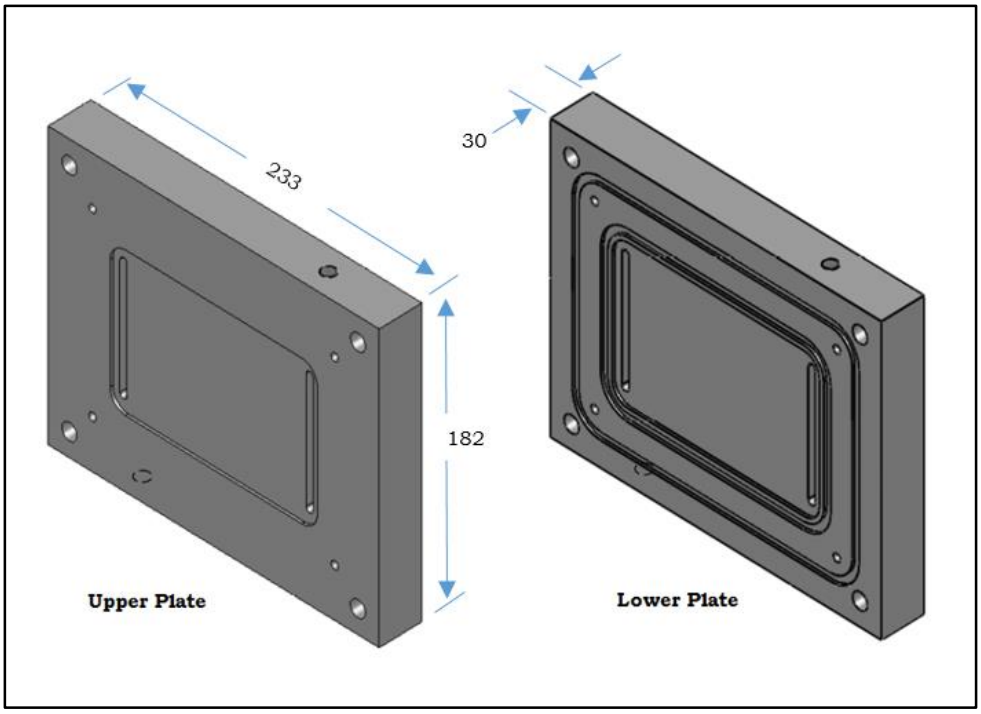

Figure 41: Schematic diagram of upper and lower plates of MD compartment (dimensions in mm)

As shown in figure (41) each plate is 23.3 cm in length, 18.2 cm in width and 3.0 cm for the thickness. More detailed graphical drawings of compartment cells with all the dimensions are represented in **APPENDIX C**.

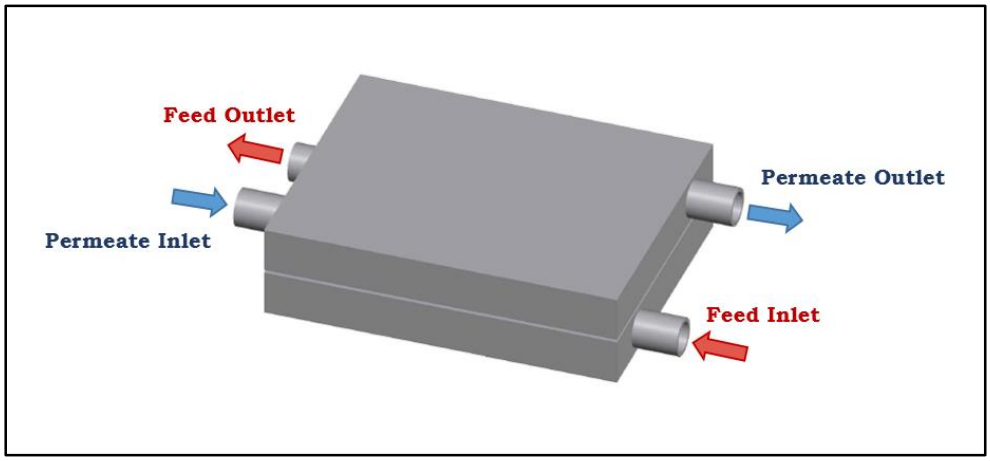

Figure 42: Feed and Permeate Inlet and Outlet streams in MD system

Membrane Distillation (MD) compartment can easily rearranged for concurrent or counter-current flows. For our experiments, counter-current configuration is used for feed and permeate flows. Hot feed flow is passing through the bottom plate reaching the membrane while the permeate cold flow is passing through the top plate. It is chosen to pass saline water through the lower cell in order to avoid salt precipitation on membrane surface that can happen if saline water have been processing through upper cell.

Figure (42) illustrates inlet and outlet streams of feed and distilled water in/out membrane compartment.

4.4.4 Membrane Installation

After the membrane have been cut into the proper rectangular size, it is installed in the inner side of the bottom plate. PP flat sheet has two different surfaces, the shiny face and the dull face. When placing the membrane on the bottom block, the shiny side has to face feed saline water where the dull side should face the distilled water. The membrane is placed on the bottom plate O-ring, just over the spacer. Bottom O-rings are made of two layers of double Viton material to provide a leak-proof seal. O-rings are supplied by Sterlitech and are very significant in

the compartment as its function is to prevent feed seawater to mix with the permeate flow in the upper plate. These two O-ring with a diameter of 75 mm is placed into the particulate space with 2 mm depth provided in the bottom cell. In order to fix membrane sheet on the bottom plate and prevent movement, four guide-pins are used along the bottom plate corners. Each membrane hole is placed over one guide-pin. All the components; membrane, spacer, lower and upper blocks are tightly fixed using four pieces of Allen screw bolt and nuts. Washers are used between the blocks and Allen screw bolt and nuts from both sides of compartment for better fixation due to the slippery nature of Teflon material. It also distributes the load across the plate and provides better fixation of the screws. C Clamp Holders are used for additional fixation of the cells.

Two inlet tubes and two outlet tubes are connected to the compartment from the upper and lower blocks. The used tubes are 3/8-inch female national pipe thread (FNPT) that are fixed with National Pipe Thread (NPT) that prevent fluid from seeking out at connections. Figure (43) represents all the components of flat sheet membrane compartment.

Figure (44) illustrates the sequence of flat sheet membrane installation into the compartment with the spacer.

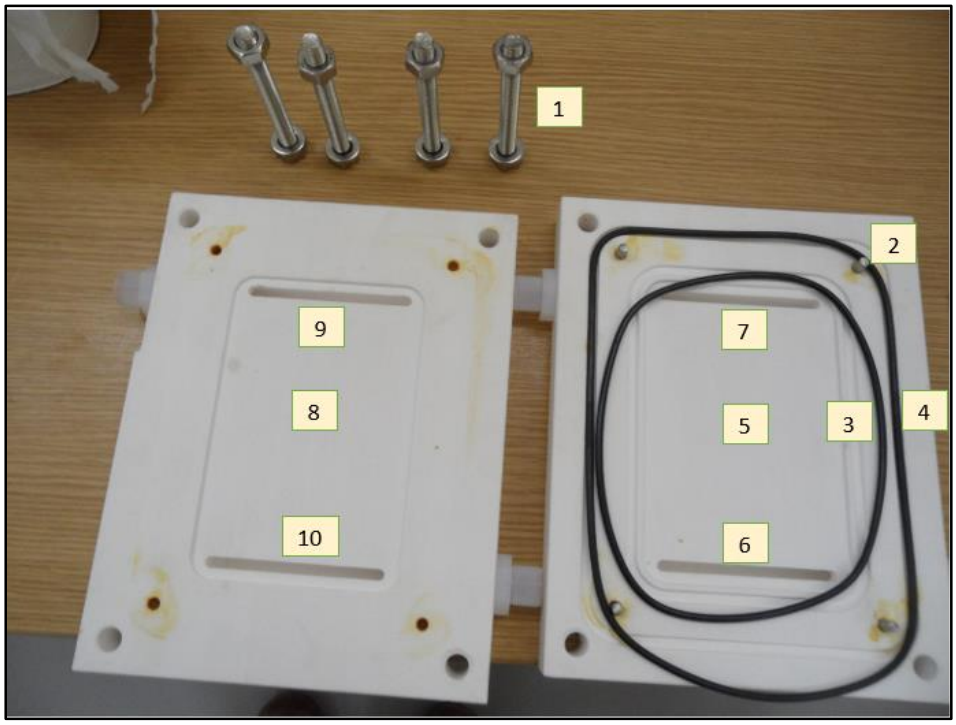

Figure 43: The inner side of the upper and lower plates of membrane compartment

1: Allen Screw Bolts and Nuts

2: Guide Pin

3: Inner O-ring

4: Outer O-ring

5: Membrane Cavity (Feed manifold)

6: Feed Inlet Port

7: Feed Outlet Port

8: Membrane Cavity (Distilled manifold)

9: Distilled Inlet Port

10: Distilled Outlet Port

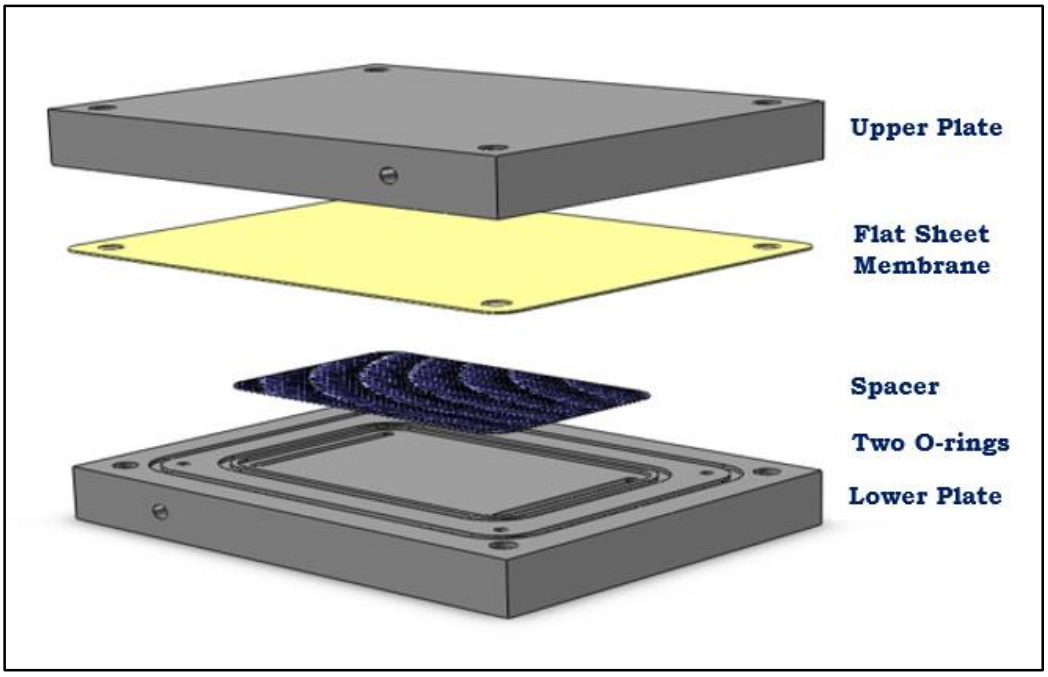

Figure 44: The order of placing the spacer and the membrane in the compartment

It is recommended to place the spacer between the membrane sheet and the feed water to increase the turbulence and decrease the boundary layer.

4.4.5 Fluid Mechanism

The flow in membrane distillation (MD) system is facing counter-current configuration. Hot feed stream is entering the compartment from **feed inlet port** in the bottom cell. Feed stream is passing inside the compartment through the first manifold over the membrane cavity and exiting from the other manifold in the other side of the cell. Feed stream is leaving the compartment from the **feed outlet port** in the lower plate. Inside the membrane cavity, feed stream is passing along the spacer and membrane surface. While the feed stream is passing from one port to another, vapor molecules are keep permeating through the membrane and collecting in the membrane cavity through manifold of upper cell. The remaining feed water with the rejected brine is passing through the

opposite feed port in the lower plate to be pumped back to the heater. Same mechanism is applied for the upper cell where distilled cold water is entering from **permeate inlet port** into the compartment to pass through the manifold. In the membrane cavity, distilled water is mixed with the permeate to leave the upper plate from the manifold on the other side of the plate. The permeate water is passing out through **permeate outlet port** to be cooled down and sent back to the tank. The design of the inlet and outlet ports allocated in opposite directions to ensure the total circulation of water lengthwise the membrane surface.

4.4.6 Material of Construction

Membrane compartment components including MD cells, O-rings, and inlet and outlet fittings are made of different materials. As it was mentioned before, the construction material of membrane compartment is Polytetrafluoroethylene PTFE, commercial name (Teflon). Teflon have been chosen based on several advantages that this material has. First of all, Teflon is a high resistance material that isolates the system and prevent heat transfer through conduction. Because of this Teflon is considered as very good isolating material. It also resists to many chemicals. Another important advantage is that (PTFE) is not a sticky material that offers a very smooth MD process with low friction coefficient. Another advantages of Teflon material are:

- Non wetting material (high hydrophobicity)
- The ability to perform at extreme temperatures (-24 – 260 ℃)
- Ultra Violet (UV) and weather resistance

Two O-rings are made of double synthetic fluorocarbon rubber (Viton) with a diameter of 2 mm and placed in the inner side of lower plate. Viton material is preferable due to its leak-proof property in addition to many other advantages such as:

- Excellent resistance to high temperatures, solvents and many chemicals

- The ability to perform at extreme temperatures (-26 – 204 ℃)
- Low permeability
- Compression set resistance [142]

Last of all, the inlet and outlet fittings to the compartment are made of PFA (Perfluoroalkoxy) Teflon nuts and ETFE (Ethylene tetrafluoroethylene) body (Parker, USA). These fittings are chosen due to their high resistance to many solvents and chemicals in addition to the ability to perform at extreme temperatures (up to 200 ℃) and pressure (100 psi).

4.4.7 Spacer Characteristics

Spacers are used in Direct Contact Membrane Distillation (DCMD) systems to enhance the flow for maximum permeate flux production. Spacer's main function is to distribute feed water along the membrane for maximum contact with the membrane. It also protects the membrane from the hydraulic pressure affected the membrane from feed and permeate sides. Polypropylene (PP) High Foulant spacer was introduces to the system with 14.5 cm in length, 9.7 cm width, and 0.156 cm thickness supplied by Sterlitech (USA). Characteristics of the used spacer are listed in table (16) below.

Table 16: PP Spacer Characteristics

Spacer Characteristics	
Material	Polypropylene (PP)
Length (mm)	145
Width (mm)	97
Thickness (mm)	1.56
Filament size (mm)	0.78
Mesh size (mm)	3.23
Hydrodynamic angle	90
Voidage (%)	80 – 85

Figure (45) represents the real Polypropylene (PP) spacer used in flat sheet membrane distillation system.

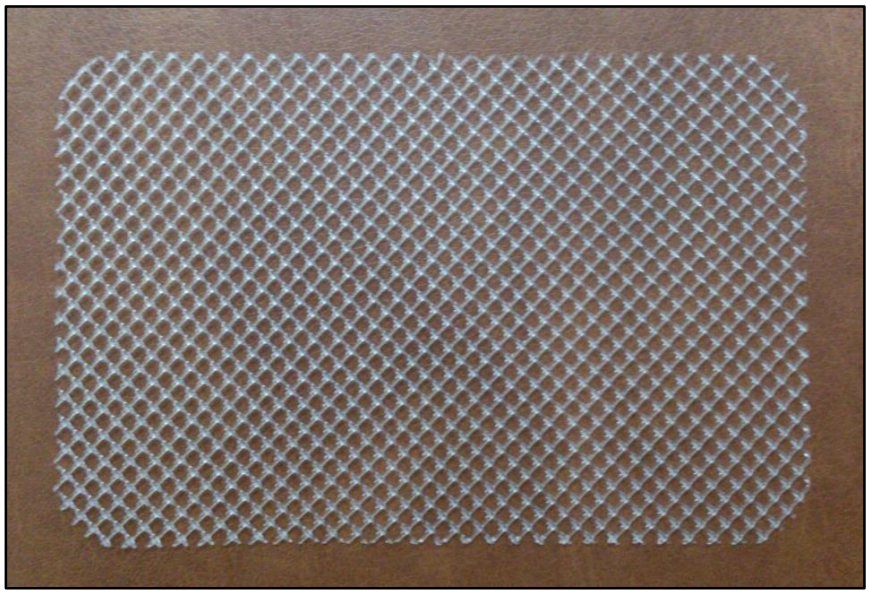

Figure 45: PP spacer used in MD system

Figure (46) shows the main spacer dimensions such as spacer thickness, hydrodynamic angle, and filament size.

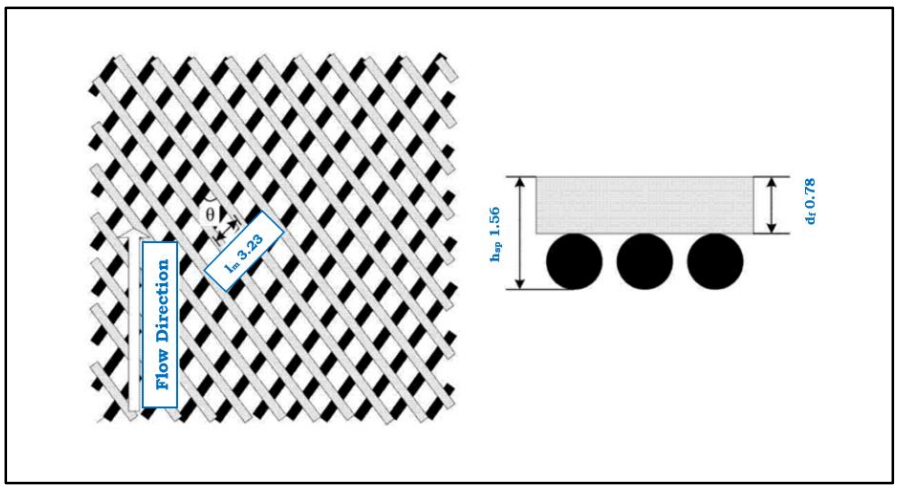

Figure 46: Spacer dimensions

Some spacer characteristics such as filament size, mesh size and spacer voidage are explained in detailed **in the Approach section (4.7).**

4.4.8 Hollow Fiber membrane

The commercial hollow fiber membranes of (MD020CP2N) with the module were purchased from Microdyn-Nadir® Tubular and Capillary modules for Microfiltration that is manufactured in Germany. The module is performed at a cross-flow configuration that minimizes dead zones of the module and is suitable for membrane desalination. Inside the module, hydrophobic ACCUREL® polypropylene (PP) membranes are potted by special Polyurethane material. The hollow fiber membranes and the housing are made of polypropylene (PP). Main characterizations of these membranes are high porosity, symmetrical design and large pore distribution. High porosity of the membranes (75 – 85%) cause high permeability of permeate through pores. The pores size of the membranes are exactly 0.2 microns. The symmetrical homogenous design of the membranes avoids any mechanical damage and scratches. Chemical cleaning in the opposite direction of the flow can withdraw any depositions occur on the membrane

surface. Therefore, citric acid can be used for cleaning as Polypropylene (PP) membranes have high chemical resistance to many acids [143].
The module contains 40 hollow fiber capillaries with an inner diameter of 1.8 mm and membrane inside area of 0.1 m^2. More characteristics of hollow fiber membrane module are present in Table (17) below such as fiber inside and outside diameters.

Moreover, figure (47) represented hollow fiber membrane module that was used for DCMD. The module is covered with isolated tape to minimize heat lose. Distilled water is chosen to be placed inside the capillaries, while feed saline water is placed in the shell side.

Table 17: Characteristics of used Hollow Fiber membrane characteristics

Hollow Fiber membrane characteristics	
Manufacture	MICRODYN
Membrane Material	Polypropylene (PP)
Housing Material	Polypropylene (PP)
Potting Material	Polyurethane
Number of fibers	40
Fiber Inner diameter (mm)	1.8
Membrane thickness (mm)	0.65
Shell Inner diameter (m)	0.021
Shell Outer diameter (m)	0.025
Module Length (m)	0.50
Membrane Length (m)	0.45
Pore size (μm)	0.2
Porosity (%)	75 – 85
Membrane Active Area (m^2)	0.1
Contact Angle (PP)	134.8

A cross sectional view is also illustrated in the figure (47) showing the number of fibers in the module.

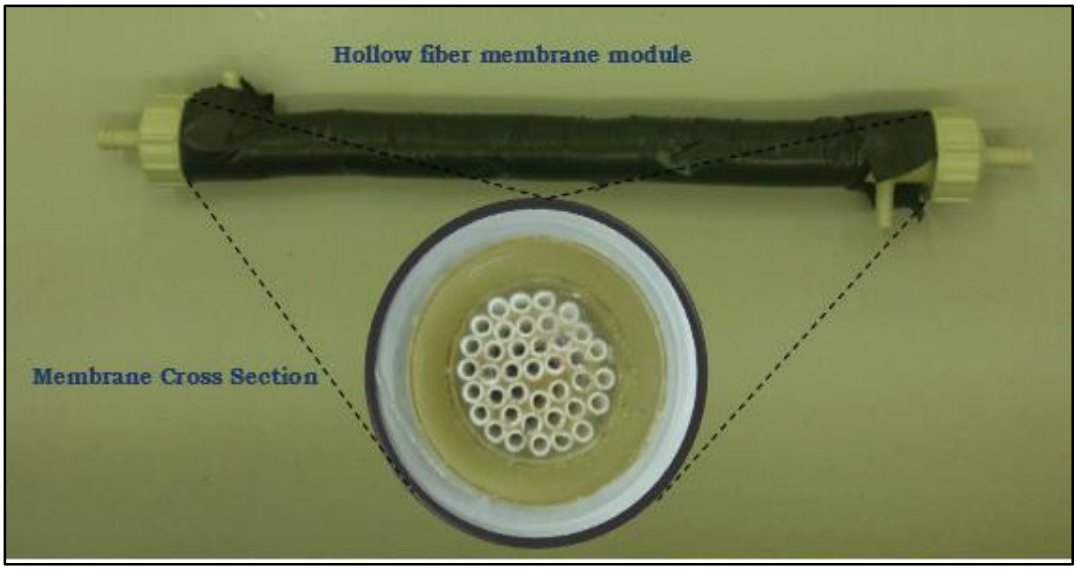

Figure 47: Hollow Fiber membrane module and a cross-section of the module

More detailed graphical drawing of hollow fiber module is represented in **APPENDIX C**.

4.5 Auxiliary Equipment

Many units are required rather than the membrane and feed water to process membrane distillation. This equipment are balances, pumps, heater, cooler, temperature and pressure sensors, flowrate meters, and data acquisition system. Each equipment will be explained in details in this section. The main auxiliary equipment was representing before in figure (36). Other secondary devices are shown in the more detailed sections below.

4.5.1 Pumps

Two peristaltic pumps are used in the system to circulate the water into and out the membrane compartment. One pump is used for hot feed flow and the other one is used for the cool distilled flow. Peristaltic pumps are frequently used in DCMD systems and the advantages behind using them are the accuracy and

reliability of use, easily operated, and low-costed maintained. Pumps are fit under Thermo Scientific (FH100X) model that is digitally operated. These pumps are also easily cleaned and are suitable for the required flowrates. Thermo Scientific (FH100X) pump can operate at a flowrate less than 4 LPM. Maximum flowrate of 3 LPM was used.

Table 18: Peristaltic pump (FH100X) specifications

Peristaltic pump (FH100X)	
Pump Type	Reversible
Flowrate Capacity (LPM)	0 – 4
Speed (RPM)	4 – 400
Maximum Pressure (bar)	4
Accuracy (%)	± 0.25
Dimensions (cm)	31.7 × 27.9 × 15.2

Table 18 lists some specifications of the used pumps in DCMD system [144].

4.5.2 Tubing

Feed and permeate water are pumped into and out the membrane through flexible tubing. Vincon (C-219-A) PVC tubing (ABH02028) with 3/8" ID × 9/16" OD × 3/32" Wall from Saint Gobain, USA supplied by Murdock Industrial are used. Tubing are connecting feed and permeate tanks with the membrane passing through the pumps.

Figure (48) represents Vincon tubing for feed and permeate before it has been covered with insulation.

Table 19: Vincon tubing (ABH02028) specifications

Vincon tubing (ABH02028)	
Tubing Material	PVC
Inner Tubing Diameter (mm)	9.5
Outer Tubing Diameter (mm)	14.3
Wall thickness (mm)	2.4
Color	Transparent
Temperature Range (℃)	-43 – 80

Table (19) lists some of the specifications of the used tubing in lab-scale bench DCMD system.

Figure 48: Vincon Feed and Permeate Tubing

These types of tubes are transparent providing ease of use and are preferred for peristaltic pumps. It also can resist high temperatures which are applied in MD system.

4.5.3 Heater and Cooler

A heater and a cooler are essential equipment in MD process. A heater is used to heat feed water to a specific temperature before facing the membrane. A cooler is used to cool the distilled water that will be used to condense the vapor molecules across the membrane. The heating and refrigerating circulators undergo the F32-MA model and are supplied by Julabo, Germany. One of the advantages that the circulators have is the LED digital screen that demonstrates the current temperature of the water inside the circulate and the set point temperature. It also has a warning alarm for the water level and exceeding set-point temperature. Finally, the water bath can easily be opened to clean and fix water level from the drain screw [145]. Heating/Cooling circulators are capable for a wide range of temperatures (-35 – 200 ℃) that's why they are preferable for MD systems. The used temperature for the heating circulator was in the range of (45 – 65) ± 5 ℃, while the used temperature for the cooling circulator was in the range of (20 ± 5 ℃).

Table 20: Heating/Cooling circulators (F32-MA) specifications

Heating/Cooling circulators (F32-MA)	
Supplier	Julabo, Germany
Refrigerant	R134a
Dimensions (W × L × H) cm	31 × 42 × 64
Heating Coils	Hastelloy C-276
Temperature Stability (℃)	± 0.02
Temperature Range (℃)	-35 – 200

Each circulator can hold up to 8 liters of liquid and for the cooler, refrigerant R134a is used. The heating circulator is dealing with saline water at high temperature so there is a possibility of corrosion that causes failure of equipment and decreases water quality. Therefore, special heating coils are designed from

Hastelloy C-276 (Nickel (Ni) – Molybdenum (Mo) – Chromium (Cr) alloy with addition of Tungsten) that will resist the corrosion. Table (20) presents some specifications of the used Heating/Cooling circulators in MD system.

4.5.4 Weighing Balances

Two balances are used for the MD system. One balance is used to measure the weight of collected permeate flux. This balance is considerate as the most important auxiliary equipment as it will investigate the flux trend. Permeate flux is calculated by dividing the weight of permeate water over the active area of the membrane over time. The other balance is measuring feed weight to ensure the reduced amount of water. The used NewClassic precision balances have Model code of: VWR# 97035–640, Mettler Toledo that manufactured in Italy. The maximum weighting capacity is 8.2 kg, hence feed tank with no more than 6 liters is used. The balances are very accurate as the minimum capacity range is 0.01g.

Table 21: Weighting Balances (VWR# 97035–640) specifications

Weighting Balances (VWR# 97035–640)	
Capacity range (g)	120-8200
Readability (g)	0.01-0.1
Weighing pan dimensions (mm)	170 × 200
Dimensions W × L × H (mm)	194 × 347 × 96

Table (21) presents some specifications of the weighting balances used for measuring the permeate and feed tanks in MD system.

4.5.5 Temperature measurement

The temperature of the inlet and outlet streams to the membrane compartment are measured using Thermo resistance RTDs (Model: RTD-NPT-72-E, Omega Engineering, UK). The temperature is measured using probes that are fixed over the tubes and the maximum measuring temperature can reach 230℃. No more than 70 ℃ temperature for feed stream was measured. NPT fittings are installed online to avoid leakage.

Table 22: Thermo resistance RTDs (Model: RTD-NPT-72-E) specifications

Thermo resistance RTDs (Model: RTD-NPT-72-E)	
Supplier	Omega Engineering, UK
Maximum Temperature (℃)	230
Maximum Pressure (psi)	2500

Table (22) presents some specifications of the thermocouples used for measuring the permeate and feed streams temperature.

4.5.6 Pressure measurement

The pressure of the inlet and outlet streams to the membrane compartment are measured using pressure transmitters (Model: PX309-030GI, Omega Engineering, UK) [146]. The measured pressure in these experiments were in the range of (1 psi). NPT fittings are used to avoid leakage.

Table 23: Pressure Transmitters (Model: PX309-030GI) specification

Pressure Transmitters (Model: PX309-030GI)	
Supplier	Omega Engineering, UK
Operating Temperature (℃)	-40 – 85
Pressure range (psi)	1 – 5
Output power (mA)	4 – 20
Accuracy (%)	± 0.25

Table (23) presents some specifications of pressure transmitters used for measuring the pressure of permeate and feed streams.

4.5.7 Flow Meter

Two flow meters are installed to measure the flowrates of feed and permeate streams. The flow meter that is measuring the hot seawater flowrate has Magmeter model: FMG82, Omega Engineering, UK. It has NPT fittings that are installed online to avoid leakage. This model is corrosion and temperature resistance. It can handle a maximum temperature of 93 ℃ and a salinity of 70,000 ppm. Operating range reaches 11 LPM and it covers the experimental range.

Table 24: Flow meter (Magmeter Model: FMG82) specifications

Flow meter (Magmeter Model: FMG82)	
Supplier	Omega Engineering, UK
Maximum Temperature (℃)	93
Maximum Salinity (ppm)	70,000
Maximum Pressure (psi)	150
Operating Range (LPM)	0 – 11
Output power (mA)	4 – 20
Accuracy (%)	± 1

Table (24) lists some specifications of flow meters used for measuring the flow rate of feed stream.

The flow meter that is measuring the distilled flowrate has Magmeter model: FPR-1506, Omega Engineering, UK. It has NPT fittings that are installed online to avoid leakage. Operating range reaches 5 LPM and it covers the experimental range. Pelton-type turbine wheel is used to measure the flowrate assuming a linear relationship between wheel's rotations and flowrate and there is no need for conductivity.

Table 25: Flow meter (Magmeter Model: FPR-1506) specifications

Flow meter (Magmeter Model: FPR-1506)	
Supplier	Omega Engineering, UK
Material	PTFE
Maximum Temperature (℃)	70
Maximum Pressure (psi)	10
Flow Range (LPM)	0.5 – 5

Table (25) lists some specifications of flow meters used for measuring the flow rate of distilled stream.

4.5.8 Conductivity Meter

The main function of conductivity meter is to test quality of distilled water. It is also used to measure saline water and rejected brine conductivities in order to calculate rejected percentage. WTW Multi 3420 Multiparameter Meter with Tetracon 925 conductivity measuring cell is used to determine the conductivity. Another device is used for measuring the conductivity and Total Dissolved Solids (TDS) for quality of water. It is manufactured by AQUALYTIC, Germany and has

a product name: SD 320 Con. This conductivity meter is very applicable for drinking water applications [147].

Table 26: Conductivity meter (Model: SD 320 Con) specifications

Conductivity meter (Model: SD 320 Con)	
Supplier	AQUALYTIC, Germany
Dimensions (W x H x D) mm	164 x 128 x 37
Temperature Range (℃)	-5 – 100
Conductivity Rande (mS/cm)	0 – 2000
TDS (mg/l)	0 – 5000
Accuracy (%)	± 0.1

Table (26) lists some specifications of the conductivity meter used for measuring the electrical conductivity of permeate water.

Figure 49: AQUALYTIC conductivity meter

Figure (49) pictures AQUALYTIC conductivity meter used in these experiments to measure electrical conductivity of permeate water in addition to (TDS).

4.5.9 Digital Display

Digital displays are used to ensure temperature, pressure, and flowrate measurements of feed and distillate streams. These digital display meters have Model: DP25B-E-230-A, Omega Engineering, UK. Display meters work by converting the received voltage into readable values of temperature, pressure, and flowrate. Two colors are used to simplify monitoring the displays, blue color for distilled streams, and red color for feed streams.

4.5.10 Containers

Several liquid containers are used in MD system such as permeate and feed tanks and glass bottles for storing the samples. Feed and permeate tanks are supplied by behr Labor-Technik (Germany). These tanks are made of Polyethylene material that is resistant to many substances and can handle various range of liquids. It is also very safe for food processing and capable with permeate water generation. This material can be used at high temperature and handle temperatures of 80℃.

Figure 50: Glass bottles with Permeate samples

Glass bottles that used for storing permeate samples are also supplied by behr Labor-Technik (Germany). The bottle is made of glass and the inner side of gasket inside the screw is coated with PTFE. Screw material is (PP). Therefore, permeate sample will face only glass and a layer of PTFE. The screw and the gasket are high thermal resistant that can handle a temperature of 121℃ and 50℃, respectively. Figure (50) represents some of the permeate samples that are stored in the glass bottles.

4.5.11 Data Acquisition System

All the measured data of the experiments including permeate weight are stores and controlled by Data Acquisition System. The measurements include Temperature, Pressure, Flowrate, Permeate weight, and time. National Instruments (NI) data acquisition hardware (Chasis Model cDAQ-9188) and analog input Module (Model: NI-9219, United States) in addition to computer are used. National Instruments (NI) cDAQ-9188 is an 8-slot NI Compact DAQ Ethernet chassis which is designed to remote and distributed sensor and

measured data signals. DAQ is an intermediate device between the measured signals and a computer. Its main function is to allow the computer to read and analyze the measurements. National Instruments (NI) is basically a 4 analog-to-digital convertors (ADCs) connected in universal C-Series that analyses all the measurements [148]. These universal C-Series are connected to DAQ Ethernet chassis for functioning analog input, analog output, digital input/output, and counter/timer measurement system.

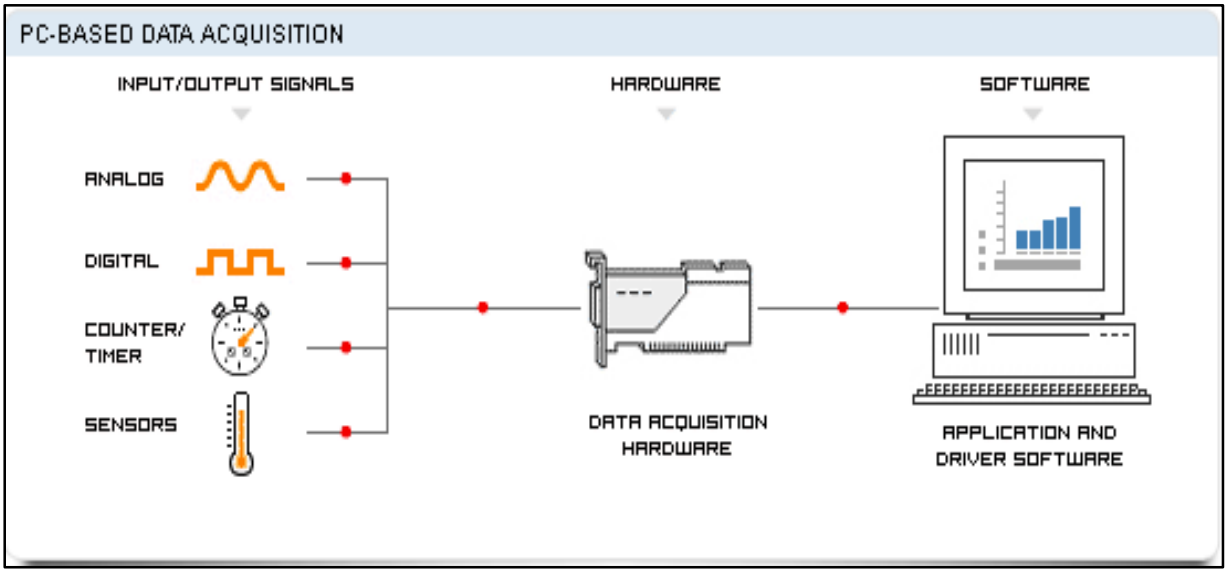

Figure 51: schematic diagram of the Data AQ system [149]

Ethernet serial server interfaces (Model: NI ENET 232, National Instruments, USA) provide additional ports RS232, RS422, and RS485 for permeate weight measurements. LabVIEW data acquisition software that is installed in the computer has a function of storing and processing all measurements data. To sum everything up, data acquisition system consists of sensors, Data Acquisition measurement hardware and a computer with programmable software [149]. Figure (51) simplifies the Data Acquisition System by graphical illustrations.

Table 27: Data Acquisition System characteristics

Data Acquisition System (Model: NI-9219)	
Operating System	Windows
Current Range (A)	- 0.025 – 0.025
Voltage Range (V)	-60 – 60
Operating Temperature (℃)	-40 – 70
Measurement Type	Current RTD Resistance Strain / Bridge-based sensor Temperature Thermocouple Voltage

Table (27) listed some of the Data Acquisition System specifications that was responsible for all the collected data.

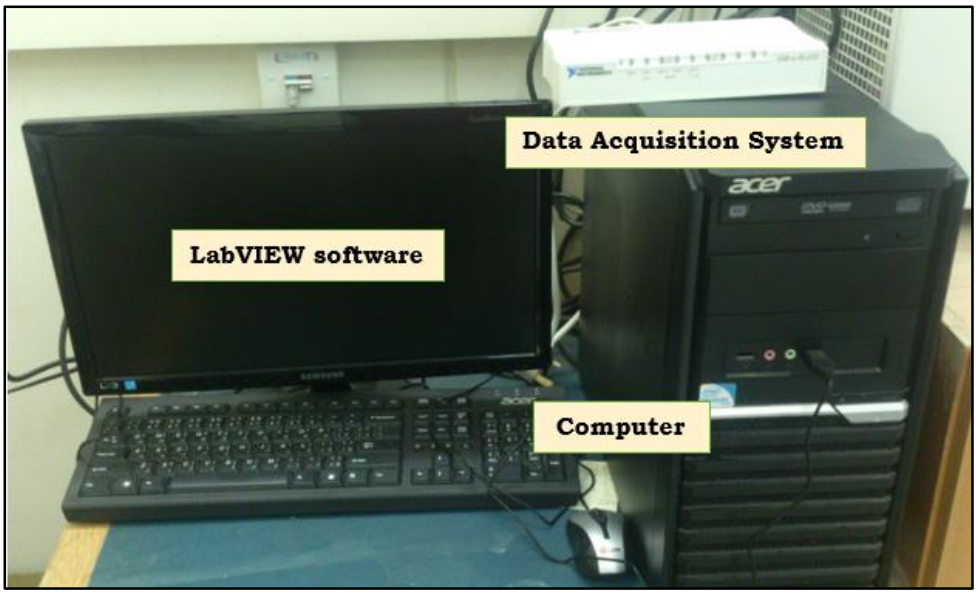

Figure 52: Data Acquisition System connected to the PC

Figure (52) shows Data Acquisition system that is connected to the LabVIEW software installed in the computer. These devices were used in the Lab in order to evaluate all the experimental part.

4.6 Experimental Procedure

In this work, a comparison study between the performance of hollow fiber membrane and flat sheet membrane is investigated. All the experiments are conducted under various operating conditions to study the effect of some factors such as feed temperature and flowrate. Several tests are performed on the permeate water at the end of the experiments to ensure quality of water such as conductivity measurements, salt rejection, and anions/cations measurements of the resulted fresh water. This section is explaining the experimental procedure that was conducted in order to achieve the research objectives. Experimental details are explained in the section below.

Several sets of experiments are made for the two types of membranes; hollow fiber and flat sheet membranes. All the experiments are conducted at similar operating conditions to meet the objectives of the study.

4.6.1 Hollow Fiber membrane

Starting with the hollow fiber membrane experiments, 5 experiments are conducted for each flowrate and 4 different experiments are processed at each feed temperature.

Table 28: Experimental codes of Hollow Fiber membrane experiments at different feed temperatures and flowrates

Feed Tem. / Flowrate	**65** ℃	**60** ℃	**55** ℃	**50** ℃	**45** ℃
1.5 (L/m)	HF6515	HF6015	HF5515	HF5015	HF4515
2.0 (L/m)	HF6520	HF6020	HF5520	HF5020	HF4520
2.5 (L/m)	HF6525	HF6025	HF5525	HF5025	HF4525
3.0 (L/m)	HF6530	HF6030	HF5530	HF5030	HF4530

Table (28) summarizes all the experiments that are processed using hollow fiber membrane at different feed temperatures and flowrates.

4.6.1.1 Effect of temperature

The effect of feed temperature on the production of permeate flux is studied by conducting the experiments on various feed temperature. Five different feed temperatures were studied (45 - 65℃) with 5℃ temperature increment between the runs. Distilled temperature is kept constant at 20℃. Each experiment lasts 4 hours.

4.6.1.2 Effect of flowrate

The effect of feed circulation rate on the production of permeate flux is studied by conducting the experiments on various feed and permeate flowrates. The flowrate is changed adjusting pump speed. Four different feed and permeate flowrates were studied (1.5 – 3.0 L/m) with 0.5 L/m flowrate increment between the runs. Each experiment lasts 4 hours.

4.6.2 Flat Sheet membrane

Also the flat sheet membrane experiments are conducting 5 experiments for each flowrate and 4 different experiments are processed at each feed temperature.

Table 29: Experimental codes of Flat Sheet membrane experiments at different feed temperatures and flowrates

Feed Tem. / Flowrate	**65** ℃	**60** ℃	**55** ℃	**50** ℃	**45** ℃
1.5 (L/m)	FS6515	FS6015	FS5515	FS5015	FS4515
2.0 (L/m)	FS6520	FS6020	FS5520	FS5020	FS4520
2.5 (L/m)	FS6525	FS6025	FS5525	FS5025	FS4525
3.0 (L/m)	FS6530	FS6030	FS5530	FS5030	FS4530

Table (29) summarizes all the experiments that are processed using flat sheet membrane at different feed temperatures and flowrates.

4.6.2.1 Effect of temperature

The effect of feed temperature on the production of permeate flux is studied by conducting the experiments on various feed temperature. Five different feed temperatures were studied (45 - 65℃) with 5℃ temperature increment between the runs. Distilled temperature is kept constant at 20℃. Each experiment lasts 4 hours.

4.6.2.2 Effect of flowrate

The effect of feed circulation rate on the production of permeate flux is studied by conducting the experiments on various feed and permeate flowrates. The flowrate is changed adjusting pump speed. Four different feed and permeate flowrates were studied (1.5 – 3.0 L/m) with 0.5 L/m flowrate increment between the runs. Each experiment lasts 4 hours.

4.6.3 Operating Conditions

As it was mentioned above all the conducted experiments are varying between (45 - 65℃) feed temperatures and (1.5 – 3.0 L/m) feed and permeate flowrates.

Table 30: Parameters and conditions of DCMD system

Parameter		Range
Feed Operating Temperature (℃)		45 – 65
Distilled Operating Temperature (℃)		20
Feed Flowrate (L/m)		1.5 – 3.0
Distilled Flowrate (L/m)		1.5 – 3.0
Pressure range (atm)		1
Feed Seawater	Conductivity (mS/cm)	65.0
	pH	8
Permeate (Hollow Fiber)	conductivity ($\mu S/cm$)	~ 40.0
	pH	6
Permeate (Flat Sheet)	conductivity ($\mu S/cm$)	~ 2.0
	pH	6

Distilled temperature is kept constant at 20℃. Each experiment lasts 4 hours. Hot Seawater is used as feed solution for all experiments with 65 $\mu S/cm$ approximately. For distilled stream, deionized cold water is used that is mixed with permeate during the experiments. The conductivity of deionized distilled

water is 65 $\mu S/cm$ approximately. All the parameters and conditions of the lab scale DCMD system are summarized in the table (30) above.

By conducting all these experiments, flux results of both membranes will be provided in the results section before being compared and analyzed. Moreover, the explanation of all conditions affecting the flux in addition to heat thermal coefficients that affect the results will be explained in the **Discussion section** in **Chapter 5**.

4.6.4 Repeatability of Experiments

After all the experimental runs were conducted with different feed temperatures and flowrates, a number of randomly selected experimental runs were repeated. All the repeated experiments show a very low error percentage near zero that did not exceed 0.2%.

4.7 Approach

The used approach in order to evaluate the thermal convective coefficients in flat sheet and hollow fiber membranes is explained in this section. All the steps and used correlations are listed in sequent of their usage.

4.7.1 Convective Heat Transfer Considerations

After the permeate results of hollow fiber and flat sheet membranes are generated from the DCMD system, the explanation of archived flux amount is made according to scientific proper terms. It was noticed that permeate flux is affected by thermal coefficients. Therefore, heat transfer coefficients were calculated for both hollow fiber and flat sheet membrane to verify flux difference. In this section

the methodology of calculation part of thermal coefficients is provided. All the steps and used equations are listed in this section for both membranes.

4.7.1.1 Flat Sheet Membrane

The main target of this section is to calculate the heat transfer coefficient of DCMD system using flat sheet membrane on the hot feed side. To achieve this target, several dimensionless numbers should be calculated such as Reynolds number (Re), Prandtl number (Pr), and Nusselt number (Nu). Reynolds number (Re) and Prandtl number (Pr) can be calculated using equations (14) and (15) mentioned before in the Heat Transfer section in **Chapter 3**. As thermal coefficients are calculated for the hot side of the membrane only, Prandtl number (Pr) that is a dimensionless number depends only on the hot feed seawater properties.

All seawater properties are calculated based on seawater salinity of 60 g/kg [150]. These properties include seawater density, viscosity, heat capacity, and thermal conductivity. Table (31) listed seawater properties at feed temperature of 65℃. Similar properties of seawater at 45℃, 50℃, 55℃, and 60℃ feed temperature are collected in order to evaluate thermal coefficient at different feed temperatures.

Table 31: Seawater properties at feed temperature of 65℃

Seawater Property	**Values at temperature of 65** ℃
Density (kg/m^3)	1024.0
Viscosity (Ns/m^2)	0.0005
Heat Capacity (J/kg. K)	3904.0
Thermal Conductivity (W/m. k)	0.6510

As turbulent promoter (spacer) is introduced in the flat sheet membrane system, all the used correlations are applied into spacer-filled channels. All the equations are used for spacer-filled channel. Some correlations are different from free-spacer channel as the spacer affect the flow velocity and the hydraulic diameter. Phattaranawik et al. [51], [74], [76], [134], [151], [152] developed several correlations to estimate heat transfer coefficients in spacer-filled channels.

The velocity of feed flow in the spacer-filled channel (v_s) can be calculated using equation (58) below:

$$\boldsymbol{v_s = \frac{Q}{A\,\varepsilon}} \tag{58}$$

where Q is the feed volumetric flowrate, ε is membrane porosity, and A is cross-sectional area of empty channel which is perpendicular to flow direction and can be calculated by measuring flow path length and channel height in the membrane compartment.

The hydraulic diameter in the spacer-filled channel (D_h) is calculated be using equation (59) below:

$$\boldsymbol{D_h = \frac{4\,\varepsilon_s}{\frac{2}{h_{sp}} + (1-\varepsilon)S_{vsp}}} \tag{59}$$

where h_{sp} is the spacer thickness, ε_s is spacer porosity that can be calculated using equation (60), and S_{vsp} is specific spacer surface that is determined by using equation (61).

$$\boldsymbol{\varepsilon_s = 1 - \frac{4\,{d_f}^2}{2\,l_m\,h_{sp}\sin\theta}} \tag{60}$$

$$\boldsymbol{S_{vsp} = \frac{4}{d_f}} \tag{61}$$

where d_f is diameter of spacer filament, l_m is mesh size, and θ is hydrodynamic angle. All these parameters are measured using electronic Vernier Caliper. All the calculated and measured spacer characteristics are listed in table (32) below:

Table 32: Parameters of the used spacer

Parameter	Measured or Calculated value
Thickness (mm)	1.56
Diameter of spacer filament (mm)	0.78
Mesh size (mm)	3.23
Hydrodynamics angle	90
Spacer porosity (%)	81
Specific surface of spacer (mm^{-1})	5128

After spacer parameters have be evaluated and hydraulic diameter is calculated, Reynolds number (Re) can be determined. Pr and Re numbers are used to estimate Nusselt number (Nu) according to Nu correlations. Different experimental conditions advise different Nu correlations. **APPENDIX B** summarizes different Nu correlations that found in literature. Nu correlation for spacer-filled channel suggested by Phattaranawik, [73] Manawi [47] and other researchers [74], [76] is expressed in equation (62). This correlation is used to calculate Nu number as it is applied on similar operating conditions that were used in our research.

$$\boldsymbol{Nu = 0.664\, k_{dc}\, Re^{0.5}\, Pr^{0.33} \left[\frac{2\, D_h}{l_m}\right]^{0.5}} \tag{62}$$

where k_{dc} is spacer correction factor that is referred to [47], [50], [73], [74], [76] and can be evaluated using equation (63).

$$\boldsymbol{k_{dc} = 1.654 \left[\frac{d_f}{h_{sp}}\right]^{-0.039} \varepsilon_s^{0.75} \left(\sin\left(\frac{\theta}{2}\right)\right)^{0.086}} \tag{63}$$

After all the affected parameters by spacer are evaluated and all the dimensionless numbers were calculated and fitted under the proper range, heat transfer coefficient (h) can be easily determined with the help of equation (13) mentioned before in Heat Transfer section in **Chapter 3**.

4.7.1.2 Hollow Fiber Membrane

Similar steps of heat transfer coefficient calculation in flat sheet membrane are applied in hollow fiber membrane. As for flat sheet membrane, several dimensionless numbers should be calculated such as Reynolds number (Re), Prandtl number (Pr), and Nusselt number (Nu) in order to achieve the objective. Reynolds number (Re) and Prandtl number (Pr) are calculated using equations (14) and (15) mentioned before in the Heat Transfer section in **Chapter 3**. As thermal coefficients are calculated for the hot side of the membrane only, Prandtl number (Pr) that is a dimensionless number depends only on the hot feed seawater properties exactly as it was proceeded for the flat sheet membrane thermal coefficients calculations.

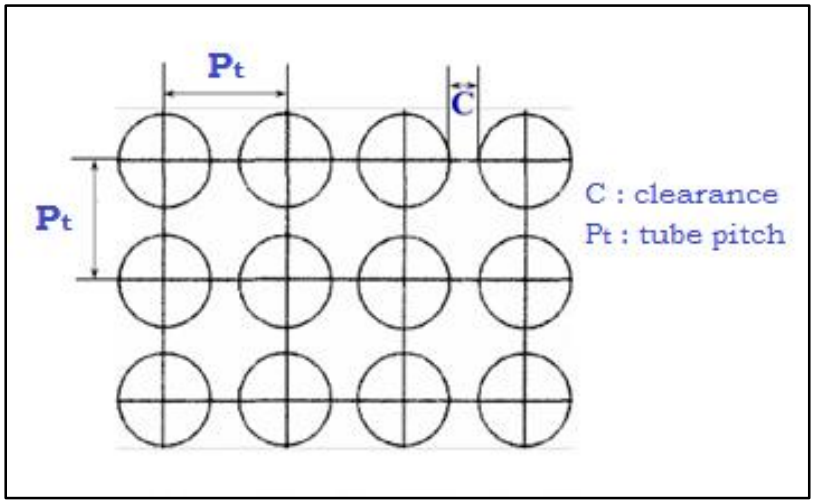

Figure 53: Square pitch arrangement of the hollow fiber tubes in the module

Kern's method of shell and tube heat exchanger design is applied on the hollow fiber module to calculate the equivalent diameter. The principle of hollow fiber membrane is very similar to the shell and tube heat exchanger. [153] Calculating the equivalent diameter and velocity of the flow are needed to evaluate Reynolds

number (Re). Starting with the equivalent diameter, square pitch arrangement of the hollow fiber tubes is assumed to be in the module as shown in figure (53).

In order to evaluate the equivalent diameter, equation (64) is used and several hollow fiber tubes parameters have to be measured and estimated. These parameters are represented in figure (53) and are listed in table (33).

$$\mathbf{D}_e = \frac{\mathbf{1.27}}{\boldsymbol{d_o}} \left(\boldsymbol{P_t}^2 - \mathbf{0.785}\, \boldsymbol{d_o}^2 \right) \tag{64}$$

where d_o is the tube outside diameter, and P_t is tube pitch.

To calculate the velocity of the flow by equation (58) as it was mentioned before in flat sheet calculations section, the cross-sectional area of the membrane that is perpendicular to the flow in hollow fiber membrane module is needed to be evaluated. Cross-sectional area is given by equation (65) [153] and all the required parameters are listed in table (33) below.

Table 33: Hollow fiber membrane parameters in square pitch arrangement

Parameter	Measured or calculated value
Tube pitch (mm)	2.9
Tube outside diameter (mm)	2.8
Shell inner diameter (mm)	21
Baffle spacing (mm)	500
Number of fibers	40

It is shown in table (33) that the clearance between the tubes is 5 mm and as baffles are not used in this configuration, baffle spacing is assumed to be the length of the module.

$$A_s = \frac{(P_t - d_o)\, D_s l_b}{P_t} \tag{65}$$

where Q is the feed volumetric flowrate, and A_s is cross-sectional area of empty channel which is perpendicular to flow direction. P_t, d_o, D_s and l_b are tube pitch, tube outside diameter, shell inside diameter, and baffle spacing.

After calculating flow velocity in the module and equivalent diameter, Re number can be estimated. Pr and Re numbers are used to estimate the Nusselt number from Nu correlations listed in **APPENDIX B**. From different Nu correlations found in literature, one was chosen to be used in this research. Wang and Gu reported in their study [108] of hollow fiber membrane heat exchanger different Nu correlations according to seawater feed arrangement; lumen side or shell side. Nu correlation that applicable for feed water on the shell side of membrane was chosen to satisfy our operating conditions. This Nu correlation is given by equation (66).

$$Nu = (0.53 - 0.58\,\emptyset)\, Re^{0.53}\, Pr^{0.33} \tag{66}$$

where $\emptyset$ is packing density of the membranes and can be evaluated using equation (67).

$$\emptyset = n \left[\frac{2\pi r_o}{\pi D_s}\right]^2 \tag{67}$$

where r_o is tube outside radius and n is number of hollow fiber tubes inside the module. All these parameters can be found in table (33). The final step is evaluating heat transfer coefficient with the help of equation (13) as it was proceeded in flat sheet thermal coefficients calculations.

4.8 Water Quality

The permeate water achieved by membrane distillation system using flat sheet and hollow fiber membranes was tested to ensure water quality. The presence of different anions and cations, electrical conductivity measurements, pH

measurements, and salt rejection calculations were proceeded in order to asses permeate quality.

4.8.1 Cations Analysis

Inductively Coupled Plasma-Optical Emission Spectroscopy (ICP-OES) is used to determine the cations of trace metals and elements present in permeate water. The used ICP-OES device has (iCAP 6000 Series, Thermo Scientific, USA) model. The procedure starts with the preparation of blank solutions of 100 ml Nitric Acid diluted with ultra-pure water. The next step is standards preparation. After that, blanks, standards, and all permeate samples generated from flat sheet membrane and hollow fiber membrane distillation process are placed in the auto-sampler rack of the ICP-OES device in order to receive cations analysis with compatible software.

Figure 54: ICP Spectrometer apparatus

Figure (54) pictures the ICP-OES device used in the laboratory for cations analysis.

4.8.2 **Anions Analysis**

Ion Chromatography (IC) is used to determine the anions of trace metals and elements present in permeate water. The used IC devise has (850, Metrohm, Swaziland) model. Ion Chromatography (IC) can measure the concentration of major anions fluoride, chloride, bromide, nitrate, sulfate, and phosphate. Figure (55) pictures Ion Chromatography apparatus used in the laboratory for anions analysis.

Figure 55: Ion Chromatography apparatus

Chapter 5: Results and Discussion

In this chapter, the results of all the conducted experiments of direct contact membrane distillation (DCMD) process are represented. The results are discussed in order to understand the theory behind the observed experimental results. The first section will cover the experimental work that includes permeate flux generation for both types of membranes. The second part will cover the convective heat transfer considerations of some dimensionless numbers (Re, Pr, Nu) and heat transfer coefficients, *h*. Finally, water quality analysis will be done on the generated permeate water.

Experimental Results

All the achieved results from the experimental work and the convective heat transport study are present in the sections below. The experimental part includes the study of flat sheet and hollow fiber membranes performance in terms of generated permeate flux. The convective heat transport study explains the results achieved from the calculations of flow pattern and thermal coefficients.

5.1 Distillate Flux Results

5.1.1 Flat Sheet membrane module

In this section, the experimental work is performed to study the effect of changing the operation conditions on DCMD system. Different operating conditions include feed and permeate temperature and feed flowrates are tested on flat sheet membrane. Same operating conditions that applied on flat sheet membranes would be applied later on hollow fiber membrane in order to compare between them. Permeate flux is the main characteristic parameter that is affected by operating conditions and indicate the optimum conditions to achieve higher

flux. Each parameter in this section would be discussed later in discussion section for better understanding.

5.1.1.1 Effect of Feed Temperature

The effect of feed temperature on permeate flux was studied on flat sheet membranes in this DCMD system. The studied feed temperatures all are varied between five different temperatures (45, 50, 55, 60, and 65 ℃) while keeping the flow rate constant at each run. The permeate temperature is set to 20 ℃ and all the experiments are run for approximately 4 hours.

5.1.1.2 Effect of Flow Rate

The effect of feed flow rate on the permeate flux was studied on flat sheet membranes in this DCMD system. Four different feed flow rates were applied for this section. All the flow rates were varied between (1.5, 2.0, 2.5, and 3.0 LPM). For each flow rate, the permeate and feed temperatures are kept constant. Permeate temperature is set to 20 ℃ and all the experiments are run for approximately 4 hours.

Figures (56 - 59) illustrate the resulted permeate fluxes for flat sheet membrane experiments at different flowrates and feed temperatures.

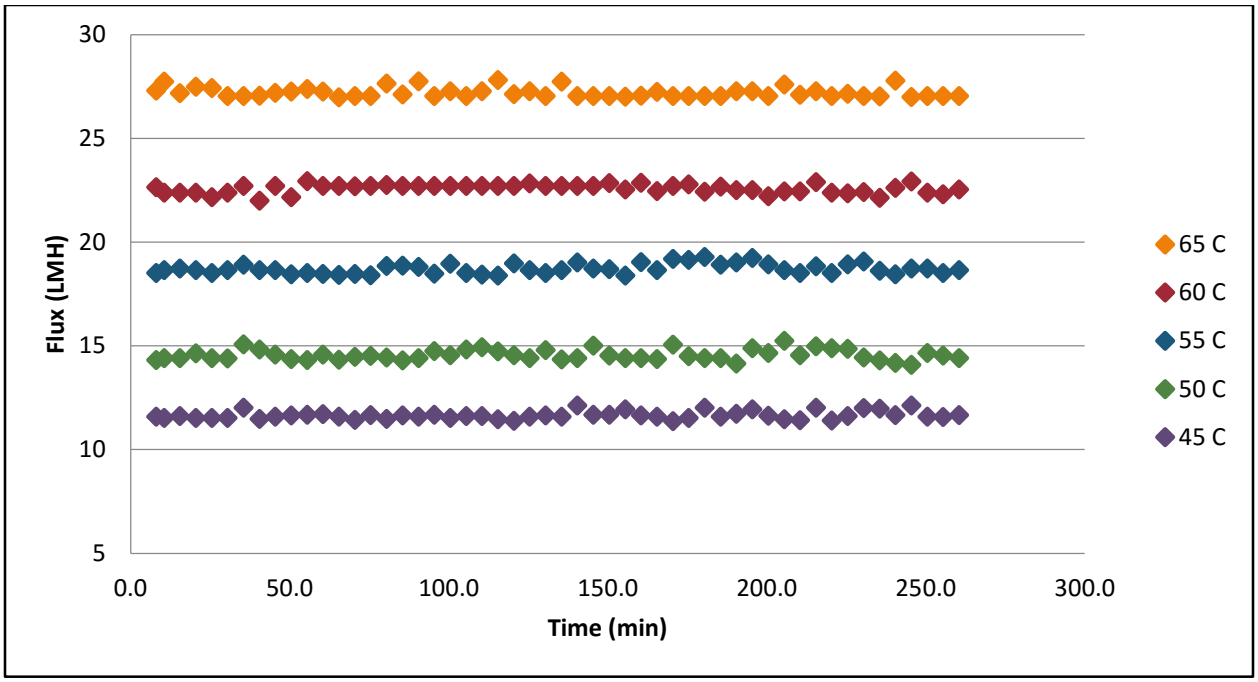

Figure 56: Permeate Flux profile of Flat Sheet membrane at different feed temperatures (Q= 1.5 LPM, Tp=20 ℃)

Figure (56) represents the effect of changing feed temperature on the permeate flux using flat sheet membrane. Feed temperatures were varied between (45, 50, 55, 60, and 65 ℃) while the permeate temperature was kept at 20 ℃. Feed and permeate flow rates are maintained at 1.5 LPM.

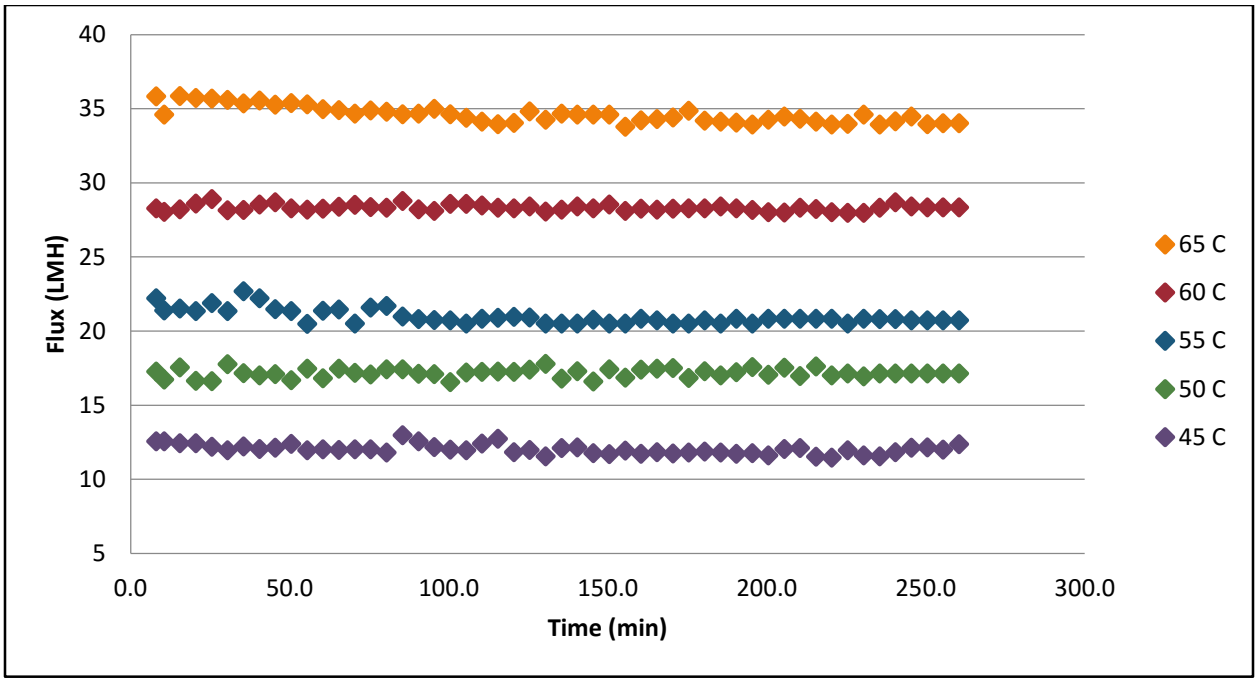

Figure 57: Permeate Flux profile of Flat Sheet membrane at different feed temperatures (Q= 2.0 LPM, T_p=20 ℃)

Figure (57) represents the effect of changing feed temperature on the permeate flux using flat sheet membrane. Feed temperatures were varied between (45, 50, 55, 60, and 65 ℃) while the permeate temperature was kept at 20 ℃. Feed and permeate flow rates are maintained at 2.0 LPM.

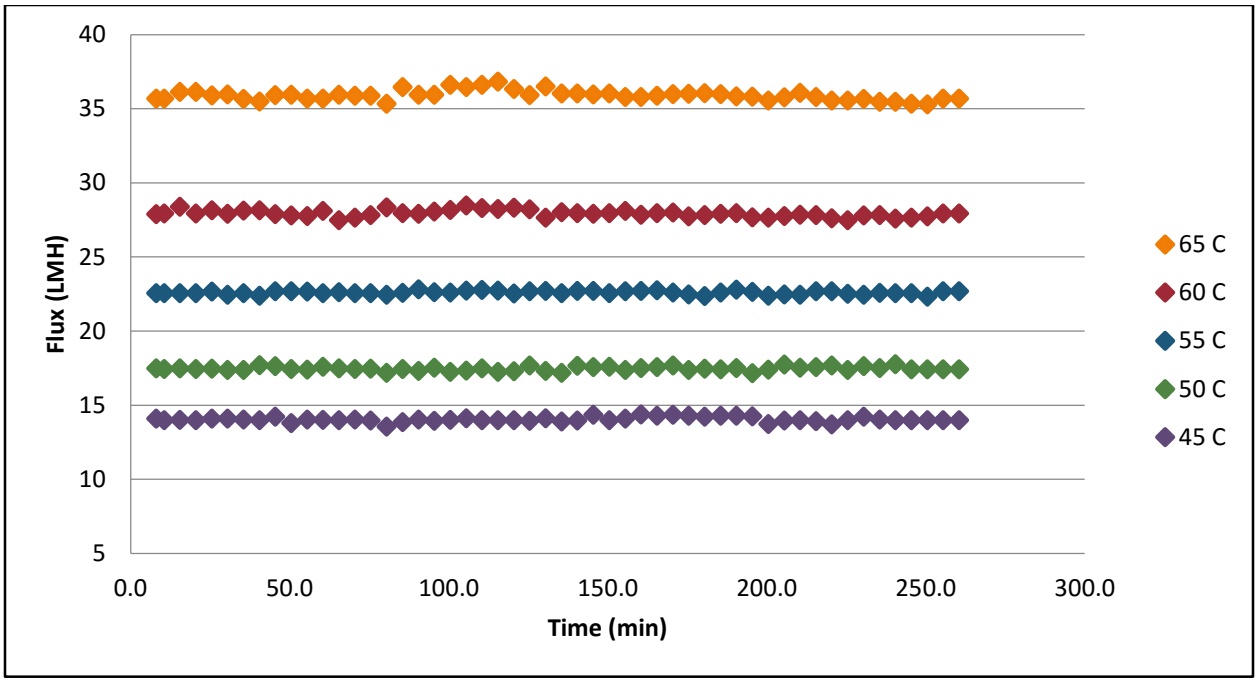

Figure 58: Permeate Flux profile of Flat Sheet membrane at different feed temperatures (Q= 2.5 LPM, T_p=20 ℃)

Figure (58) represents the effect of changing feed temperature on the permeate flux using flat sheet membrane. Feed temperatures were varied between (45, 50, 55, 60, and 65 ℃) while the permeate temperature was kept at 20 ℃. Feed and permeate flow rates are maintained at 2.5 LPM.

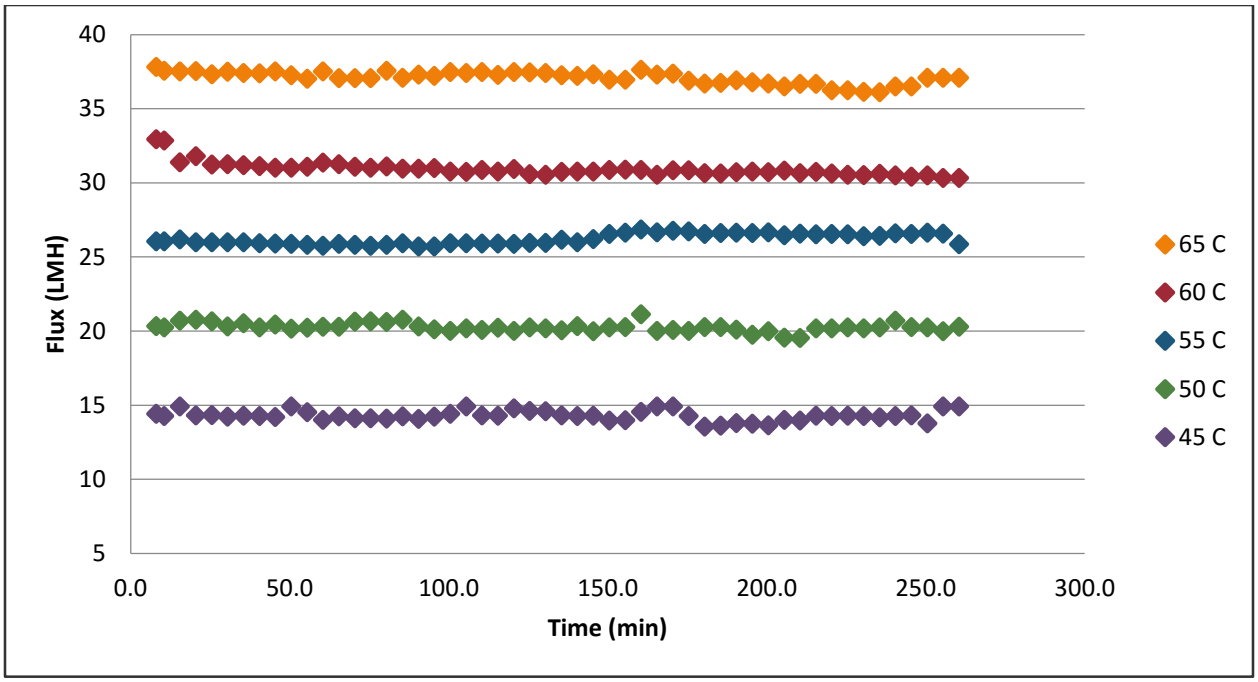

Figure 59: Permeate Flux profile of Flat Sheet membrane at different feed temperatures (Q= 3.0 LPM, T_p=20 ℃)

Figure (59) represents the effect of changing feed temperature on the permeate flux using flat sheet membrane. Feed temperatures were varied between (45, 50, 55, 60, and 65 ℃) while the permeate temperature was kept at 20 ℃. Feed and permeate flow rates are maintained at 3.0 LPM.

All feed inlet/outlet temperatures to flat sheet membrane module during the experimental time and just before shutting-down the apparatus are summarized in table (34) below in addition to temperature difference across the membrane at different feed flowrates.

Table 34: Flat Sheet Module terminal temperatures

Feed Flowrate (LPM)	Feed Inlet Temperature (℃)	Feed Outlet Temperature (℃)	ΔT
1.5	45.50	43.00	2.50
	50.40	47.60	2.80
	55.10	51.70	3.40
	60.00	56.20	3.80
	65.10	60.90	4.20
2.0	45.50	43.70	1.80
	50.30	48.00	2.30
	55.20	52.50	2.70
	59.90	57.30	2.60
	65.30	61.70	3.60
2.5	45.50	43.70	1.80
	50.00	47.90	2.10
	55.10	52.70	2.40
	59.80	56.80	3.00
	65.30	62.60	2.70
3.0	45.40	44.20	1.20
	50.90	49.80	1.10
	54.90	52.90	2.00
	60.20	58.20	2.00
	65.40	63.10	2.30

Results showed that temperature difference across the membrane decreases with increasing feed flowrate.

5.1.2 Hollow Fiber membrane module

In this section, the experimental work is performed to study the effect of changing the operation conditions on DCMD system. Different operating conditions include feed and permeate temperature and feed flowrates are tested on hollow fiber membrane in order to compare with flat sheet membrane. Permeate flux is the main characteristic parameter that is affected by operating conditions and indicate the optimum conditions to achieve higher flux. Each

parameter in this section would be discussed later in discussion section for better understanding.

5.1.2.1 Effect of Feed Temperature

The effect of feed temperature on permeate flux was studied on hollow fiber membrane in this DCMD system. The studied feed temperatures all are varied between five different temperatures (45, 50, 55, 60, and 65 ℃) while keeping the flow rate constant at each run. The permeate temperature is set to 20 ℃ and all the experiments are run for approximately 4 hours.

5.1.2.2 Effect of Flow Rate

The effect of feed flow rate on the permeate flux was studied on hollow fiber membrane in this DCMD system. Four different feed flow rates were applied for this section. All the flow rates were varied between (1.5, 2.0, 2.5, and 3.0 LPM). For each flow rate, the permeate and feed temperatures are kept constant. Permeate temperature is set to 20 ℃ and all the experiments are run for approximately 4 hours.

Figures (60 – 63) illustrate the resulted permeate flux for flat sheet membrane experiments at different flowrates.

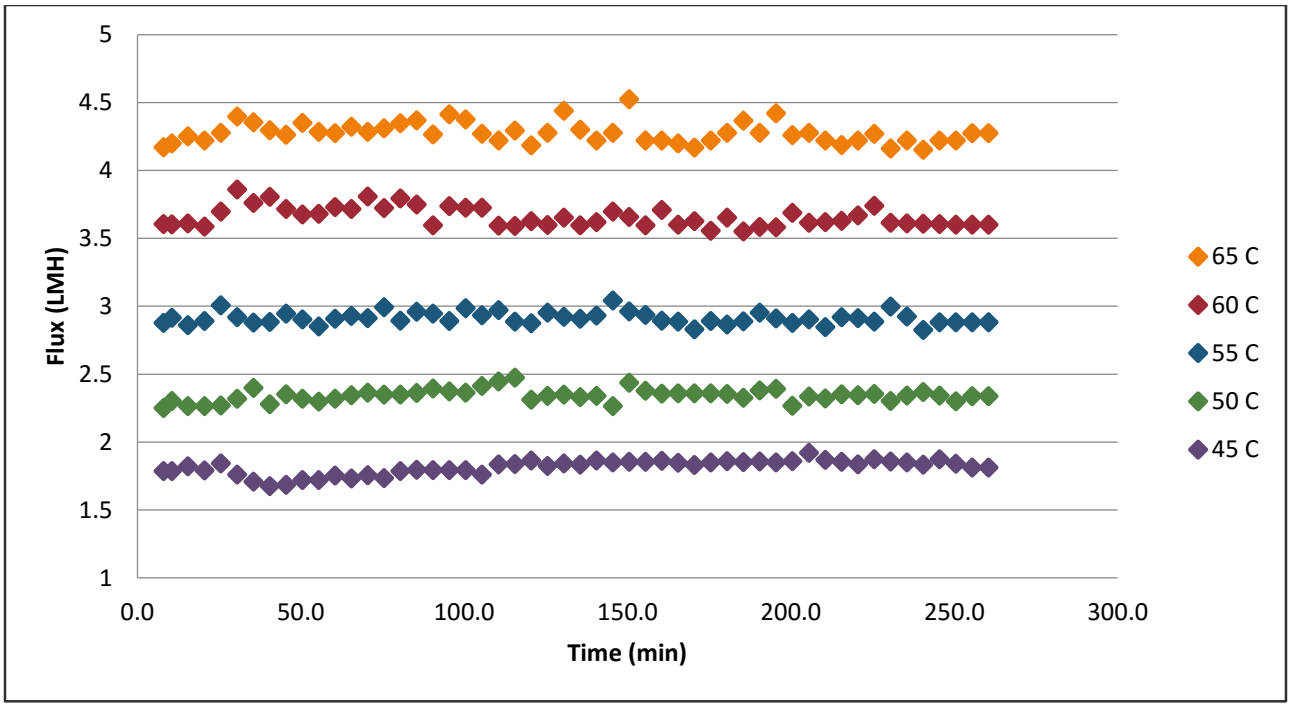

Figure 60: Permeate Flux profile of Hollow Fiber membrane at different feed temperatures (Q= 1.5 LPM, Tp=20 ℃)

Figure (60) represents the effect of changing feed temperature on the permeate flux using hollow fiber membrane. Feed temperatures were varied between (45, 50, 55, 60, and 65 ℃) while the permeate temperature was kept at 20 ℃. Feed and permeate flow rates are maintained at 1.5 LPM.

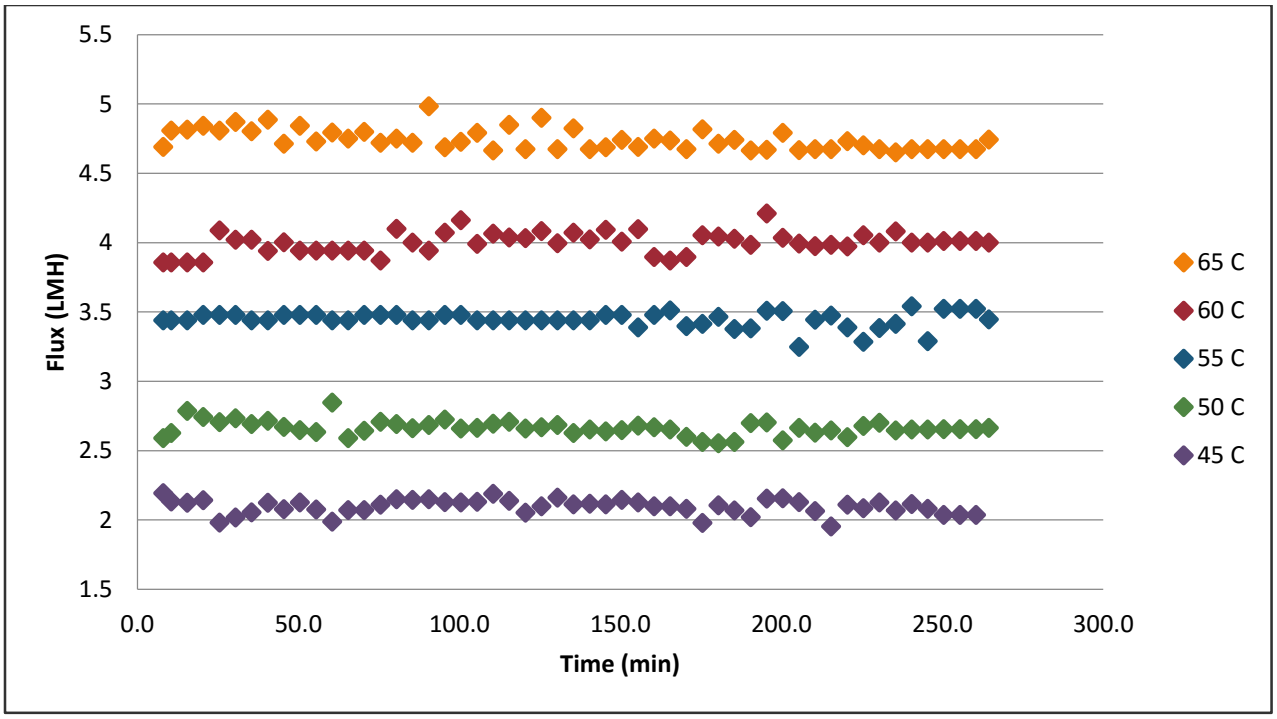

Figure 61: Permeate Flux profile of Hollow Fiber membrane at different feed temperatures (Q= 2.0 LPM, Tp=20 ℃)

Figure (61) represents the effect of changing feed temperature on the permeate flux using hollow fiber membrane. Feed temperatures were varied between (45, 50, 55, 60, and 65 ℃) while the permeate temperature was kept at 20 ℃. Feed and permeate flow rates are maintained at 2.0 LPM.

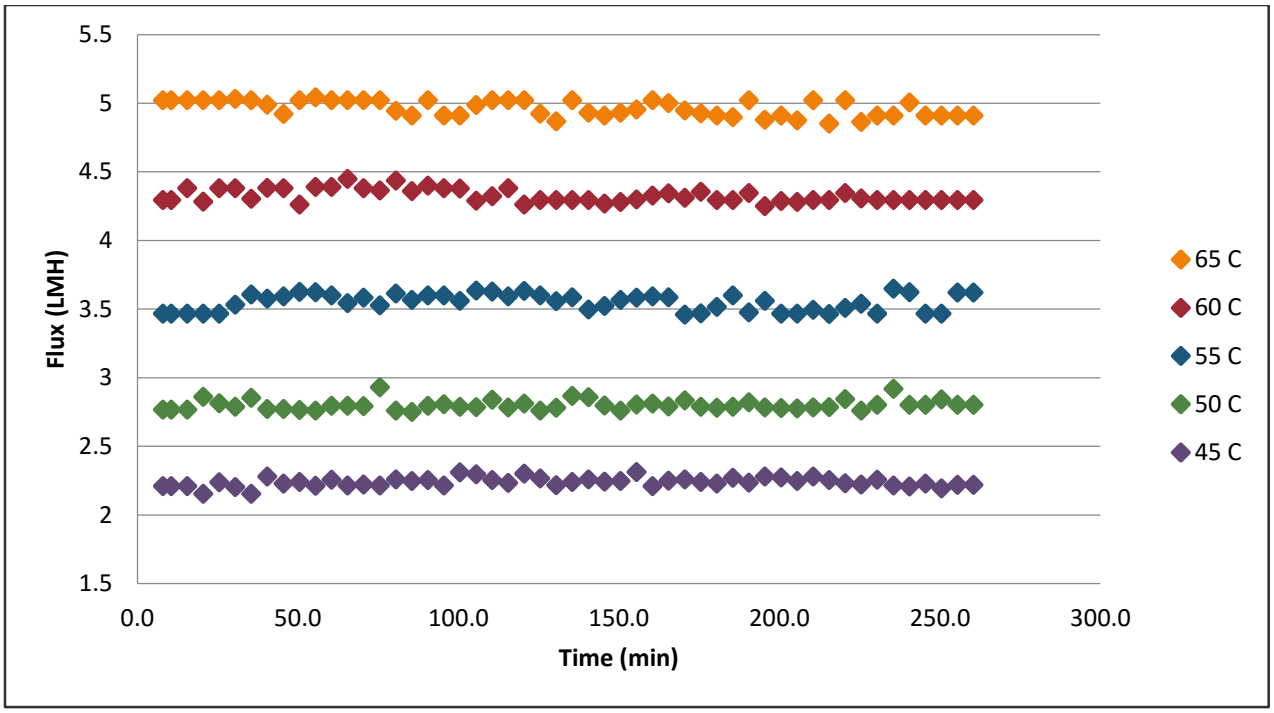

Figure 62: Permeate Flux profile of Hollow Fiber membrane at different feed temperatures (Q= 2.5 LPM, Tp=20 ℃)

Figure (62) represents the effect of changing feed temperature on the permeate flux using hollow fiber membrane. Feed temperatures were varied between (45, 50, 55, 60, and 65 ℃) while the permeate temperature was kept at 20 ℃. Feed and permeate flow rates are maintained at 2.5 LPM.

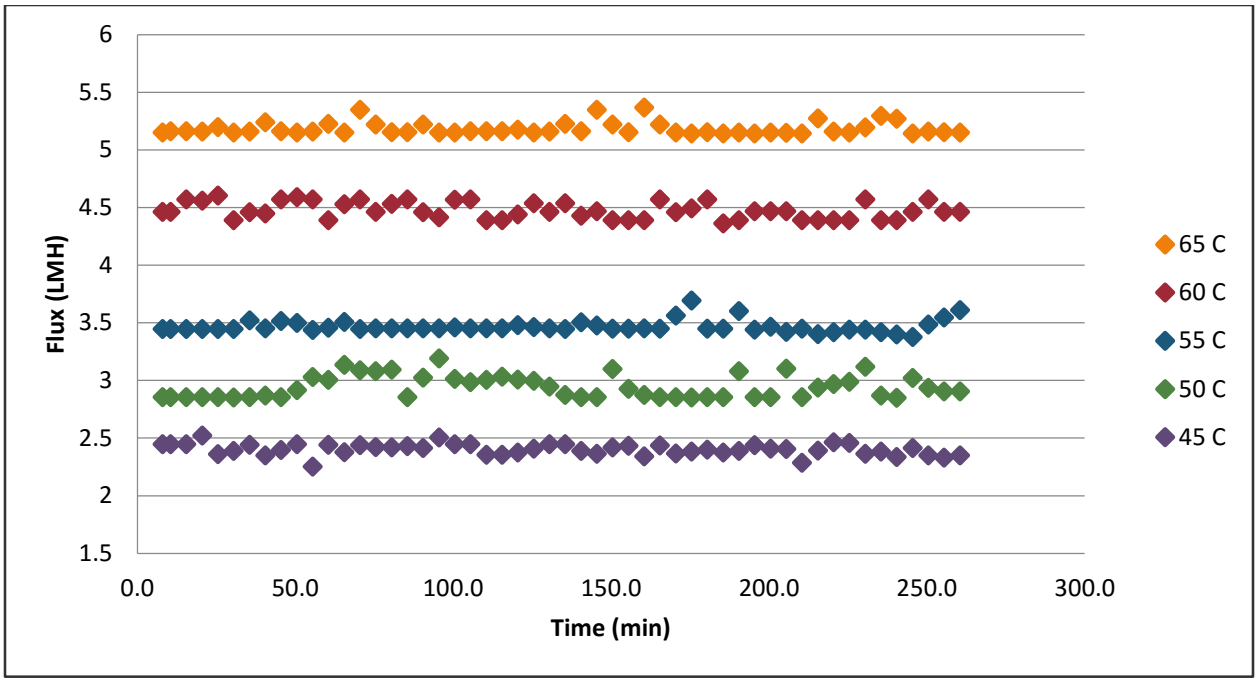

Figure 63: Permeate Flux profile of Hollow Fiber membrane at different feed temperatures (Q= 3.0 LPM, Tp=20 ℃)

Figure (63) represents the effect of changing feed temperature on the permeate flux using hollow fiber membrane. Feed temperatures were varied between (45, 50, 55, 60, and 65 ℃) while the permeate temperature was kept at 20 ℃. Feed and permeate flow rates are maintained at 3.0 LPM.

All feed inlet/outlet temperatures to hollow fiber membrane module during the experimental time and just before shutting-down the apparatus are summarized in table (35) below in addition to temperature difference across the membrane at different feed flowrates.

Table 35: Hollow Fiber Module terminal temperatures

Feed Flowrate (LPM)	Feed Inlet Temperature (℃)	Feed Outlet Temperature (℃)	ΔT
1.5	46.00	40.90	5.10
	50.70	46.00	4.70
	55.40	50.40	5.00
	59.80	53.00	6.80
	65.30	58.40	6.90
2.0	45.60	42.00	3.60
	51.20	47.10	4.10
	55.40	50.20	5.20
	60.40	55.10	5.30
	65.10	59.60	5.50
2.5	46.10	42.80	3.30
	50.90	47.30	3.60
	55.50	51.70	3.80
	60.20	55.90	4.30
	65.10	60.60	4.50
3.0	46.60	44.00	2.60
	51.10	48.20	2.90
	56.00	52.90	3.10
	60.80	57.60	3.20
	64.80	60.70	4.10

Results showed that temperature difference across the membrane decreases with increasing feed flowrate.

Discussion

All the achieved results from the experimental part are discussed and compared to other literature results in this section below. The results are discussed according to different affecting parameters. Moreover, the heat transport convective study of flow pattern and thermal coefficients calculations is presented in the sections below.

5.2 Permeate Flux Performance

5.2.1 Flat Sheet membrane

The permeate flux performance is studied at different feed temperatures and flowrates of flat sheet membrane of DCMD system. The results of 20 experimental runs are combined and represented in one graph to show the effect of operating conditions.

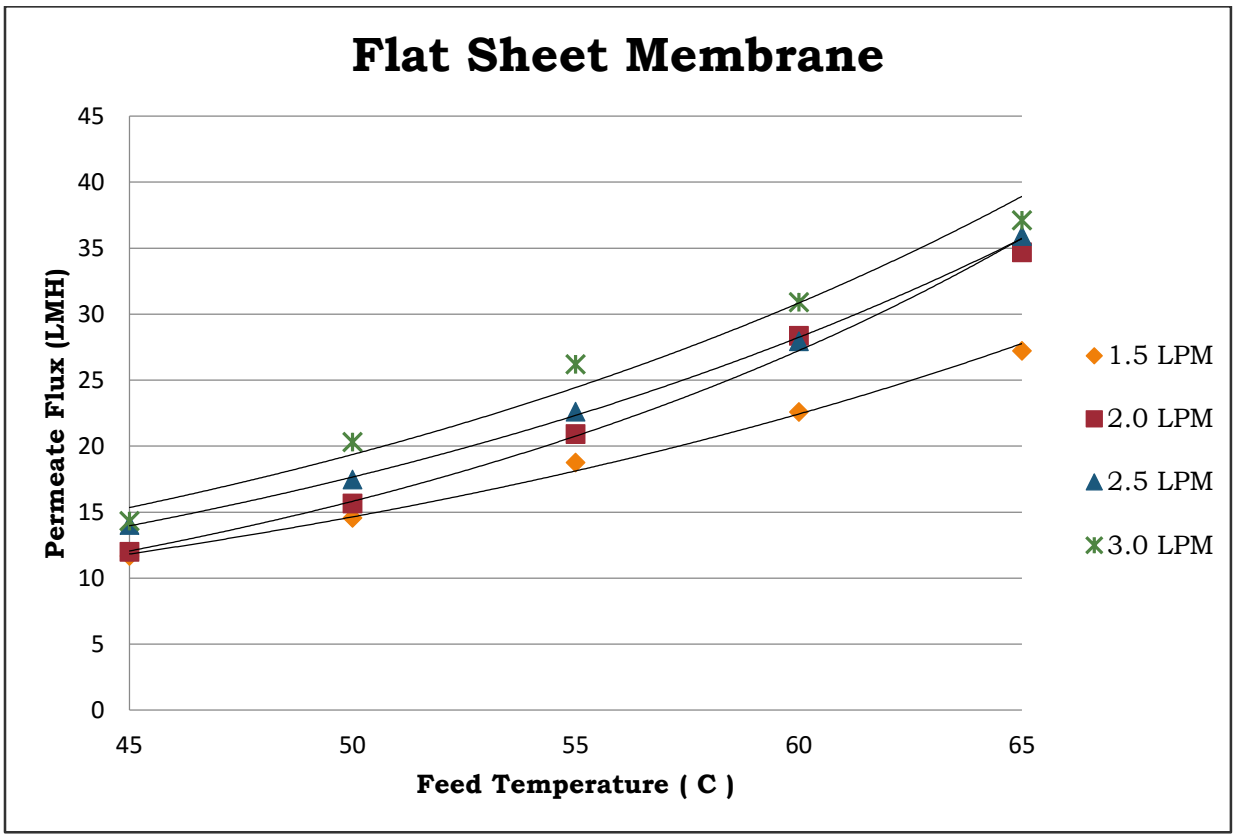

Figure 64: Permeate flux profile of Flat Sheet membrane at different flowrates

Figure (64) shows that feed temperature and flowrate have direct effect on the permeate flux. As feed temperature rises from (45 – 65)℃ , the flux increases. The permeate temperature is kept constant at 20℃. Similar to feed temperature,

increasing feed flow rate will enhance the permeate flux. At lowest feed and permeate flowrates (1.5 LPM) and lowest feed temperature of 45℃, a permeate flux of 12 LMH is achieved. The highest permeate flux that can be achieved in the flat sheet membrane is 37 LMH at feed and permeate flowrates of 3.0 LPM and feed temperature of 65℃. Comparing to literature results, Zhang et al. [154] accomplished a flux of nearly 40 LPM in a spacer filled channel of compressible PTFE membrane. A permeate flux of almost 40 LPM is also obtained by Nguyen et al. [155] at similar operating conditions and they pointed that at higher feed temperatures, membrane wetting started to occur. The results of permeate fluxes obtained from our experiments were in good agreement with the results found in literature [47], [48], [53], [58], [74], [88], [93], [129], [156], [157]. Some researchers found the permeate flux for flat sheet membrane can achieve as high as 190 LPM if operating conditions are wisely chosen [75], [117]. Other results that found in literature are varying a lot from what we have, and this could be due to different operating conditions such as higher or lower flowrates, different membrane materials, different membrane morphology from the one used in our laboratory, and many other factors that affect the flux [52], [68], [158], [159]. As example, a research on LDPE membrane in a spacer-filled channel generate less than 10 LHM flux [38]. At same operating conditions, more than 15 LHM permeate flux is achieved. This conclude that the membrane material is also affecting the flux.

The increase of permeate flux due to higher flowrates is also plotted in figure (64). The flowrates are varying from (1.5 – 3.0) LPM and it is shown that the effect of increasing the flowrate is not as high as the feed temperature effect. The small enhancement of the flux by flowrate related to the increase of Reynolds number. Therefore, heat transfer coefficient became higher and the potential of driving the vapor from feed to distilled is increased. Shim et al. reported that an increase of feed flowrate from 4.5 LPM to 7.0 LPM enhances the flux by almost 20% [156]. Special accurateness of feed and permeate flowrates should be taken into

consideration at lower feed temperature, as specific temperature difference (more than 10) between the hot and cold sides should be maintained [47]. The values of flux affected by feed flowrate and obtained from our experiments are consistent with the majority of literature results [50], [58], [154], [157], [158].

All the operating conditions parameters are further discussed in details and the results are compared to literature results in this section below:

5.2.1.1 Feed Temperature

Starting with feed temperature that has greatest effect on the flux. This is due to exponential relation between vapor pressure and temperature in the Antoine equation [80], [115]. Increasing feed temperature lead to increase the difference of temperatures across the membrane from that generate more flux. This means that the highest fluxes occur at high feed temperature and low permeate temperature. However, the relation is not directly proportional and this is due to temperature polarization that lower the flux [88]. In general, the highest amount of flux is generated at high feed temperatures (60 – 85℃). Alkhudhiri et al. also shows that permeate flux production is more depended on the feed temperature than permeate temperature by keeping constant temperature difference across the membrane will generate more flux at higher feed temperature [35]. In addition, Srisurichan et al. pointed that high feed temperature increases mass transfer coefficient leading to higher production of flux [81]. Another factor that lower the flux production is temperature polarization and Phattaranawik et al. [74], [75] believed that at higher feed temperature, the effect of temperature polarization is negligible.

5.2.1.2 Permeate Temperature

As mentioned before, not only the feed temperature can affect the permeate flux, the distilled temperature is also an important factor of enhancement the flux

generation. However, the effect of permeate temperature is not high as feed temperature [35], [47], [50]. Banat and Simandl [116] represent that effect of distilled temperature on permeate flux is almost negligible at constant feed temperature.

5.2.1.3 Feed/Permeate Flowrate

Permeate flux is increasing as the hydrodynamic conditions increase. As feed velocity increases, fluid mixing is improved in the channel by increasing the turbulence and minimizing the dead zones [80]. By increasing the flowrates, flow velocities are increased. Higher velocities decrease temperature boundary layer resistance across the membrane hence, reduce the effect of temperature and concentration polarization on the flux. As a result, heat transfer coefficients are increased, producing more permeate flux [6], [81], [118]. Bouchrit et al. [42] noticed in his study that a linear increasing of flux occurs when both the permeate and flux flowrates increase. Alike the feed flowrate, permeate flowrate is also affecting the flux. However, enhancing only the cold side flowrate is showing negligible effect on the flux [35].

5.2.1.4 Turbulent Promoter (Spacer)

A polymeric (PP) mesh spacer is used for flat sheet membrane in order to increase the turbulence of the flow and reduce temperature and concentration polarization effect. Spacer's function was not only increasing heat transfer coefficients, but also increasing flow velocity inside the compartment. A study was done by Manawi et al. [47] showing that an increase of about 50% of the flux occur when a spacer is introduced to the system under identical operating conditions. Different spacer characteristics are explained previously in section (4.4.7) in **chapter 4**.

5.2.1.5 Flow Configuration

A counter-current flow configuration was used for the system as it was investigated by Manawi et al. [47] in a previous research that the flux is enhanced by 6% when counter-current system is used.

5.2.2 Hollow Fiber membrane

The permeate flux performance is studied at different feet temperatures and flowrates of hollow fiber membrane of DCMD system. The results of 20 experimental runs are combined and represented in one graph to show the effect of operating conditions.

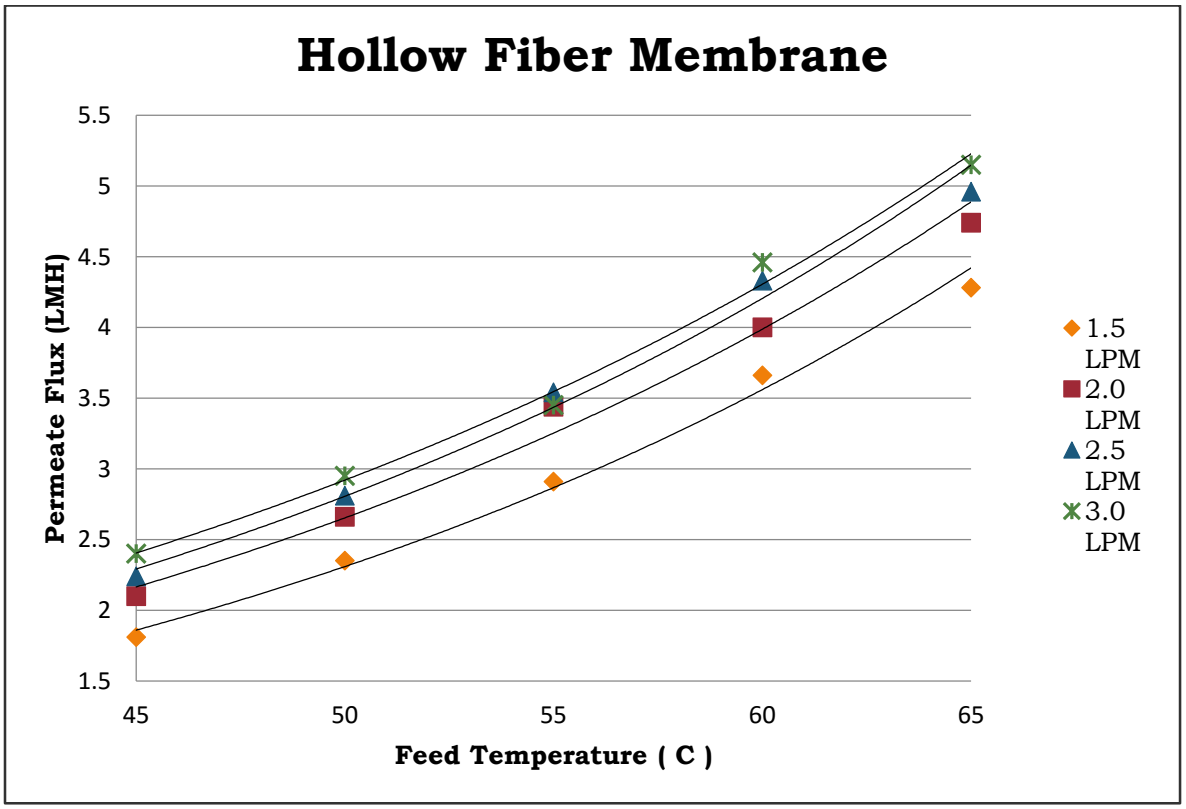

Figure 65: Permeate flux profile of Hollow Fiber membrane at different flowrates

Figure (65) represents the flux profile as a function of feed temperature and flowrate. These two parameters have direct effect on the permeate flux. As feed temperature rises from (45 – 65)℃ , more permeate flux is generated. The permeate temperature is kept constant at 20℃. Similar to feed temperature, increasing feed flow rate will enhance the permeate flux. At lowest feed and permeate flowrates (1.5 LPM) and lowest feed temperature of 45℃, a permeate flux of 1.8 LMH is achieved. The highest permeate flux that can be achieved in the flat sheet membrane is 5.2 LMH at feed and permeate flowrates of 3.0 LPM and feed temperature of 65℃. Experiments with similar operating conditions and PP membrane material conducted by Chung et al. [128] accomplished exactly same results that are doubled when feed temperature reached 80℃. Permeate flux in hollow fiber membrane can exceed 38.0 LMH at 85℃ feed temperature [101]. Mainly, the results obtained for hollow fiber flux are consistent with many results found in literature [46], [98], [107], [108], [126]. As feed temperature is the most important factor affecting the flux, the porosity in hollow fiber membrane has essential impact. Lower permeate fluxes even at higher feed temperature were found in these researches where low porosity membranes are used [39], [49], [79].

It is also shown in figure (65) that the permeate flux is less affected by feed and permeate velocities at high values of flowrates.

All the operating conditions parameters are further discussed in details and the results are compared to literature in the sections below:

5.2.2.1 Feed Temperature

Starting with feed temperature that has great effect on the flux. This is due to exponential relation between saturated vapor pressure and temperature in the Antoine equation. As vapor pressure difference across the membrane increases, more flux is achieved. Related to the equation, a parabolic curve of permeate flux occur as the temperature increases. The highest amount of flux is achieved near

the boiling point temperature. However, as high feed temperature produces more flux, more heat transfer to the permeate side rising the temperature of the distilled. As permeate temperature rises, flux production drops [135]. This shows that all condition parameters in hollow fiber membranes are connected together. In addition to condition parameters, membrane morphology helps achieving better results. Cheng et al. [100] explained in his research that increasing feed temperature won't affect the flux with long membrane fibers. As the membrane increases in length, less flux is generated. Geng et al. [160], [161] found that flux is declining slowly with increasing the length of membrane to reach 30 cm. At a length greater than 30 cm, insignificant amount of flux is generated. The reason behind flux declining is that feed temperature difference between inlet and outlet decreases with increasing fiber length [108], [154], [157]. Consequently, the driving force decreases. Therefore, flux increment is affected by fiber length and the optimum length should be chosen. Hollow fiber membrane material, [46], [161] the number of membrane modules [162] and many other factors are also affecting the permeate flux at high feed temperature.

5.2.2.2 Permeate Temperature

As mentioned before, not only the feed temperature can affect the permeate flux, the distilled temperature is also an important factor of enhancement the flux generation in hollow fiber membranes. However, the effect of permeate temperature is not high as feed temperature. In some researches where very low permeate temperature is used (8.6℃), mass flux can be doubled [100].

5.2.2.3 Feed/Permeate Flowrate

In hollow fiber membrane module, flowrate is more affecting parameter than in flat sheet membrane. Permeate flux is affected as the hydrodynamic conditions change. However, the permeate temperature and flowrate is not affecting the

production flux a feed temperature and flowrate do. Therefore, enhancement of flux according to permeate can occur only at very high permeate flowrate or very low permeate temperature [135]. By increasing the flowrates, flow velocities are increased affecting Reynolds numbers and hence the heat transfer coefficients [105]. As thermal convective parameters rise; more production of flux occurs.

As vapor molecule pass through the membrane from the hot side to the cold side, the temperature at the surface of membrane became lower that the temperature at feed bulk creating a boundary layer. This phenomenon is called temperature polarization and it decreases the tendency of flux generation. Song et al. [135] explained in this research that increasing feed flowrate minimizes the boundary layer leading to higher flux production. Nevertheless, Yang et al. [126] mentioned that there is no advantage of increasing the flowrate if the flow reached turbulent regime as the flux would not change much.

Song et al. [135] reported in his research that the permeate flux can be doubled when feed velocity increases four times at high feed temperature. However, increasing the flowrate in hollow fiber module can be a critical issue. From one side, it minimizes temperature polarization and from the other side increasing the flowrate lower the residence time and increase feed average temperature. As a result, reducing the retention time along the module, higher temperature difference across the membrane. As a consequence, more flux is generated. For this reason, only the optimum flowrate can enhance the flux. In addition to this, Cheng et al. [109] reported that the increase of flux due to permeate flowrate is temporary. After a while, flux starts to decline if permeate flowrate is increasing more than the feed flowrate. It happens due to the geometry of hollow fiber and the changes of temperature along fiber length. Maximum flux occurs at the inlet of permeate stream where large ΔT between hot and cold temperatures, then the flux starts to decline. Eventually, each hollow fiber modules with different dimensions has its optimum permeate flowrate that produce the highest flux.

Novel techniques are investigated to increase the turbulence in hollow fiber modules. These new designs implement spacers, different baffles, and improved hollow fibers such as twisted and braided fibers. These modified hollow fiber membranes can enhance the permeate flux up to 36% and in some specific designs up to 90% [84], [85].

5.2.2.4 Flow Configuration

A counter-current flow configuration was used for hollow fiber membrane system as it was investigated by Sirkar [79] in a research that counter-current configuration in hollow fiber membranes generates more flux than co-current flow under the same operating conditions.

5.3 Comparison of Permeate Flux

In this section the permeate flux profiles of flat sheet membrane and hollow fiber membrane at identical operating conditions are graphically represent on one graph for an easy comparison between them. Similar graphs are conducted for each flowrate.

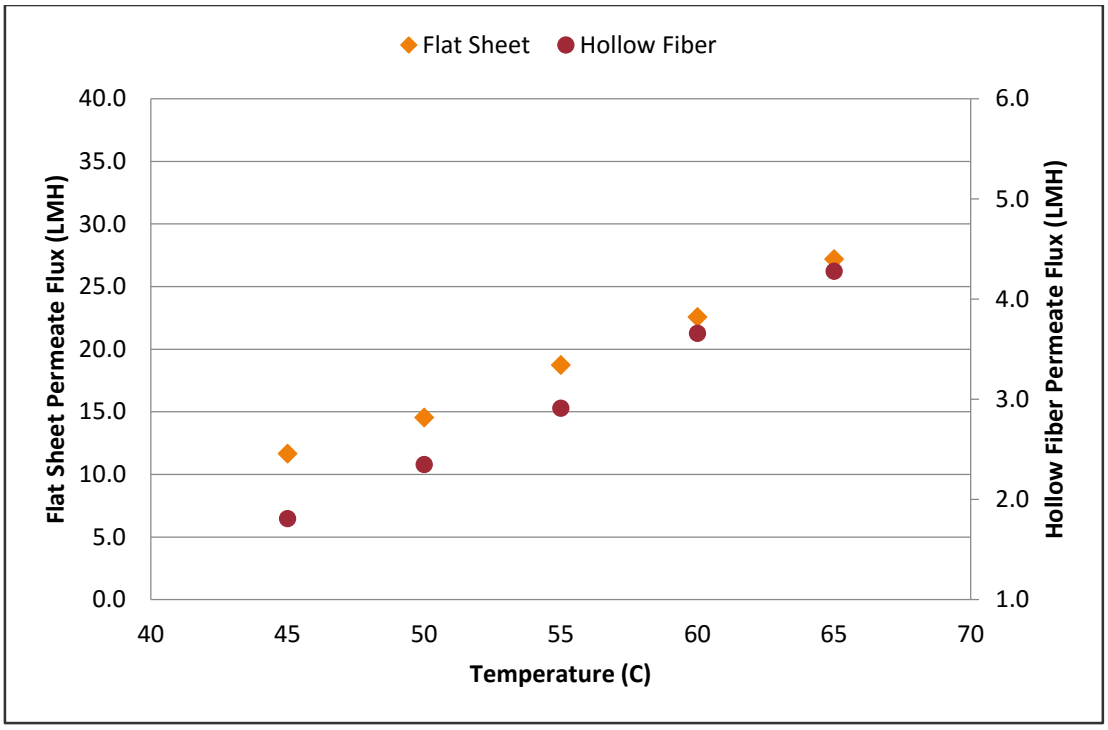

Figure 66: Comparison of permeate flux between flat sheet membrane and hollow fiber membrane at flowrate (1.5 LPM)

In figure (66) above, a comparison between flat sheet membrane and hollow fiber membrane is made in terms of permeate flux generation. All the experiments were conducted at identical operating conditions of temperatures and flowrates. At a flowrate of 1.5 LPM and feed temperature of 65℃ flat sheet membrane can generate permeate flux of (27.2 L/m^2.h) which is almost 6 times higher the flux of hollow fiber membrane (4.3 L/m^2.h).

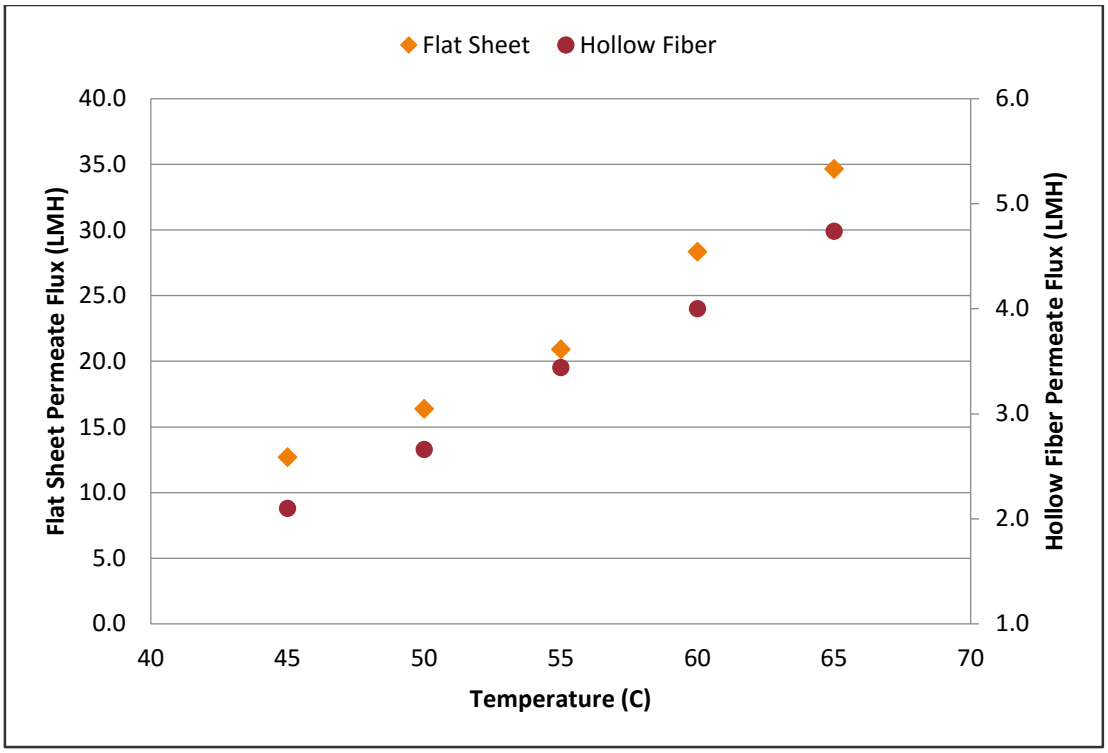

Figure 67: Comparison of permeate flux between flat sheet membrane and hollow fiber membrane at flowrate (2.0 LPM)

In figure (67) below, a comparison between flat sheet membrane and hollow fiber membrane is made in terms of permeate flux generation. All the experiments were conducted at identical operating conditions of temperatures and flowrates. At a flowrate of 2.0 LPM and feed temperature of 65℃ flat sheet membrane can generate permeate flux of (34.7 L/m^2.h) which is almost 7 times higher the flux of hollow fiber membrane (4.7 L/m^2.h).

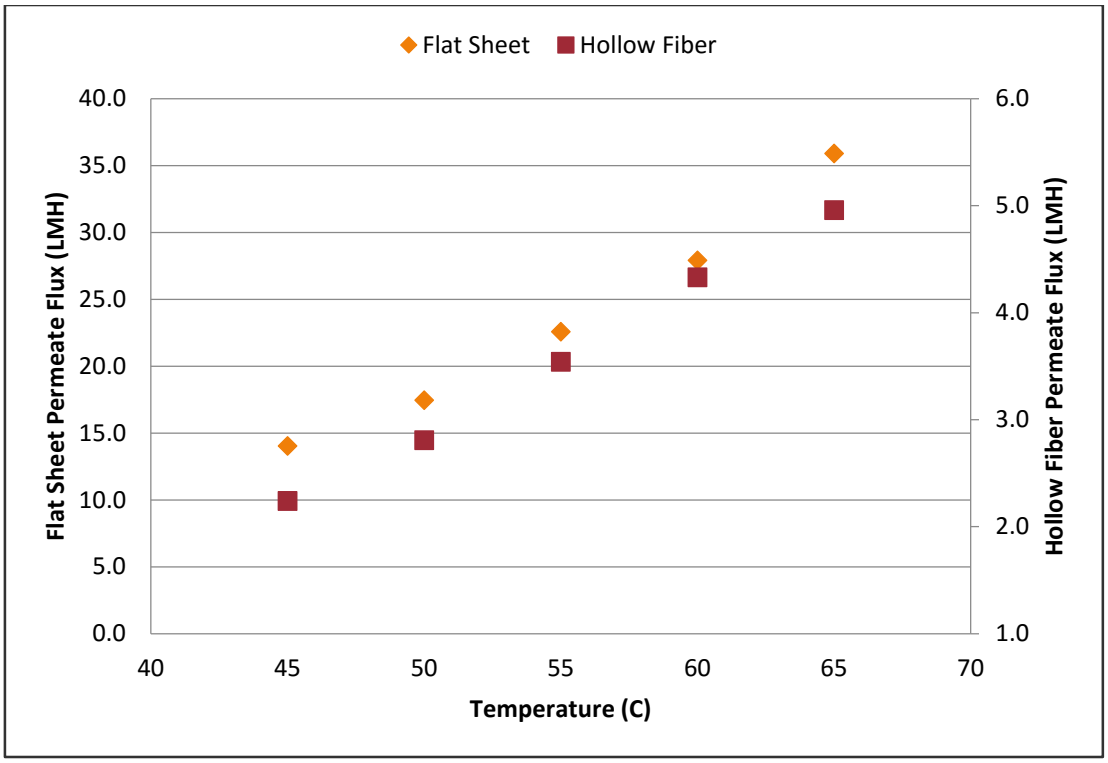

Figure 68: Comparison of permeate flux between flat sheet membrane and hollow fiber membrane at flowrate (2.5 LPM)

In figure (68) above, a comparison between flat sheet membrane and hollow fiber membrane is made in terms of permeate flux generation. All the experiments were conducted at identical operating conditions of temperatures and flowrates. At a flowrate of 2.5 LPM and feed temperature of 65℃ flat sheet membrane can generate permeate flux of (36.0 L/m^2.h) which is almost 7 times higher the flux of hollow fiber membrane (5.0 L/m^2.h).

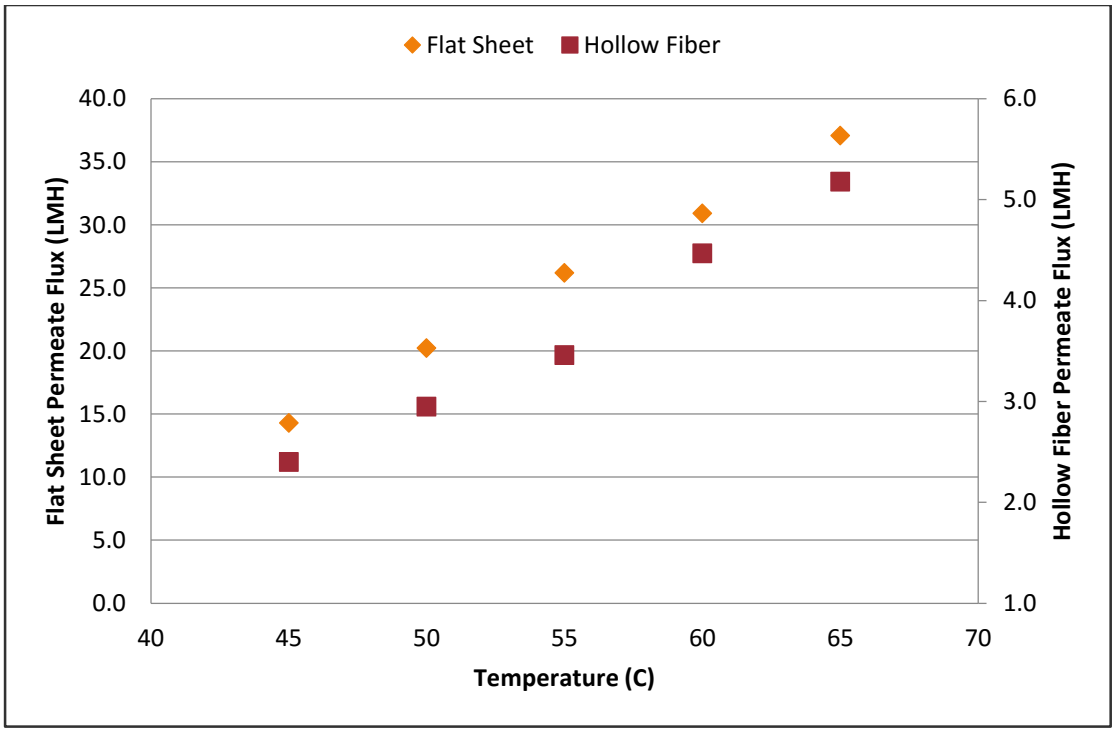

Figure 69: Comparison of permeate flux between flat sheet membrane and hollow fiber membrane at flowrate (3.0 LPM)

In figure (69) above, a comparison between flat sheet membrane and hollow fiber membrane is made in terms of permeate flux generation. All the experiments were conducted at identical operating conditions of temperatures and flowrates. At a flowrate of 3.0 LPM and feed temperature of 65℃ flat sheet membrane can generate permeate flux of (37.1 L/m^2.h) which is almost 7 times higher the flux of hollow fiber membrane (5.2 L/m^2.h).

5.4 Convective Heat Transfer Study

This section will discuss the generated amounts of permeate flux from the experimental part and relate it to theoretical aspects (section 3.4). In order to understand and compare the obtained results to literature and other studies, the factors leading to flux enhancement were studies and explained. The factors

include operating conditions such are feed temperature and flowrate and how they will affect the dimensionless numbers (Re, Nu, Pr) hence the permeate flux. First of all, dimensionless numbers (Re, Pr) are calculated according to various operating conditions. Prandtl number (Pr) depends on fluid properties, so it will be affected by changing feed temperature. Reynolds number (Re) will be influenced by feed temperature and feed flowrate. A proper correlation for Nusselt number (Nu) is chosen depending on Reynolds number (Re) and operating conditions in order to evaluate the heat transfer coefficients (h), W/m^2 K. The improvement of permeate flux generation is directly related to heat transfer coefficients. Therefore, the effect of each parameter will be studied separately later in this chapter. Also, the effect of flow patter and membrane configuration is taking into account. All the calculations steps are applied on flat sheet membrane and hollow fiber membrane. For flat sheet membrane, the turbulent promoter (spacer) is also considered as an important factor of affecting heat transfer coefficients. All the studies factors can be summarized as:

- The effect of temperature
- The effect of flowrate
- The effect of module configuration and turbulent promoter

The effect of each factors will be applied on flat sheet and hollow fiber membranes where the results will be present, analyzed and compared to other studies and researches.

5.4.1 Flat Sheet membrane

5.4.1.1 Reynolds Number, Re

Reynolds Number (Re) is calculated for flat sheet membrane experiments at different flowrates using equation (14) mentioned before in Heat Transfer section in **Chapter 3**. The procedure of calculating Re numbers is explained in details in the Approach section in **Chapter 4**. Table (34) listed the calculated values of

Re numbers for feed temperature of 65 ℃ only. However, Re numbers are calculated for all feed temperatures (45, 50, 55, 60, and 65 ℃).

Table 36: Reynolds number at different flowrates of flat sheet membrane at 65 ℃

Flow Rate (LPM)	Flow Velocity (m/s)	Reynolds Number
1.5	0.15	283
2.0	0.20	513
2.5	0.25	641
3.0	0.30	770

Table 36 represents Reynolds Number (Re) of spacer-filled channel with flat sheet membrane at 65 ℃. It is observed that Reynolds number increases with increasing the flowrate. Experiments show that Reynolds number occur between **283** and **770** for five different temperatures (45, 50, 55, 60, and 65 ℃) and four flowrates (1.5, 2.0, 2.5, and 3.0 LPM). Even though, Reynolds number is low and fit in the laminar region, turbulent model is more applicable [154]. Therefore, the flow pattern is assumed to be transition to turbulent flow. Shakaib et al. [151] reported for spacer-filled channel that Re number laid between (115 – 800) for a velocity of (0.05 – 0.35 m/s) and the turbulent model is applied when velocity is higher than 0.15 m/s. The values of Reynolds number are consistent with literature results [118], [129].

5.4.1.2 Heat Transfer Coefficient, h

Heat Transfer Coefficient (*h*) is calculated for flat sheet membrane experiments at different flowrates using equation (13) mentioned before in Heat Transfer section in **Chapter 3**. The procedure of calculating Heat Transfer Coefficient (*h*) is explained in details in the Approach section in **Chapter 4**.

In the figure (70) below, heat transfer coefficient is evaluated for flat sheet spacer-filled channel at different flowrates (1.5, 2.0, 2.5, and 3.0 LPM) for five different temperatures (45, 50, 55, 60, and 65 ℃).

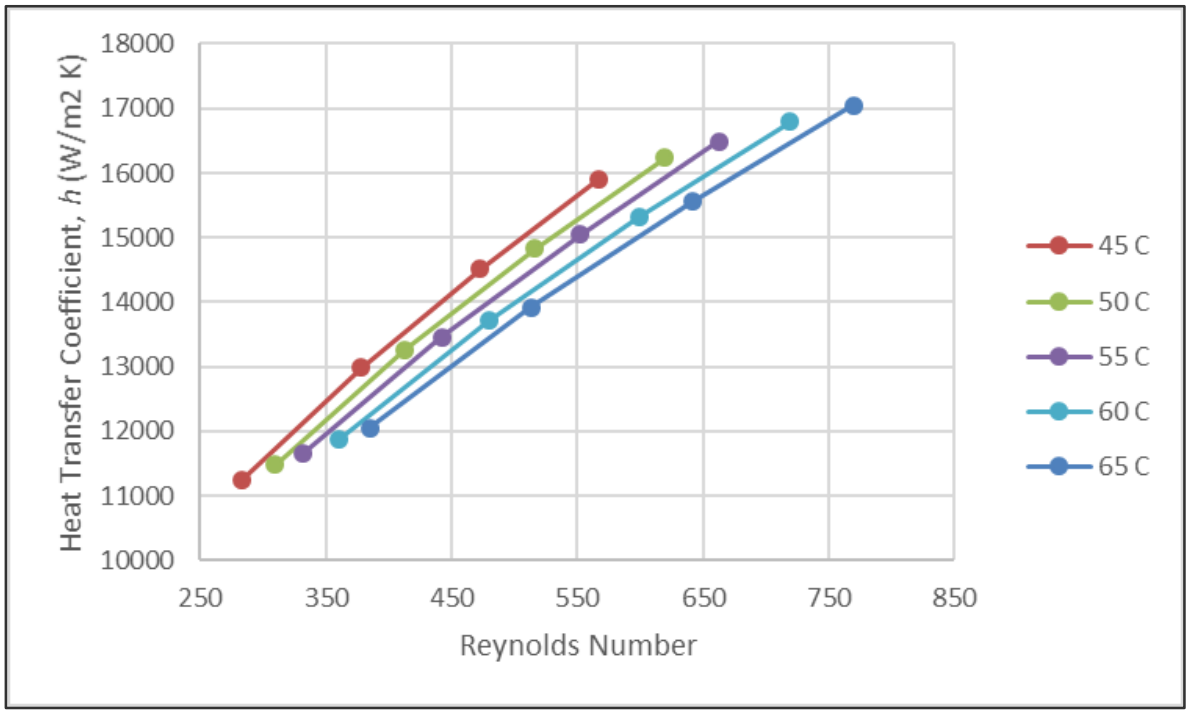

Figure 70: Heat Transfer Coefficient for flat sheet membrane at different flowrates and temperatures

Reynolds number has a proportional relationship with feed temperature and feed flowrate, therefore heat transfer coefficient is increased. Consequently, more permeate flux is generated. The conducted experiments on flat sheet membrane in a spacer-filled channel result heat transfer coefficient of (**11246 - 17044** W/m^2 K) at different feed conditions. Phattaranawik et al. and reported for PTFE flat sheet membrane at similar operating conditions and for turbulent regime that heat transfer coefficient occur between (17026 to 21432 W/m^2 K) for a spacer-filled channel at higher feed temperature [74]. The resulted values of heat

transfer coefficients are reliable and agree with many of literature results [68], [115]. However, for heat transfer coefficient we noticed a scatter in values of thermal coefficients. This is probably due to the many different dimensionless correlations used in order to calculate heat transfer coefficients [47], [58], [163]. Each correlation is valid for a specific range only with particular conditions.

APPENDIX D summaries different heat transfer coefficients found in literature for flat sheet membrane.

5.4.1.3 Prandtl number, Pr

As Prandtl number depends on the physical properties of seawater, it will change according to seawater feed temperature. Feed temperature ranges from 45 – 65℃ in flat sheet membrane system and Prandtl number decrease from 4.3 to 3.0 as feed temperature became higher.

5.4.2 Hollow fiber membrane

5.4.2.1 Reynolds Number, Re

Reynolds Number (Re) is calculated for hollow fiber membrane experiments at different flowrates using equation (14) mentioned before in Heat Transfer section in **Chapter 3**. The procedure of calculating Re numbers is explained in details in the Approach section in **Chapter 4**. Table (35) listed the calculated values of Re numbers for feed temperature of 65 ℃ only. However, Re numbers are calculated for all feed temperatures (45, 50, 55, 60, and 65 ℃).

Table 37: Reynolds number at different flowrates of hollow fiber membrane at 65 ℃

Flow Rate (LPM)	Flow Velocity (m/s)	Reynolds Number
1.5	0.07	143
2.0	0.09	191
2.5	0.11	239
3.0	0.14	287

Table 37 represents Reynolds Number (Re) of spacer-free channel with hollow fiber membrane at 65 ℃. As in flat sheet membrane, Reynolds number increases with increasing the flowrate. Experiments show that Reynolds number occur between **106** and **287** for five different temperatures (45, 50, 55, 60, and 65 ℃) and four flowrates (1.5, 2.0, 2.5, and 3.0 LPM). Similar for flat sheet membrane, the flow fits the transitional to turbulent regime even though Re was less than 300. Bui et al. related the small values of Reynolds number due to the tortuosity of hollow fibers that produce more turbulence [106]. Another comparison of Reynolds number proposed by Geng et al. where AGMD for PP membrane with similar operating conditions and it was found that Re occur in the range of (46 – 153) [160]. For our hollow fiber membrane, the calculated Reynolds numbers are consistent with the majority of literature results [72], [79], [105], [107].

5.4.2.2 Heat Transfer Coefficient, h

Heat Transfer Coefficient (*h*) is calculated for hollow fiber membrane experiments at different flowrates using equation (13) mentioned before in Heat Transfer section in **Chapter 3**. The procedure of calculating Heat Transfer Coefficient (*h*) is explained in details in the Approach section in **Chapter 4**.

In figure (71) below, heat transfer coefficient is evaluated for hollow fiber spacer-free channel at different flowrates (1.5, 2.0, 2.5, and 3.0 LPM) for five different temperatures (45, 50, 55, 60, and 65 ℃). All the performed experiments on

hollow fiber membrane at different operating conditions result heat transfer coefficients in the range of (**1385 – 2163** W/m^2 K). X. Yang et al. provided an increase of heat transfer coefficient by 60% when curly fibers are used instead of randomly packed module [85]. Moreover, heat transfer coefficient can reach (3150 and 3750 W/m^2 K) respectively, when window baffled and helical baffled modules are introduced to the system at high flowrates [84]. As for flat sheet membrane, a scatter in values of heat transfer coefficients occur for hollow fiber membrane due to the variety of correlations used [72], [108], [164].

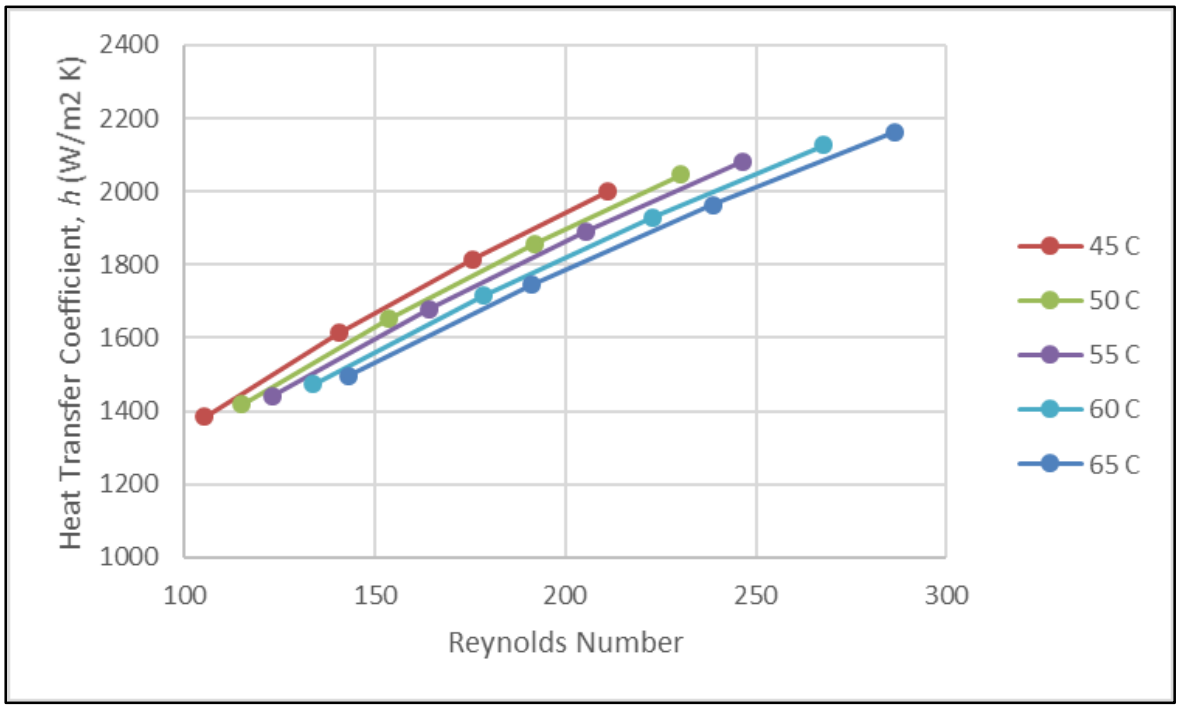

Figure 71: Heat Transfer Coefficient for hollow fiber membrane at different flowrates and temperatures

APPENDIX D summaries different heat transfer coefficients found in literature for hollow fiber membrane.

5.4.2.3 Prandtl number, Pr

As Prandtl number depends on the physical properties of seawater, it will change according to seawater feed temperature. Feed temperature ranges from 45 – 65 ℃ in hollow fiber membrane system and Prandtl number decrease from 4.3 to 3.0 as feed temperature became higher.

5.5 Summary of Results

In this section a summary of the achieved results of flat sheet membrane and hollow fiber membrane is conducted in order to evaluate the difference between two membranes.

The table (38) below summarizes all the significant results obtained from hollow fiber and flat sheet membranes for a complete comparison.

Table 38: Summary Table of flat sheet and hollow fiber results

	Hollow Fiber Membrane	Flat Sheet Membrane
Minimum Flux ($L/m^2.h$)	1.8	11.7
Maximum Flux ($L/m^2.h$)	5.2	37.1
Flow Velocity (m/s)	0.07 – 0.14	0.15 – 0.30
Re	106 – 287	283 – 770
Nu	2 – 3	22 – 33
h (W/m^2 K)	1385 – 2163	11246 – 17044

It was found that the flux for hollow fiber membrane at lowest feed temperature and lowest flowrate was (1.8 $L/m^2.h$) while the flux for flat sheet membrane at the same conditions was (11.7 $L/m^2.h$). At the highest operating conditions, the

flux for hollow fiber membrane was (5.2 L/m^2.h) while the flux for flat sheet membrane at the same conditions was (11.7 L/m^2.h). This represents a big difference between the two membranes where flat sheet produces nearly 7 times higher flux due to difference in flow regime as discussed before. Increasing feed temperature by increment of 5℃, results similar increase in the flux for flat sheet and hollow fiber membranes. For hollow fiber membrane, an increment of 5℃ of feed temperature results (15 – 30%) increase of the flux. For flat sheet membrane, an increment of 5℃ of feed temperature results (18 – 42%) increase of the flux.

The flowrate for the two membranes was identical in a range of (1.5 – 3.0 LPM). However, the permeate flux is slightly affected by the operating flowrate. For hollow fiber membrane, an increment of 0.5 L/min of operating flowrates results an average increase of permeate flux by 4%. For flat sheet membrane, an increment of 0.5 L/min of operating flowrates results an average increase of permeate flux by 8%.

However, the velocity in hollow fiber compartment was half the velocity with flat sheet membrane due to the morphology in hollow fiber module. Therefore, the feed Reynolds numbers in flow channel ranged between 283 to 770 for the flat sheet module while the Reynolds numbers ranged between 106 to 287 for the hollow fiber module. In addition to flow parameters, the convective heat transfer coefficients in the hot side is much greater in the flat sheet module than in the hollow fiber module. It is indicated by Nusselt number (Nu) that is 11 times higher for the flat sheet module than for the hollow fiber in the hot side of the membrane. The maximum hot side convective heat transfer coefficient for the flat sheet module was estimated to be 17044 W/m^2.h compared to 2163 W/m^2.h for the hollow fiber module. As heat transfer coefficients increases, heat transfer resistance (boundary layer) decreases. Therefore, more mass transfer occurs between the membrane.

5.6 Water Quality Analysis

In this section, the quality of the permeate water collected from DCMD system with flat sheet and hollow fiber membranes is analyzed. Water quality analysis includes Inductively Coupled Plasma – Optical Emission Spectroscopy (ICP – OES) analysis, Ion Chromatography (IC) analysis, pH and electrical conductivity measurements, and salt rejection calculations.

5.6.1 Anions/Cations Analysis

Water quality analysis of Inductively Coupled Plasma – Optical Emission Spectroscopy (ICP – OES) and Ion Chromatography (IC) is conducted on the permeate water achieved by bench-scale DCMD system using flat sheet and hollow fiber membranes. The analysis is carried out on permeate water generated at different operating conditions. ICP and IC analysis were conducted on whole samples of permeate water. Some of water quality analysis of randomly chosen experiments conducted by ICP and IC are summarized in tables (39 – 41).

Table 39: Chemical Analysis of the permeate at feed temperature of 45℃ and 1.5 LPM flowrate

Composition	Hollow Fiber Concentration level (mg/L)	Flat Sheet Concentration level (mg/L)
Anions		
Chloride	12.029	0.138
Sulphate	UDL	UDL
Cations		
Calcium	0.21	0.06
Sodium	9.03	UDL
Magnesium	0.07	0.02
Potassium	0.21	0.10
pH	5.9	6.76
Conductivity ($\mu s/cm$)	51.16	2.07

Table (39) represents the chemical analysis conducted on the permeate water generated at experimental conditions of 45℃ feed temperature and 1.5 LPM flowrate using both flat sheet and hollow fiber membranes. Distilled cooling water is at 20℃. At these experimental operating conditions, the conductivity of the permeate achieved by hollow fiber membrane is approximately 25 times higher than the conductivity of permeate achieved by flat sheet membrane.

The analysis showed that using flat sheet membranes provides higher distilled water quality in terms of electrical conductivity. Moreover, more cations and anions are present in the distilled water generated by the hollow fiber membrane than flat sheet membrane. Some compositions concentration is under the detection limit of ICP-OES device. Table (42) listed the detection limits of some elements for the ICP-OES apparatus.

Table 40: Chemical Analysis of the permeate at feed temperature of 55℃ and 2.0 LPM flowrate

Composition	Hollow Fiber Concentration level (mg/L)	Flat Sheet Concentration level (mg/L)
	Anions	
Chloride	4.858	0.119
Sulphate	UDL	UDL
	Cations	
Calcium	0.08	0.03
Sodium	3.19	UDL
Magnesium	0.25	0.02
Potassium	0.24	0.05
pH	5.81	5.76
Conductivity ($\mu s/cm$)	23.32	1.83

Table (40) represents the chemical analysis conducted on the permeate water generated at experimental conditions of 55℃ feed temperature and 2.0 LPM flowrate using both flat sheet and hollow fiber membranes. Distilled cooling

water is at 20℃. At these experimental operating conditions, the conductivity of the permeate achieved by hollow fiber membrane is approximately 13 times higher than the conductivity of permeate achieved by flat sheet membrane.

Table 41: Chemical Analysis of the permeate at feed temperature of 65℃ and 3.0 LPM flowrate

Composition	Hollow Fiber Concentration level (mg/L)	Flat Sheet Concentration level (mg/L)
	Anions	
Chloride	28.557	0.399
Sulphate	0.230	UDL
	Cations	
Calcium	0.39	0.06
Sodium	16.93	UDL
Magnesium	1.27	0.04
Potassium	0.86	0.08
pH	5.95	5.05
Conductivity ($\mu s/cm$)	84.07	3.30

Table (41) represents the chemical analysis conducted on the permeate water generated at experimental conditions of 65℃ feed temperature and 3.0 LPM flowrate using both flat sheet and hollow fiber membranes. Distilled cooling water is at 20℃. At these experimental operating conditions, the conductivity of the permeate achieved by hollow fiber membrane is approximately 25 times higher than the conductivity of permeate achieved by flat sheet membrane.

Table 42: The ICP-OES Detection Limits

Element	Detection Limit (mg/L)	Element	Detection Limit (mg/L)
Al	0.23	**Mn**	0.01
Ca	0.15	**Na**	0.04
Cu	0.01	**Ni**	0.01
K	0.08	**Ti**	0.04
Mg	0.00	**Zn**	0.28

The minimum electrical conductivity achieved by flat sheet membrane is 1.83 $\mu S/cm$. For flat sheet membrane, the electrical conductivity does not exceed 5 $\mu S/cm$. The minimum electrical conductivity achieved by hollow fiber membrane is 23.32 $\mu S/cm$. The average electrical conductivity achieved by hollow fiber membrane is 40 $\mu S/cm$ besides it never exceed 100 $\mu S/cm$. The high values of electrical conductivity in hollow fiber membranes present only in the last sets of experiments when membrane wetting start to occur.

Table 43: The compositions of Rayyan Drinking water in Qatar

Composition	Rayyan Water Concentration level (mg/L)
Anions	
Chloride	32
Sulphate	7
Cations	
Calcium	13
Sodium	6
Magnesium	5
Potassium	< 1
pH	7.2

The compositions concentration of Rayyan fresh drinking water of Qatar is represent in table (43) for better understanding and comparison of the achieved results by both membranes.

Rayyan drinking water company is considered as low-sodium product. It is shown from the results that sodium concentration in the permeate water achieved by hollow fiber membrane is higher than the amount present in drinking water. However, flat sheet membrane produces extremely clean drinking water. All element concentrations including Sodium concentration fall within the permissible levels of drinking water. The concentration level of sodium in drinking water is suggested by World Health Organization [165] to be 20 mg/L.

All other tested elements concentration present in the permeate water that is produced either by flat sheet or hollow fiber membranes is much lower than the compositions in drinking water. Moreover, the application of desalinated water directly from the sea requires pH adjustments and the addition of some anti-sealants to minimize calcium carbonate precipitation on the membrane hence membrane wetting. [88] Membrane wetting lowers water quality by increasing the electrical conductivity of the permeate.

5.6.2 Salt Rejection

Salt rejection percentage is calculated based on the initial seawater feed concentration and final permeate concentration according to equation (57) mentioned before in **Chapter 3**. Salt Rejection percentage is calculated for four different randomly picked up runs of hollow fiber and flat sheet membranes are represented in table (44).

Table 44: Salt Rejection (%) of Hollow Fiber and Flat Sheet membranes

Run	Salt Rejection (%)	
	Hollow Fiber Membrane	Flat Sheet Membrane
HF6530/FS6530	99.83	99.99
HF5520/FS5520	99.87	99.99
HF4515/FS4515	99.92	99.99
HF5025/FS5025	99.92	99.99

High salt rejection is achieved by using flat sheet (about 100%) and hollow fiber (about 99.9%) membranes in the bench-scale DCMD system.

Francis et al. [46] who studied the different hollow fiber membranes in DCMD system achieved high salt rejection of 99.99%. Similar results are also achieved by Francis et al. [48] studying the desalination of Red sea water by using different flat sheet membranes in DCMD system.

Chapter 6: Conclusions and Recommendations

Membrane Distillation (MD) is a thermally driven membrane separation technology that can take the advantage of low-grade heat produced by various industries. As the low-grade heat is a process byproduct, the integration of membrane distillation system into the industrial site became important in terms of space footprint.

This thesis presented results from a bench-scale Direct Contact Membrane Distillation (DCMD) system for the desalination of real saline water collected from the Arabian Gulf. Two different hydrophobic Polypropylene (PP) membranes configurations which are flat sheet membrane and hollow fiber membranes were used. The main objective of this study was to compare the flux performance of hollow fiber and flat sheet membranes under various operating conditions.

By the end of this research, several conclusions were made:

- Membrane distillation is a viable technology that can produce fresh water from saline water.

After evaluating permeate flux performance of flat sheet and hollow fiber membranes, several conclusions were made:

- Flat sheet membranes generate much higher permeate flux than hollow fiber membrane under various operating conditions. The highest permeate flux achieved by flat sheet membrane is (37.1 $kg/m^2.h$) which approximately 7 times higher than the flux achieved by hollow fiber membrane (5.2 $kg/m^2.h$). Such high difference in permeate flux is referred to the high compactness of hollow fiber membranes.
- The permeate flux increases with increasing feed operating temperature for both, flat sheet membrane and hollow fiber membrane. However, the effect of increasing feed temperature on flux is much greater in flat sheet membrane than hollow fiber membrane. An increment of 5℃ feed temperature results (15 – 30%) increase of the flux in hollow fiber membrane and (18 – 42%) increase of the flux in flat sheet membrane.

- The permeate flux slightly increases with increasing the operating flowrate for both, flat sheet membrane and hollow fiber membrane. Approximately, similar trends occur for both, flat sheet and hollow fiber membranes. An increment of 0.5 L/min of operating flowrates results an average increase of permeate flux of 4% in hollow fiber membrane and 8% increase of the flux in flat sheet membrane.

After evaluating flow patterns and thermal coefficients of the feed side in flat sheet and hollow fiber, the following conclusions were made:

- Hot feed flow velocities in flat sheet and hollow fiber modules were calculated at various operating conditions. The calculated velocity of the flow in flat sheet compartment is twice higher the velocity in hollow fiber module. The lower flow velocity in hollow fiber module happen due to the lack of turbulence promoters or equivalent.
- Reynolds numbers (Re) of hot feed flow in flat sheet compartment and hollow fiber module were calculated. The Reynolds numbers of feed flow in flat sheet compartment ranged between (283 – 770) which is higher than Reynolds numbers in hollow fiber module that ranged between (106 – 287). The low values of Re in hollow fiber module related to the tortuosity of the flow in the module. Even when Re numbers are ranged in the laminar region, transitional to turbulent flow region is applied.
- Nusselt numbers (Nu) of hot feed flow in flat sheet compartment and hollow fiber module were calculated. The Nusselt numbers of feed flow in flat sheet compartment ranged between (22 – 33) which is 11 times higher than Nusselt numbers in hollow fiber module that ranged between (2 – 3).
- Heat transfer coefficients of hot feed flow in flat sheet compartment and hollow fiber module were calculated. Much higher heat transfer coefficients are achieved in flat sheet membrane hot side than in hollow fiber membrane. Heat transfer coefficients of flat sheet membrane ranged between (11246 – 17044 $W/m^2 K$) while heat transfer coefficients of hollow fiber membrane ranged between (1385 – 2163 $W/m^2 K$) only. This explains

the low amount of permeate flux generated by hollow fiber membrane. As heat transfer coefficient increases, the boundary layer across the membrane decrease, allowing more mass transfer (permeate flux) to be generated.

After examining the quality of the permeate water produced by flat sheet and hollow fiber membranes, the following conclusions were made:

- The DCMD system produce high quality permeate water with high salt rejection using flat sheet and hollow fiber membranes. Approximately 100% salt rejection is achieved by flat sheet membrane and nearly 99.9% salt rejection is accomplished by hollow fiber membrane.
- The electrical conductivity of permeate water produced by using flat sheet membrane is much lower than the electrical conductivity of permeate produced by hollow fiber membrane. The average electrical conductivity achieved by hollow fiber membrane is 40 $\mu S/cm$ besides it never exceed 100 $\mu S/cm$. However, the electrical conductivity achieved by flat sheet membrane never exceed 5 $\mu S/cm$. High values of conductivity in hollow fiber membranes present only in the last sets of experiments when membrane wetting start to occur.
- Cations and Anions analysis conducted by (ICP-OES) and (IC) tests indicated the low concentration of elements present in the permeate water produced by flat sheet and hollow fiber membranes. Less occurrence of the anions and cations in the produced permeate water is reached by flat sheet membrane. However, all elements concentration falls within the permissible limits of water quality.

Our investigation shows that hollow fiber modules with basic configuration consistently gave lower distillate flux. We investigated the likely reasons and found that it was mainly due to the flow pattern and associated convective heat transfer.

Despite the recent work in the literature on hollow fiber module design, reported flux is still lower than in flat sheet modules. We recommended a step change in hollow fiber module design using advanced computational fluid dynamics where local (Re) and (Nu) numbers can be estimated numerically for various module configurations in terms of turbulence promoters inserts like baffles.

Other recommendations are also proposed to improve the performance of membrane distillation systems:

- Comparison of permeate flux profile of hollow fiber membranes and flat sheet membrane based on temperature and concentration polarization coefficients.
- Membrane wetting and fouling evaluation on a comparison based between hollow fiber and flat sheet membranes.
- Pretreatment of seawater in order to minimize the biological fouling of the membranes.
- A greater understanding of the wetting phenomenon can minimize the risk of membrane wetting of the commercial membranes
- Membrane synthesizing with specific membranes characteristics such are pore sizes and membrane material for particular purpose such as real saline water desalination.
- Enhancement of membrane hydrophobicity by synthesizing new membranes to minimize membrane wetting
- Membrane distillation integration with industrial processes and utilization of low-grade heat produced by various ranges of industries.
- Membrane distillation integration with renewable source of energy such as solar energy.
- For the experimental devices, using stronger tubing material is recommended that provide more stable performance at extreme operating conditions of high temperature and flowrate.

References

[1] I. A. Shiklomanov, "Chapter 2: World Fresh Water Resourses," in *Water in Crisis*, P. H. Gleick, Ed., New York, 1993.

[2] J. Zhu, L. Jiang and T. Matsuura, "New insights into fabrication of hydrophobic/hydrophilic composite hollow fibers for direct contact membrane distillation," *Chemical Engineering Science,* no. 137, p. 79–90, 2015.

[3] "World Health Organization (WHO)," June 2015. [Online]. Available: http://www.who.int/topics/water/en/. [Accessed April 2016].

[4] N. Gohil, "WHY THE WATER CRISIS IS GRAVER THAN YOU THINK? THE GLOBAL WATER CRISIS," [Online]. Available: http://earth5r.com/why-the-water-crisis-is-graver-than-you-think-the-global-water-crisis/#. [Accessed April 2016].

[5] A. Cipollina, G. Micale, and L. Rizzuti, Seawater Desalination: Conventional and Renewable Energy Processes, Springer, 2009.

[6] T.-C. Chen and C.-D. Ho, "Immediate assisted solar direct contact membrane distillation in saline water desalination," *Membrane Science,* no. 358, pp. 122-130, 2010.

[7] P. S. Goh, T. Matsuura, A. F. Ismail and N. Hilal, "Recent trends in membranes and membrane processes for desalination," *Desalination,* 2015.

[8] M. A. Raouf, "Water Issues in the Gulf: Time for Action," 2009. [Online]. Available: http://www.mei.edu/content/water-issues-gulf-time-action. [Accessed March 2016].

[9] "Human Development Report 2006, Beyond scarcity: Power, poverty and the global water crisis," 2006. [Online]. Available: http://hdr.undp.org/en/content/human-development-report-2006. [Accessed March 2016].

[10] I. A. Z. Aidrous, "How to Overcome the Fresh Water Crisis in the Gulf," 18 August 2014. [Online]. Available: http://russiancouncil.ru/en/inner/?id_4=4190#top-content. [Accessed April 2016].

[11] "Zero Discharge Seawater Desalination: Integrating the Production of Freshwater, Salt, Magnesium, and Bromine," *Reclamation ,* no. 11, 2008.

[12] N. Voutchkov, Desalination Engineering: Planning and Design, McGraw Hill Professional, 2012.

[13] O. Saif, "The Future Outlook of Desalination in the Gulf: Challenges & opportunities faced by Qatar & the UAE," 2012. [Online]. Available: http://collections.unu.edu/view/UNU:2647. [Accessed March 2016].

[14] GRID-Arendal, "Sick Water? The central role of wastewater management in sustainable development," 2010. [Online]. Available: http://www.unep.org/pdf/SickWater_screen.pdf. [Accessed March 2016].

[15] S. Uddin, "Environmental Impacts of Desalination Activities in the Arabian Gulf," *International Journal of Environmental Science and Development,* vol. 5, no. 2, pp. 114-117, 2014.

[16] J. H. Reif and W. Alhalabi, "Solar-thermal powered desalination: Its significant challenges and potential," *Renewable and Sustainable Energy Reviews ,* no. 48, p. 152–165, 2015.

[17] M. S. Al. Ansari, "Concentrating Solar Power to Be Used in Seawater Desalination within the Gulf Cooperation Council," *Energy and Environment Research,* vol. 3, no. 1, 2013.

[18] M. A. Dawoud and M. M. Al Mulla, "Environmental Impacts of Seawater Desalination: Arabian Gulf Case Study," *Environment and Sustainability,* vol. 1, no. 3, pp. 22-37, 2012.

[19] A. N. Mabrouk and H. E. Fath, "Technoeconomic study of a novel integrated thermal MSF–MED desalination technology," *Desalination,* no. 371, p. 115–125, 2015.

[20] D. A. Roberts, E. L. Johnston and N. A. Knott, "Impacts of desalination plant discharges on the marine environment: A critical review of published studies," *Water Research,* no. 44, pp. 5117-5128, 2010.

[21] H. J. Krishna, "Introduction to Desalination Technologies," 2004. [Online]. Available: http://texaswater.tamu.edu/readings/desal/introtodesal.pdf. [Accessed March 2016].

[22] H. Ettouney, "Chapter 2 Conventional Thermal Processes," in *Seawater Desalination: Conventional and Renewable Energy Processes*, Springer, 2009.

[23] S. Gray, R. Semiat, M. Duke, A. Rahardianto and Y. Cohen, "Reference Module in Earth Systems and Environmental Sciences," in *Seawater Use and Desalination Technology* , 2011, pp. 73-109.

[24] V. Namboodiri and N. Rajagopalan, "Desalination," in *Comprehensive Water Quality and Purification*, Elsevier, 2013, pp. 98-119.

[25] C. M. Fellows and A. Al-Hamzah, "Chapter 23: Thermal Desalination: Current," in *Mineral Scales and Deposits: Scientific and Technological Approaches*, Elsevier, 2015.

[26] R. Semiat, "Multi-effect distillation (MED) in water and wastewater treatment technologies," 2011. [Online]. Available: http://www.eolss.net. [Accessed February 2016].

[27] T. Younos and K. E. Tulou, "Overview of Desalination Techniques," *Contemporary Water Resarch & Education,* no. 132, pp. 3-10, 2005.

[28] D. Paulson, "Nanofiltration: The Up-And-Coming Membrane Process," 18 May 2015. [Online]. Available: http://www.wateronline.com/doc/nanofiltration-the-up-and-coming-membrane-process-0001. [Accessed April 2016].

[29] LUMINOR, "Reverse Osmosis Education," 2016. [Online]. Available: http://www.luminoruv.com/education_rev_osmosis.php. [Accessed April 2016].

[30] B. Yamada, "Water Talks," 13 September 2011. [Online]. Available: http://www.slideshare.net/waterauthority/water-talks-regional-seawater-desalination. [Accessed April 2016].

[31] M. R. Qtaishat and T. Matsuura, "Modelling of pore wetting in membrane distillation compared with pervaporation," in *Pervaporation, Vapour Permeation and Membrane Distillation*, 2015, pp. 385-413.

[32] P. Wang and T.-S. Chung, "Recent advances in membrane distillation processes: Membrane development, configuration design and application exploring," *Membrane Science ,* no. 474, p. 39–56, 2015.

[33] M. Khayet, "Membranes and theoretical modeling of membrane distillation: A review," *Advances in Colloid and Interface Science,* no. 164, pp. 56-88, 2011.

[34] E. Drioli, A. Ali and F. Macedonio, "Membrane distillation: Recent developments and perspectives," *Desalination,* no. 356, pp. 56-84, 2015.

[35] A. Alkhudhiri, N. Darwish and N. Hilal, "Membrane distillation: A comprehensive review," *Desalination,* no. 287, p. 2–18, 2012.

[36] P. Onsekizoglu, "Membrane Distillation: Principle, Advances, Limitations and Future Prospects in Food Industry," in *Distillation - Advances from Modeling to Applications*, 2012, p. 282.

[37] S. Lin, N. Y. Yip and M. Elimelech, "Direct contact membrane distillation with heat recovery: Thermodynamic insights from module scale modeling," *Membrane Science ,* no. 453, p. 498–515, 2014.

[38] H. C. Duong, P. Cooper, B. Nelemans, T. Y. Cath and L. D. Nghiema, "Optimising thermal efficiency of direct contact membrane distillation by brine recycling for small-scale seawater desalination," *Desalination ,* no. 374, p. 1–9, 2015.

[39] S. T. Bouguecha, S. E. Aly, M. . H. Al-Beirutty, M. M. Hamdi and A. Boubakri, "Solar driven DCMD: Performance evaluation and andthermal energy efficiency," *Chemical Engineering Research and Design,* no. 100, pp. 331-340, 2015.

[40] A. M. Elzahaby, A. E. Kabeel, M. M. Bassuoni and A. R. Abd Elbar, "Direct contact membrane water distillation assisted with solar energy," *Energy Conversion and Management,* no. 110, p. 397–406, 2016.

[41] K. W. Lawson and D. R. Lloyd, "Membrane distillation," *Membrane Science,* no. 124, pp. 1-25, 1997.

[42] R. Bouchrit, A. Boubakri, A. Hafiane and S. A.-T. Bouguecha, "Direct contact membrane distillation: Capability to treat hyper-saline solution," *Desalination,* no. 376, p. 117–129, 2015.

[43] D. Hou, J. Wang, C. Zhao, B. Wang, Z. Luan and X. Sun, "Fluoride removal from brackish groundwater by direct contact membrane distillation," *Environmental Sciences,* vol. 22, no. 12, p. 1860–1867, 2010.

[44] M. Gryta, M. Tomaszewska and K. Karakulski, "Wastewater treatment by membrane distillation," *Desalination,* no. 198, p. 67–73, 2006.

[45] M. Khayet and T. Matsuura, Membrane Distillation: Principles and Applications, Elsevier, 2011.

[46] L. Francis, N. Ghaffour, A. S. Al-Saadi and G. Amy, "Performance of different hollow fiber membranes for seawater desalination using membrane distillation," *Desalination and Water Treatment,* 2014.

[47] Y. M. Manawi, M. Khraisheh, A. K. Fard, F. Benyahia and S. Adham, "Effect of operational parameters on distillate flux in direct contact membrane distillation (DCMD): Comparison between experimental and model predicted performance," *Desalination,* no. 336, pp. 110-120, 2014.

[48] L. Francis, N. Ghaffour, A. Alsaadi, S. Nunes and G. Amy, "Performance evaluation of the DCMD desalination process under bench scale and large scale module operating conditions," *Membrane Science,* no. 455, pp. 103-112, 2014.

[49] D. Singh and K. K. Sirkar, "High temperature direct contact membrane distillation based desalination using PTFE hollow fibers," *Chemical Engineering Science,* no. 116, p. 824–833, 2014.

[50] J.-G. Lee, Y.-D. Kim , W.-S. Kim, L. Francis, G. Amy and N. Ghaffour, "Performance modeling of direct contact membrane distillation (DCMD) seawater desalination process using a commercial composite membrane," *Membrane Science,* no. 478, p. 85–95, 2015.

[51] H. Maab, A. Al Saadi, L. Francis, S. Livazovic, N. Ghafour, G. L. Amy and S. P. Nunes, "Polyazole Hollow Fiber Membranes for Direct Contact Membrane

Distillation," *Industrial & Engineering Chemistry Research ,* no. 52, pp. 10425-10429, 2013.

[52] K. He, H. J. Hwang, M. W. Woo and I. S. Moon, "Production of drinking water from saline water by direct contact membrane distillation (DCMD)," *Industrial and Engineering Chemistry,* no. 17, p. 41–48, 2011.

[53] L. D. Nghiem, F. Hildinger, F. I. Hai and T. Cath, "Treatment of saline aqueous solutions using direct contact membrane distillation," *Desalination and Water Treatment,* no. 32, p. 234–241, 2011.

[54] O. A. Hamed, "Evolution Developments of Thermal Desalination Plants in the Arab Gulf Region," Beirut, 2004.

[55] T. Younos, "Environmental Issues of Desalination," *Conremporary Water Research & Education,* Vols. 11-18, no. 132, 2005.

[56] K. Khulbe, C. Feng and T. Matsuura , "Membrane Characterization," [Online]. Available: http://www.desware.net/Sample-Chapters/D05/E6-144-45-00.pdf. [Accessed April 2016].

[57] B. Tylkowski and I. Tsibranska, "Overview of Main Techniques Used For Membrane Characterization," *Chemical Technology and Metallurgy,* vol. 50, no. 1, pp. 3-12, 2015.

[58] J. Zhang, N. Dow, M. Duke, E. Ostarcev, J.-D. Li and S. Gray, "Identification of material and physical features of membrane distillation membranes for high performance desalination," *Membrane Science,* no. 349, pp. 295-303, 2010.

[59] D. Y. Cheng, "United States Patent, Method and Apparatus for Distillation," 1981.

[60] A. -S. Jonsson, R. Wimmerstedt and A.-C. Harrysson, "Membrane Distillation - A Theoretical Study of Evaporation Through Microporous Membranes," *Desalination,* no. 56, pp. 237-249, 1985.

[61] E. Drioli and Y. Wu, "Membrane Distillation : An Experimental Study," *Desalination,* no. 53, pp. 339-346, 1985.

[62] E. Drioli, V. Calabro and Y. Wu, "Microporous membranes in membrane distillation," *Pure & Appl. Chem.,* vol. 58, no. 12, pp. 1657-1662, 1986.

[63] E. Drioli, Y. Wu and V. Calabro, "Membrane distillation in the treatment of aqueous solutions," *Membrane Science,* no. 33, pp. 277-284, 1987.

[64] V. Calabro, E. Drioli and F. Matera, "Membrane Distillation in the Textile Wastewater Treatment," *Desalination,* no. 83, pp. 209-224, 1991.

[65] G. C. Sarti, C. Gostoli and S. Matuili, "Low Energy Cost Desalination Process Using Hydrophobic Membranes," *Desalination,* no. 56, pp. 277-286, 1985.

[66] S. Bandini, C. Gostoli and G. C. Sarti, "Role of Heat and Mass Transfer in Membrane Distillation Process," *Desalination,* no. 81, pp. 91-106, 1991.

[67] C. Gostoli and G. C. SARTI, "Separation of Liquid Mixtures by Membrane Distillation," *Membrane Science,* no. 41, pp. 211-224, 1989.

[68] R. W. Schofield, A. G. Fane and C. J. Fell, "Heat and Mass Transfer in Membrane Distillation," *Membrane Science,* no. 33, pp. 299-313, 1987.

[69] R. W. Schofield, A. G. Fane, C. J. Fell and R. Macoun, "Factors Affecting Flux in Membrane Distillation," *Desalination,* no. 77, pp. 279-294, 1990.

[70] K. Schneider, W. Holz and R. Wollbeck, "Membranes and Modules for Transmembrane Distillation," *Membrane Science,* no. 39, pp. 25-42, 1988.

[71] M. J. Costello, A. G. Fane, P. A. Hogan and R. W. Schofield, "The effect of shell side hydrodynamics on the performance of axial flow hollow fibre modules," *Membrane Scrience,* no. 80, pp. 1-11, 1993.

[72] M. Gryta and M. Tomaszewska, "Heat transport in the membrane distillation process," *Membrane Science,* no. 144, pp. 211- 222, 1998.

[73] J. Phattaranawik , R. Jiraratananon and A. G. Fane, "Effect of pore size distribution and air flux on mass transport in direct contact membrane distillation," *Membrane Science,* no. 215, pp. 75-85, 2003.

[74] J. Phattaranawik, R. Jiraratananon and A. G. Fane, "Heat transport and membrane distillation coefficients in direct contact membrane distillation," *Membrane Science,* no. 212, p. 177–193, 2003.

[75] J. Phattaranawik and R. Jiraratananon, "Direct contact membrane distillation: effect of mass transfer on heat transfer," *Membrane Science,* no. 188, p. 137–143, 2001.

[76] J. Phattaranawik, R. Jiraratananon, A. G. Fane and C. Halim, "Mass flux enhancement using spacer filled channels in direct contact membrane distillation," *Membrane Science,* no. 187, pp. 193-201, 2001.

[77] S. T. Hsu, K. T. Cheng and J. S. Chiou, "Seawater desalination by direct contact membrane distillation," *Desalination,* no. 143, pp. 279-287, 2002.

[78] D. Wirth and C. Cabassud, "Water desalination using membrane distillation: comparison between inside/out and outside/in permeation," *Desalination,* no. 147, pp. 139-145, 2002.

[79] B. Li and K. K. Sirkar, "Novel Membrane and Device for Direct Contact Membrane Distillation-Based Desalination Process," *Ind. Eng. Chem. Res.,* no. 43, pp. 5300-5309, 2004.

[80] T. Y. Cath, V. D. Adams and A. . E. Childress, "Experimental study of desalination using direct contact membrane distillation: a new approach to flux enhancement," *Membrane Science ,* no. 228, pp. 5-16, 2004.

[81] S. Srisurichan, R. Jiraratananon and A. G. Fane, "Mass transfer mechanisms and transport resistances in direct contact membrane distillation process," *Membrane Science,* no. 277, pp. 186-194, 2006.

[82] A. Criscuoli, M. C. Carnevale and E. Drioli, "Evaluation of energy requirements in membrane distillation," *Chemical Engineering and Processing,* no. 47, p. 1098–1105, 2008.

[83] M. Gryta, "Alkaline scaling in the membrane distillation process," *Desalination,* no. 228, p. 128–134, 2008.

[84] M. M. Teoh, S. Bonyadi and T.-S. Chung, "Investigation of different hollow fiber module designs for flux enhancement in the membrane distillation process," *Membrane Science ,* no. 311, p. 371–379, 2008.

[85] X. Yang, R. Wang and A. G. Fane, "Novel designs for improving the performance of hollow fiber membrane distillation modules," *Membrane Science,* no. 384, pp. 52-62, 2011.

[86] S. S. Ibrahim and Q. F. Alsalhy, "Modeling and Simulation for Direct Contact Membrane Distillation in Hollow Fiber Modules," *AIChE,* no. 2, pp. 589-603, 2013.

[87] A. Bahmanyar, M. Asghari and N. Khoobi, "Numerical simulation and theoretical study on simultaneously effects of operating parameters in direct contact membrane distillation," *Chemical Engineering and Processing,* no. 61, pp. 42-50, 2012.

[88] S. Adham, A. Hussain, J. M. Matar, D. Raul and A. Janson, "Application of Membrane Distillation for desalting brines from thermal desalination plants," *Desalination,* no. 314, p. 101–108, 2013.

[89] F. Macedonio, A. Ali, T. Poerio, E. El-Sayed, E. Drioli and M. Abdel-Jawad, "Direct contact membrane distillation for treatment of oilfield produced water," *Separation and Purification Technology,* no. 126, p. 69–81, 2014.

[90] C.-D. Ho, C.-H. Huang, F.-C. Tsai and W.-T. Chen, "Performance improvement on distillate flux of countercurrent-flow direct contact membrane distillation systems," *Desalination,* no. 338, p. 26–32, 2014.

[91] C.-D. Ho, H. Chang, T.-J. Yang, K.-Y. Wu and L. Chen, "Theoretical and experimental studies of laminar flow hollow fiber direct contact membrane distillation modules," *Desalination,* no. 378, p. 108–116, 2016.

[92] J. Zuo, S. Bonyadi and T.-S. Chung, "Exploring the potential of commercial polyethylene membranes for desalination by membrane distillation," *Membrane Science,* no. 497, pp. 239-247, 2016.

[93] F. Eleiwi, N. Ghaffour, A. S. Alsaadi, L. Francis and T. M. Laleg-Kirati, "Dynamic modeling and experimental validation for direct contact membrane distillation (DCMD) process," *Desalination,* no. 384, pp. 1-11, 2016.

[94] S. Munirasua, M. Abu Haijab and F. Banat, "Use of membrane technology for oil field andrefinery produced water treatment—A review," *Process Safety and Environmental Protection,* no. 100, p. 183–202, 2016.

[95] J. Swaminathan, H. W. Chung, D. M. Warsinger and J. H. Lienhard V, "Simple method for balancing direct contact membrane distillation," *Desalination ,* no. 383, pp. 53-59, 2016.

[96] D. Singh and K. K. Sirkar, "Desalination of brine and produced water by direct contact membrane distillation at high temperatures and pressures," *Membrane Science,* no. 389, pp. 380-388, 2012.

[97] I. Janajreh and D. Suwwan, "Numerical Simulation of Direct Contact Membrane Desalination (DCMD): II," in *IAJC-ISAM International Conference*, 2014.

[98] J. Zhang, . J.-D. Li, M. Duke, Z. Xie and S. Gray, "Performance of asymmetric hollow fibre membranes in membrane distillation under various configurations and vacuum enhancement," *Membrane Science,* no. 362, pp. 517-528, 2010.

[99] D. M. Warsinger, J. Swaminathan, E. Guillen-Burrieza, H. Arafat and J. H. Lienhard, "Scaling and fouling in membrane distillation for desalination applications: A review," *Desalination,* no. 356, p. 294–313, 2015.

[100] L.-H. Cheng, P.-C. Wu, C.-K. Kong and J. Chen, "Spatial variations of DCMD performance for desalination through countercurrent hollow fiber modules," *Desalination,* no. 234, p. 323–334, 2008.

[101] M. Gryta, "Effectiveness of Water Desalination by Membrane Distillation Process," *Membranes,* no. 2, pp. 415-429, 2012.

[102] M. Gryta, M. Tomaszewska and A. W. Morawski, "A Capillary Module for Membrane Distillation Process," *Chem. Papers,* no. 54, pp. 370-374, 2000.

[103] G. Chen, X. Yang, R. Wang and A. G. Fane, "Performance enhancement and scaling control with gas bubbling in direct contact membrane distillation," *Desalination,* no. 308, p. 47–55, 2013.

[104] N. C. Mat, Y. Lou and G. G. Lipscomb, "Hollow fiber membrane modules," *Chemical Engineering,* no. 4, p. 18–24, 2014.

[105] S. Al-Obaidania, E. Curcio, F. Macedoniob, G. D. Profiob, H. Al-Hinai and E. Drioli, "Potential of membrane distillation in seawater desalination: Thermal efficiency, sensitivity study and cost estimation," *Membrane Science,* no. 323, pp. 85-98, 2008.

[106] V. Bui, . L. Vu and M. Nguyen, "Modelling the simultaneous heat and mass transfer of direct contact membrane," *Membrane Science ,* no. 353, p. 85–93, 2010.

[107] H. Yu, X. Yang, R. Wang and A. G. Fane, "Numerical simulation of heat and mass transfer in direct membrane distillation in a hollow fiber module with laminar flow," *Membrane Science ,* no. 384, p. 107– 116, 2011.

[108] Z. Wang, F. Cui, G. Wang, S. Feng, M. Zhao and Z. Gu, "Analysis of DCMD-Based Hollow Fiber Membrane Heat Exchanger," *Chemical Engineering of Japan,* vol. 46, no. 8, p. 1–10, 2013.

[109] L.-H. Cheng, P.-C. Wu and J. Chen, "Modeling and optimization of hollow fiber DCMD module for desalination," *Membrane Science ,* no. 318, pp. 154-166, 2008.

[110] I. Janajreh and D. Suwwan, "Numerical Simulation of Direct Contact Membrane Desalination in Conjugate Heat Transfer Configuration: Role of Membrane Conductivity," *Sustainable Water and Environmental Systems,* no. 2, pp. 81-87, 2014.

[111] L. M. Camacho, L. Dumée, J. Zhang, J.-d. Li, M. Duke, J. Gomez and S. Gray, "Advances in membrane distillation for water desalination and purification applications," *Water,* no. 5, pp. 94-196, 2013.

[112] Ó. Andrjesdóttir, C. L. Ong, M. Nabavi, S. Paredes, A. S. Khalil, B. Michel and D. Poulikakos, "An experimentally optimized model for heat and mass transfer in direct contact membrane distillation," *International Journal of Heat and Mass Transfer,* no. 66, p. 855–867, 2013.

[113] M. Khayet, A. Vela´zquez and J. I. Mengual, "Modelling mass transport through a porous partition: Effect of pore size distribution," *Non-Equilib. Thermodyn.,* vol. 29, p. 279–299, 2004.

[114] I. Hitsov, T. Maere, K. De Sitter, C. Dotremont and I. Nopens, "Modelling approaches in membrane distillation: A critical review," *Separation and Purification Technology,* no. 142, p. 48–64, 2015.

[115] M. Qtaishat, T. Matsuura, B. Kruczek and M. Khayet, "Heat and mass transfer analysis in direct contact membrane distillation," *Desalination,* no. 219, p. 272–292, 2008.

[116] F. A. Banat and J. Simandl, "Theoretical and experimental study in membrane distillation," *Desalination,* no. 95, pp. 39-52, 1994.

[117] S. Jeong, S. Lee, H.-T. Chon and S. Lee, "Structural analysis and modeling of the commercial high performance composite flat sheet membranes for membrane distillation application," *Desalination,* no. 349, p. 115–125, 2014.

[118] L. Martinez-Diez and M. Vazquez-Gonzalez, "Temperature and concentration polarization in membrane distillation of aqueous salt solutions," *J. of Membrane Science,* no. 156, pp. 265-273, 1999.

[119] P. Termpiyakul, R. Jiraratananon and S. Srisurichan, "Heat and mass transfer characteristics of a direct contact membrane distillation process for desalination," *Desalination,* no. 177, pp. 133-141, 2005.

[120] H. J. Hwang, K. He, S. Grayb, J. Zhang and I. S. Moon, "Direct contact membrane distillation (DCMD): Experimental study on the commercial PTFE membrane and modeling," *Membrane Science ,* no. 371, pp. 90-98, 2011.

[121] L. Martínez-Diez and M. I. Va´zquez-Gonza´ lez, "Effects of Polarization on Mass Transport through Hydrophobic Porous Membranes," *Ind. Eng. Chem. Res.,* no. 37, pp. 4128-4135, 1998.

[122] Y. Yun, R. Ma, W. Zhang, A. G. Fane and J. Li, "Direct contact membrane distillation mechanism for high concentration NaCl solutions," *Desalination,* no. 188, pp. 251-262, 2006.

[123] M. Gryta, M. Tomaszewska and A. W. Morawski, "Membrane distillation with laminar flow," *Separation and Purification Technology,* no. 11, pp. 93-101, 1997.

[124] K. SMOLDERS and A. FRANKEN, "Terminology for Membrane Distillation," *Desalination,* no. 72, pp. 249-262, 1989.

[125] D. Hou, J. Wang, X. Sun, Z. Ji and Z. Luan, "Preparation and properties of PVDF composite hollow fiber membranes for desalination through direct contact membrane distillation," *Membrane Science,* no. 405– 406, p. 185– 200, 2012.

[126] X. Yang, R. Wang, L. Shi, A. G. Fane and M. Debowski, "Performance improvement of PVDF hollow fiber-based membrane distillation process," *Membrane science,* no. 369, pp. 437-447, 2011.

[127] M. S. El-Bourawi, Z. Ding, R. Ma and M. Khayet, "A framework for better understanding membrane distillation separation process," *Membrane Science,* no. 285, pp. 4-29, 2006.

[128] S. Chung, C. D. Seo, J.-H. Choi and J. Chung, "Evaluation method of membrane performance in membrane distillation process for seawater desalination," *Environmental Technology,* vol. 35, no. 17, pp. 2147-2152, 2014.

[129] M. M. A. Shirazi, A. Kargari and M. Tabatabaei, "Evaluation of commercial PTFE membranes in desalination by direct contact membrane distillation," *Chemical Engineering and Processing,* no. 76, p. 16– 25, 2014.

[130] M. Gryta, "Hydrodynamics - Optimizing Methods and Tools," in *The Influence of the Hydrodynamic Conditions on the Performance of Membrane Distillation*, InTech, 2011, p. 420.

[131] A. S. Kim, "Cylindrical cell model for direct contact membrane distillation (DCMD) of densely packed hollow fibers," *Membrane Science,* no. 455, p. 168– 186, 2014.

[132] S. Wickramasinghe, M. J. Semmens and E. Cussler, "Mass transfer in various hollow fiber geometries," *Membrane Science,* no. 69, pp. 235-250, 1992.

[133] L. Martínez-Diez, M. I. Vazquez-Gonzalez and F. J. Florido-Diaz, "Study of membrane distillation using channel spacers," *Membrane Science,* no. 144, pp. 45-56, 1998.

[134] A. Tamburini, P. Pitò, A. Cipollina, G. Micale and M. Ciofalo, "A Thermochromic Liquid Crystals Image Analysis technique to investigate temperature polarization in spacer-filled channels for Membrane Distillation," *Membrane Science,* no. 447, pp. 260-273, 2013.

[135] Z. Song, L. Li, H. Wang, B. Li and S. Wang, "DCMD flux curve characteristics of cross-flow hollow fiber membrane," *Desalination,* no. 323, pp. 107-113, 2013.

[136] S. Chhun, W. Khongnakorn and W. Youravong, "Effect of Operating Conditions of Direct Contact Membrane Distillation for Water Purification," in *International Graduate Research Conference*, 2013.

[137] A. R. Al Naamaa, "KAHRAMAA Drinking Water: Quality Requirements," 2014.

[138] D. Singh and K. K. Sirkar, "Desalination by air gap membrane distillation using a two hollow-fiber-set membrane module," *Membrane Science,* no. 421–422, p. 172–179, 2012.

[139] N. Tang, P. Cheng, X. Wang and H. Zhang, "Study on the Vaccum Membrane Distillation Performances of PVDF Hollow Fiber Membranes for Aqueous NaCl Solution," *Chemical Engineering Transactions ,* no. 17, pp. 1537-1542, 2009.

[140] M. Khayet, C. Cojocaru and M. García-Payo, "Experimental design and optimization of asymmetric flat-sheet membranes prepared for direct contact membrane distillation," *Membrane Science,* no. 351, p. 234–245, 2010.

[141] M. Al-Obaidli, "An investigation into hydrophobic membrane fouling in desalination using membrane distillation technology," Qatar University, 2015.

[142] "Viton O-rings," Sealing Devices Inc., 2016. [Online]. Available: https://www.sealingdevices.com/viton-o-rings. [Accessed March 2016].

[143] W. Lamparter, "The Art to Clear Solutions," MICRODYN-NADIR GmbH, [Online]. Available: http://www.microdyn-nadir.com/en/Products/MICRODYN/. [Accessed February 2016].

[144] "Peristalic Pumps FH100 and FH100X from Thermo Scientific," VISSERS SALES CORP., [Online]. Available: http://www.process-controls.com/Vissers_Sales/masterflex_fh100.htm. [Accessed March 2016].

[145] "F32-MA Refrigerated/Heating Circulator," JULABO, 2016. [Online]. Available: http://www.julabo.com/en/products/refrigerated-circulators/refrigerated-heating-circulators/f32-ma-refrigerated-heating-circulator. [Accessed March 2016].

[146] "High Performance Pressure Transmitters," OMEGA, [Online]. Available: http://www.omega.com/pptst/PX309_mA.html. [Accessed March 2016].

[147] "SD 300 pH, SD 320 Con," AQUALYTIC, [Online]. Available: http://en.aqualytic.de/products/handheld-meters/sd-300-ph-sd-320-con. [Accessed March 2016].

[148] "NI 9219," National Instruments, 2016. [Online]. Available: http://sine.ni.com/nips/cds/view/p/lang/en/nid/208789. [Accessed March 2016].

[149] "What Is Data Acquisition?," AM Tech, 2011. [Online]. Available: http://www.amtechdas.com/data-acquisition.htm. [Accessed March 2016].

[150] M. H. Sharqawy, J. V. Lienhard and S. M. Zubair, "A review of existing correlations and data," in *The thermophysical properties of seawater*, Desalination Publications, 2010.

[151] M. Shakaib, S. M. Hasani, I. Ahmed and R. M. Yunus, "A CFD study on the effect of spacer orientation on temperature polarization in membrane distillation modules," *Desalination,* no. 284, p. 332–340, 2012.

[152] H. Chang, J.-A. Hsu, C.-L. Chang and C.-D. Ho, "CFD study of heat transfer enhanced membrane distillation using spacer-filled channels," *Energy Procedia,* no. 75, p. 3213 – 3219, 2015.

[153] G. Towler and R. Sinnott, Chemical Engineering Design, Oxford: ELSEVIER SCIENCE & TECHNOLOGY, 2009.

[154] J. Zhang, S. Gray and J.-D. Li, "Modelling heat and mass transfers in DCMD using compressible membranes," *Membrane Science,* no. 387–388, p. 7–16, 2012.

[155] Q.-M. Nguyen and . S. Lee, "Fouling analysis and control in a DCMD process for SWRO brine," *Desalination,* no. 367, pp. 21-27, 2015.

[156] W. G. Shim, K. He, S. Gray and I. S. Moon, "Solar energy assisted direct contact membrane distillation (DCMD) process for seawater desalination," *Separation and Purification Technology,* no. 143, p. 94–104, 2015.

[157] R. D. Gustafson, J. R. Murphy and A. Achilli, "A stepwise model of direct contact membrane distillation for application to large-scale systems: Experimental results and model predictions," *Desalination,* no. 378, pp. 14-27, 2016.

[158] E. Close and E. Sørensen, "Modelling of Direct Contact Membrane Distillation for Desalination," pp. 649-654, 2010.

[159] D. Hou, H. Fan, Q. Jiang, J. Wang and X. Zhang, "Preparation and characterization of PVDF flat-sheet membranes for direct contact membrane distillation," *Separation and Purification Technology,* no. 135, p. 211–222, 2014.

[160] H. Geng, H. Wu, P. Li and Q. He, "Study on a new air-gap membrane distillation module for desalination," *Desalination,* no. 334, p. 29–38, 2014.

[161] A. S. Kim, "Cylindrical cell model for direct contact membrane distillation (DCMD) of densely packed hollow fibers," *Membrane Science,* no. 455, p. 168–186, 2014.

[162] L. Song, Z. Ma, Xiaohong Liao, P. B. Kosaraju, J. R. Irish and K. K. Sirkar, "Pilot plant studies of novel membranes and devices for direct contact membrane distillation-based desalination," *Membrane Science,* no. 323, p. 257–270, 2008.

[163] A. Ali, F. Macedonio, E. Drioli and O. A. Alharbi, "Experimental and theoretical evaluation of temperature temperature polarization phenomenon in direct contact membrane distillation," *Chemical Engineering Research and Design,* no. 91, pp. 1966-1977, 2013.

[164] H. Geng, Q. He, H. Wu, P. Li, C. Zhang and H. Chang, "Experimental study of hollowfiber AGMDmodules with energy recovery for high saline water desalination," *Desalination,* no. 344, pp. 55-63, 2014.

[165] WHO, "Sodium in Drinking-water," *World Health Organization,* vol. 2, no. 2, 2003.

APPENDIX A: Schematic Diagrams of MED and MSF systems

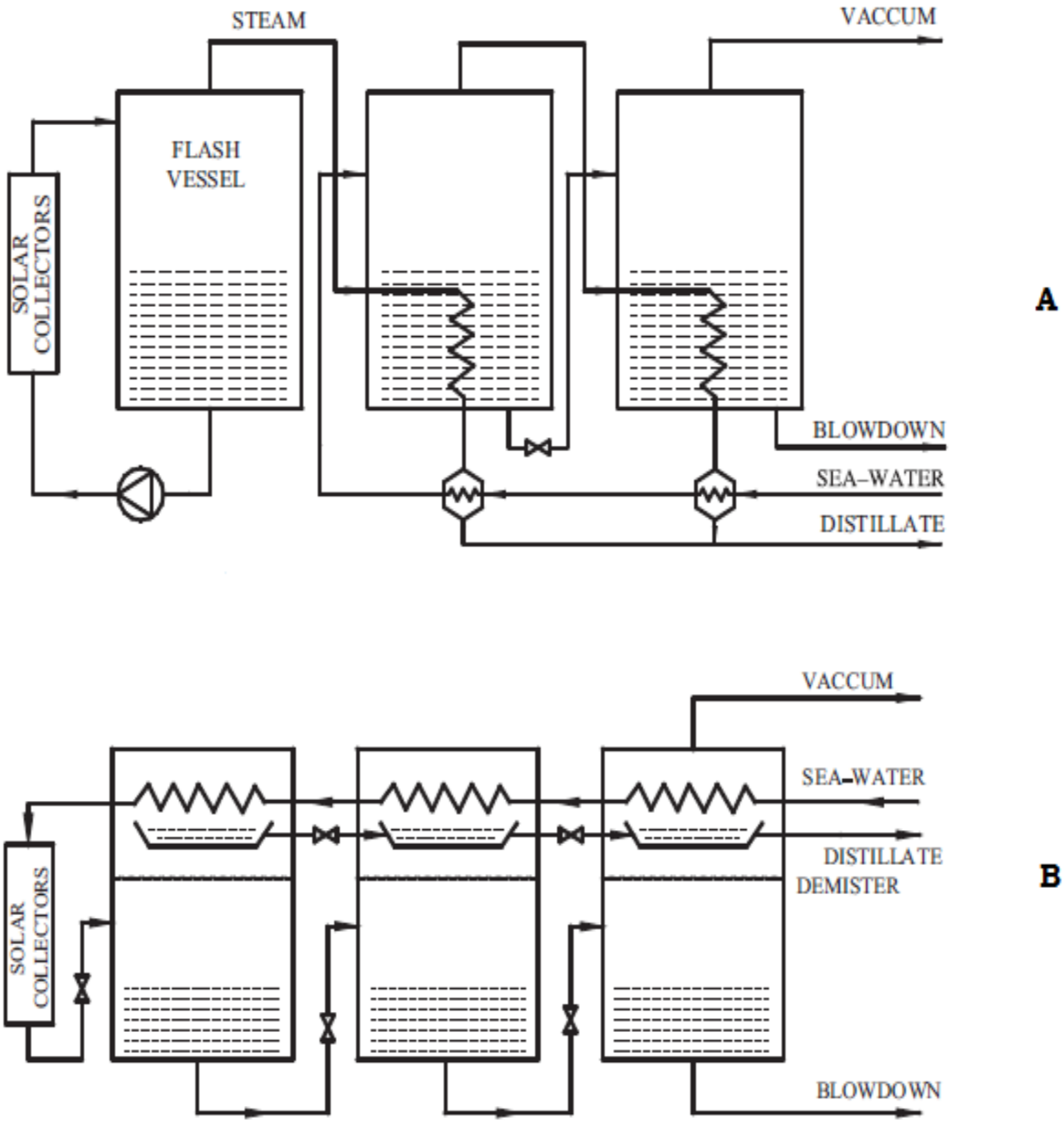

Figure 72: Schematic Diagram of A) MED system, B) MSF system

APPENDIX B: Nu Correlations of Laminar and Turbulent Flows

Nu Correlation	Ref.	Nu Correlation	Ref.
Turbulent Flow			
$Nu = 0.023\, Re^{0.8} Pr^{\frac{1}{3}}$ For cooling, (0.6 < Pr < 100) Flat Sheet or Hollow Fiber	[109] [115] [33] [35]	$Nu = 0.027\, Re^{0.8}\, \mathrm{Pr}^{0.3} \left(\frac{k_f}{D_h}\right) \left(\frac{\mu_p}{\mu_{pm}}\right)^{0.14}$ For cooling	[115]
$Nu = 0.023\ Re^{0.8}\, \mathrm{Pr}^{0.4}$ For heating, (0.6 < Pr < 100), Flat Sheet	[68] [33] [35]	$Nu = 0.027\, Re^{0.8}\, \mathrm{Pr}^{0.4} \left(\frac{k_f}{D_h}\right) \left(\frac{\mu_p}{\mu_{pm}}\right)^{0.14}$ For heating	[115]
$Nu = 0.023\ Re^{0.8}\, \mathrm{Pr}^{0.3} \times \left(\frac{\mu}{\mu_w}\right)^{0.14}$ (2500 < Re < 125000)	[35]	$Nu = 0.027\, Re^{0.8}\, Pr^{n} \left(\frac{\mu_{bf}}{\mu_{mf}}\right)^{0.14}$ For cooling (n=0.3), for heating (n=0.4)	[86] [74]
$Nu = 0.023 \left(1 + \frac{6D}{L}\right) Re^{0.8}\, Pr^{\frac{1}{3}}$ The most suitable correlation	[86] [74] [35]	$Nu = 0.027 \left(1 + \frac{6D}{L}\right) Re^{0.8}\, Pr^{\frac{1}{3}} \left(\frac{\mu}{\mu_w}\right)^{0.14}$	[115] [33] [35]
$Nu = 0.036\, Re^{0.8}\, Pr^{\frac{1}{3}}$	[115]	$Nu = 0.337\ Re^{\frac{4}{5}}\, \mathrm{Pr}^{0.33}$ Flat plate	[117]
$Nu = 0.036\, Re^{0.8}\, Pr^{\frac{1}{3}} \left(\frac{D}{L}\right)^{0.055}$	[35] [86] [74]	$Nu = 0.042\, Re^{0.59}\, \mathrm{Pr}^{0.33}$ Hollow Fiber, shell side (400 < Re < 2500)	[86] [84]
$Nu = 0.036\, Re^{0.96}\, Pr^{\frac{1}{3}} \left(\frac{D}{L}\right)^{0.055}$ Flow in tube $10 \leq \frac{L}{d} \leq 400$	[35]	$Nu = 0.029\, k\, Re^{0.3}\, \mathrm{Pr}^{0.33}$ $k = 1.9 \left(\frac{d_f}{h}\right)^{-0.039} \varepsilon^{0.75} \left(\sin\left(\frac{\theta}{2}\right)\right)^{0.086}$ Spacer-filled channel (Flat Sheet)	[154]
$Nu = \left(1 + \frac{6D}{L}\right) \left(\frac{\left(\frac{f}{8}\right) RePr}{1.07 + 12.7 \left(\frac{f}{8}\right)^{\frac{1}{2}} \left(Pr^{\frac{2}{3}} - 1\right)} \right)$ $f = [0.79 \ln(Re) - 1.64]^{-2}$	[86] [74]	$Nu = \frac{\left(\frac{f}{8}\right) Re\, Pr}{1.07 + 12.7 \left(\frac{f}{8}\right)^{\frac{1}{2}} \left(Pr^{\frac{2}{3}} - 1\right)}$ $f = [0.79 \ln(Re) - 1.64]^{-2}$	[115]
$Nu = \left(1 + \frac{6D}{L}\right) \left(\frac{\left(\frac{f}{8}\right) (Re - 1000) Pr}{1 + 12.7 \left(\frac{f}{8}\right)^{\frac{1}{2}} \left(Pr^{\frac{2}{3}} - 1\right)} \right)$ $f = [0.79 \ln(Re) - 1.64]^{-2}$	[86] [74]	$Nu = \frac{\left(\frac{f}{8}\right) (Re - 1000) Pr}{1 + 12.7 \left(\frac{f}{8}\right)^{\frac{1}{2}} \left(Pr^{\frac{2}{3}} - 1\right)}$ $f = [0.79 \ln(Re) - 1.64]^{-2}$	[115]

$Nu = \left(1 + \frac{6D}{L}\right)\left(\frac{\left(\frac{f}{8}\right)RePr}{1.2 + 13.2\left(\frac{f}{8}\right)^{\frac{1}{2}}\left(Pr^{\frac{2}{3}} - 1\right)}\right)$ $f = [0.79\ln(Re) - 1.64]^{-2}$	[86] [74]		
$Nu = \left(1 + \frac{6D}{L}\right)\left(\sqrt{\frac{f}{8}}\right)\left[12.48Pr^{\frac{2}{3}} - 7.853Pr^{\frac{1}{3}} + 3.613\ln(\mathrm{Pr}) + 5.8 + 2.78\ln\left(\frac{Re\sqrt{\frac{f}{32}}}{45}\right)\right]^{-1}$			[74]
Laminar Flow			
$Nu = 1.86\left(Re\ Pr\frac{d_h}{L}\right)^{0.33}$ Flat Sheet (Re < 2100)	[118] [84] [35] [115] [74]	$Nu = 0.13Re^{0.645}Pr^{0.38}$	[86] [74] [33]
$Nu_p = 1.86\left(Re_p\,\mathrm{Pr}_p\frac{d_{hp}}{L}\right)^{0.33} \times \left(\frac{\mu_p}{\mu_{pm}}\right)^{0.14}$ if $Gz_p = Re_p\,\mathrm{Pr}_p\frac{d_{hp}}{L} \geq 100$, (Re < 2100) Hollow Fiber, Permeate Side	[106] [86] [35]	$Nu = 0.13\ Re^{0.64}Pr^{\frac{1}{3}}$	[115] [89]
$Nu = 1.86\ Re^{0.96}\ \mathrm{Pr}^{0.33}\left(\frac{d_h}{L}\right)^{0.33}$	[35]	$Nu = 3.66$	[115]
$Nu = 1.95\left(\frac{RePr}{\frac{L}{D}}\right)^{\frac{1}{3}}$	[86] [74]	$Nu = 3.66 + \left(\frac{0.104\ RePr\left(\frac{D}{L}\right)}{1 + 0.0106\left(RePr\left(\frac{D}{L}\right)\right)^{0.8}}\right)$ The most suitable correlation	[86] [74] [35] [89]
$Nu = 1.95\ (Re\ \mathrm{Pr})^{\frac{1}{3}}$	[115] [89]	$Nu = 3.66 + \frac{0.0668\left(\frac{RePrd_h}{L}\right)}{1 + 0.045\left(\frac{RePrd_h}{L}\right)^{\frac{2}{3}}}$	[33]
$Nu = 0.74\ Re^{0.2}(GrPr)^{0.1}Pr^{0.2}$ The most suitable for Plate and frame	[35]	$Nu_p = \left(3.66 + \frac{0.0668\ Gz_p}{1 + 0.04\ Gz_p{}^{2/3}}\right) \times \left(\frac{\mu_p}{\mu_{pm}}\right)^{0.14}$ if $Gz_p = Re_p\,\mathrm{Pr}_p\frac{d_{hp}}{L} < 100$, (Re < 2100) Hollow Fiber, Permeate Side	[106] [86]
$Nu = 0.298\ Re^{0.646}Pr^{0.316}$	[35]	$Nu = 0.332\ Re^{0.5}\ \mathrm{Pr}^{0.33}$ Flat Plate (Re < 50000), (0.6 < Pr < 50)	[117]
$Nu = 0.097Re^{0.73}\mathrm{Pr}^{0.13}$	[33] [86] [89] [115] [74]	$Nu = 0.15\ Re^{0.33}\ Pr^{0.43}Gr^{0.1}\left(\frac{Pr}{Pr_w}\right)^{0.25}$ (Re < 2100)	[72] [33]

$Nu = 4.36$	[115]	$Nu = 11.5\,(RePr)^{0.23}\left(\frac{D}{L}\right)^{0.5}$ For cooling	[86] [74] [89]
$Nu = 4.36 + \frac{0.036\frac{Pe}{L/d}}{1 + 0.0011\left[\frac{Pe}{L/d}\right]^{0.8}}$ (Re < 2100)	[72] [33]	$Nu = 15\,(RePr)^{0.23}\left(\frac{D}{L}\right)^{0.5}$ For heating	[86] [89] [74]
$Nu = 4.36 + \left(\frac{0.036RePr(\frac{D}{L})}{1 + 0.0011(RePr\left(\frac{D}{l}\right)^{0.8}}\right)$	[89] [90]	$Nu = 1.62(Re\,\mathrm{Pr}\,\frac{d}{L})^{0.33}$ (Re < 2100), $\frac{L}{d} > 15$	[72] [33] [35]
$Nu_x = 4.36 + \frac{0.023\frac{Pe}{X/d}}{1 + 0.0012\left[\frac{Pe}{X/d}\right]}$ (Re < 2100)	[72]	$Nu = 1.75\sqrt[3]{Gz + 0.04\left(\frac{Gr\,Pr}{\frac{L}{d}}\right)^{0.75}}\left(\frac{\eta}{\eta_w}\right)^{0.14}$	[72] [33]
$Nu_x = \left\{4.364 + \frac{0.2633}{\left[\left(\frac{X}{dPe}\right)^{0.506}\exp\left(\frac{41X}{dPe}\right)\right]}\right\}\left(\frac{Pr}{Pr_w}\right)^{K}$ $K = 0.19\ for\ cooling,\ K = 0.2\ for$ heating	[72]	$Nu = 1.62\left(Re\,Pr\frac{d_h}{L}\right)^{0.33}$	[109]
Other Correlations			
$Nu = 0.664\,k_{dc}\,Re^{0.5}\,\mathrm{Pr}^{0.33}\left(\frac{2\,d_h}{L}\right)^{0.5}$ $k = 1.654\left(\frac{d_f}{h}\right)^{-0.039}\varepsilon^{0.75}\left(\sin\left(\frac{\theta}{2}\right)\right)^{0.086}$ Spacer-filled channel (Flat Sheet)	[47] [73] [74]	$Nu = (0.53 - 0.58\emptyset)\,Re^{0.53}\,\mathrm{Pr}^{0.33}$ $\emptyset = n\left[\frac{2\pi r}{\pi D}\right]^2$ Hollow Fiber, Shell side	[108]
$Nu = 0.023\,k_{dc}\,Re^{0.8}\,\mathrm{Pr}^{0.33}$ $k = 1.654\left(\frac{d_f}{h}\right)^{-0.039}\varepsilon^{0.75}\left(\sin\left(\frac{\theta}{2}\right)\right)^{0.086}$ Spacer-filled channel (Flat Sheet)	[50]	$Nu_p = 4.36 + \frac{0.036\,Re\,\mathrm{Pr}\left(\frac{L}{d}\right)}{1 + 0.0011\left(Re\,\mathrm{Pr}\left(\frac{L}{d}\right)\right)^{0.8}}$ Hollow Fiber, Lumen side	[108] [86]
$Nu = 0.206\,\mathrm{Pr}^{0.36}$ Hollow Fiber, Shell side	[109]	$Nu = 0.206(Re\,cos\propto)^{0.63}Pr^{0.36}$ Hollow Fiber, Shell side	[33]
$Nu = 0.116\left(Re^{\frac{2}{3}} - 125\right)Pr^{\frac{1}{3}}\left[1 + \left(\frac{d_h}{L}\right)^{\frac{2}{3}}\right]$ Transitional Region	[33]	$Nu = 1 + 1.44\left(1 - \frac{1708}{Re}\right) + \left[\left(\frac{Re}{5830}\right)^{\frac{1}{3}} - 1\right]$ Not mentioned	[35]
$Nu = \alpha\left[4.36 + \frac{0.036RePr\left(\frac{d_h}{L}\right)}{1+0.0011\left(RePr\left(\frac{d_h}{L}\right)\right)^{0.8}}\right]$ where $\alpha = 1.88\left(\frac{d_f}{h_{ch}}\right)^{-0.039}(sin\theta)^{1.33} \times \exp\left(-4.05\left(\left[ln\left(\frac{\varepsilon}{\varepsilon_m}\right)\right]^2\right)\right)$ Spacer-filled channel (Flat Sheet)			[151]

APPENDIX C: Schematic Diagram of MD Compartment

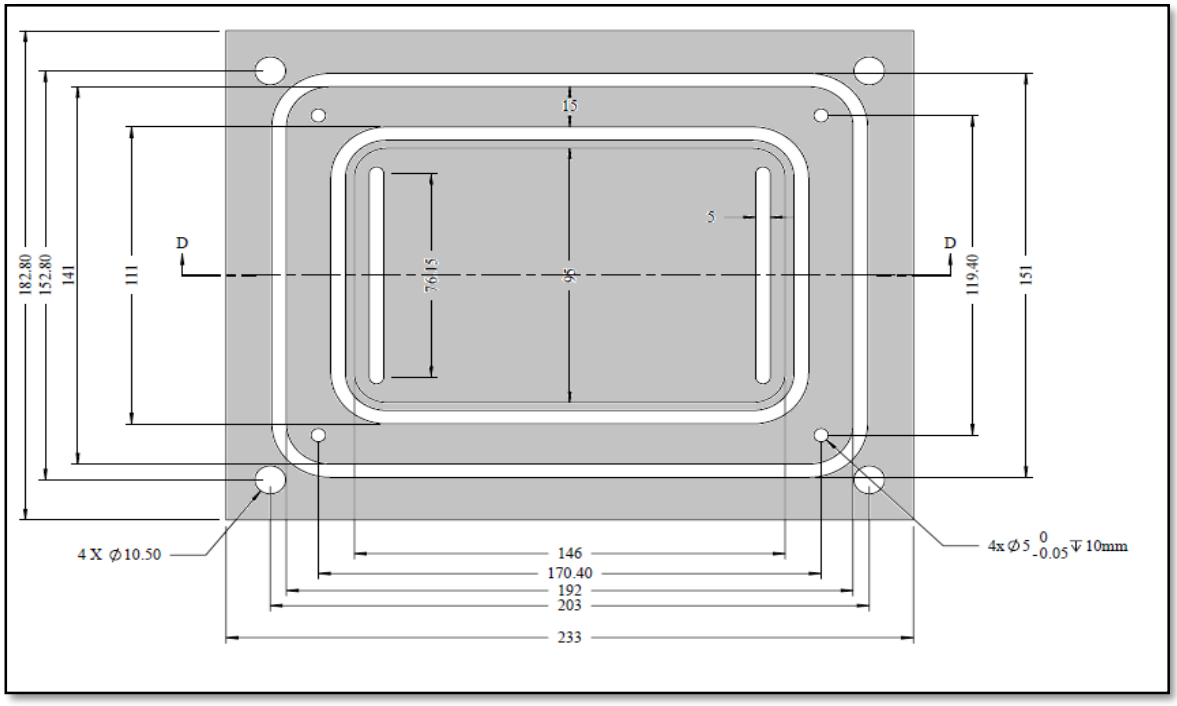

Figure 73: Dimensions of the bottom plate (top view)

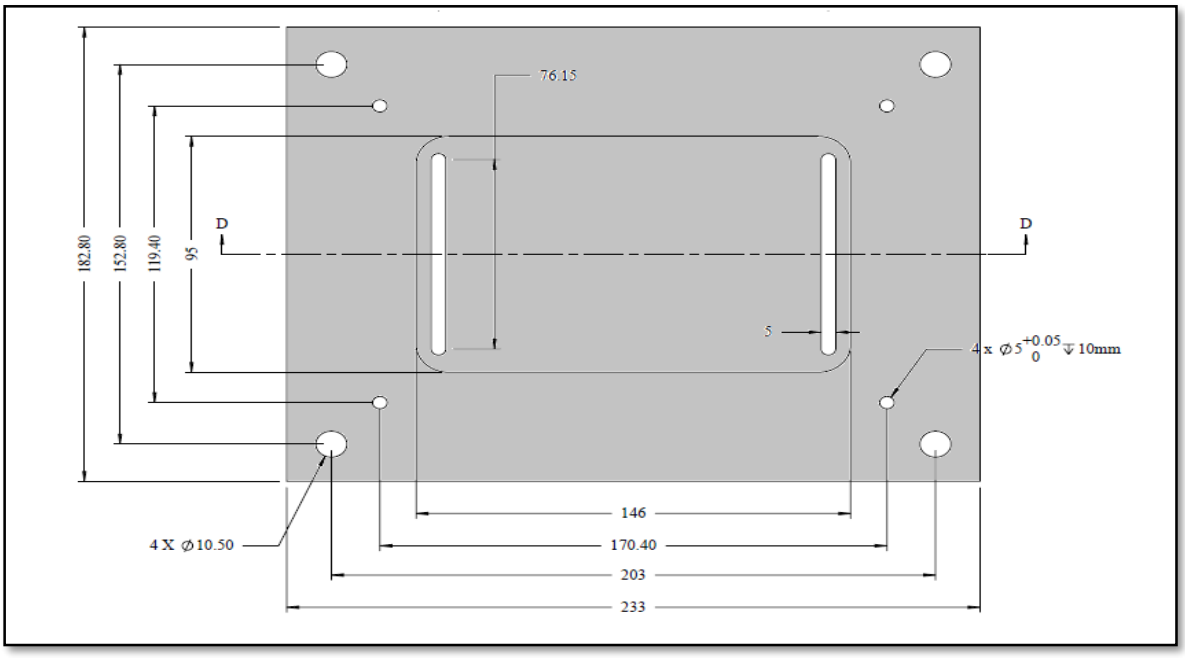

Figure 74: Dimensions of the top plate (top view)

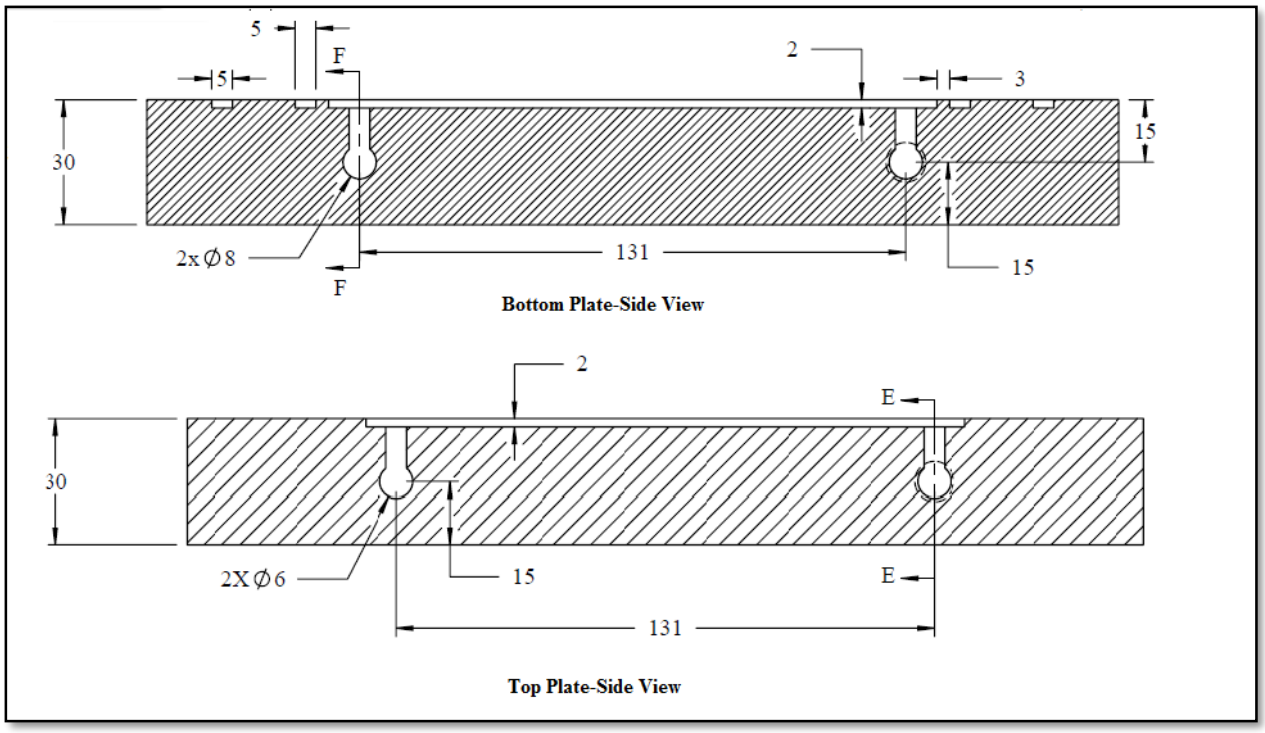

Figure 75: Dimensions of top and bottom plate looking from side view

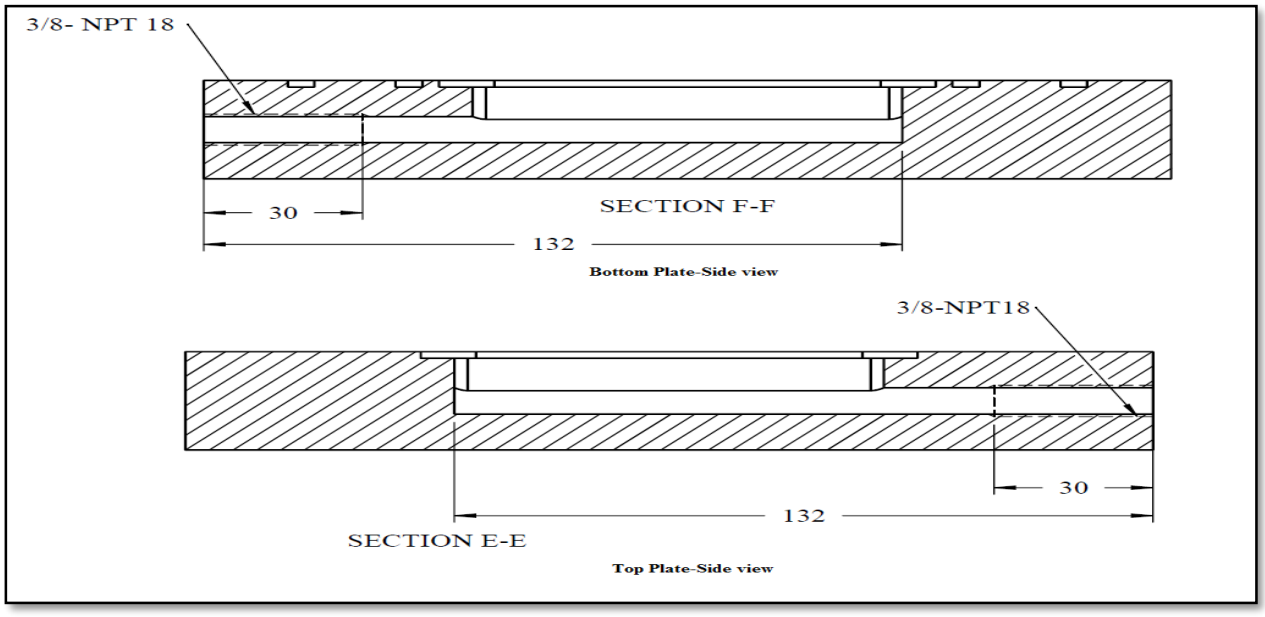

Figure 76: cross section of feed and permeate inlet and outlet looking from side view

Schematic Diagrams of Hollow Fiber Module

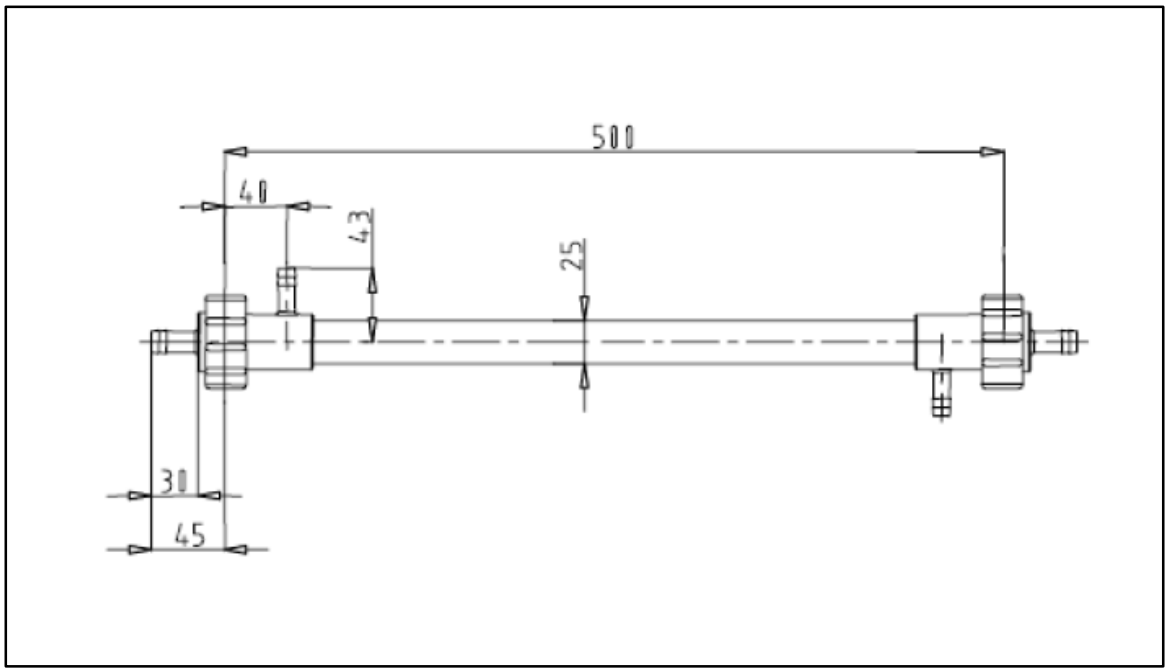

Figure 77: Hollow Fiber module dimensions

APPENDIX D: Heat Transfer Coefficient Summary Table

Membrane	Operating Conditions	Re Nu	Heat Transfer Coefficient (W/m² K)	Ref.
Flat Sheet Membrane				
PP membrane *Spacer filled channel	**Flowrate:** (LPM) 1.5	**Re: (without spacer)** 1105 **Re: (with spacer)** 6379	***h: (without spacer)*** 1190 ***h: (with spacer)*** 2163	[47]
PTFE/PP membrane	**Velocity:** (m/s) (0.09-0.34)	**Re:** (482-1822)	***h:*** (1705 – 3314)	[117]
Different membrane geometry	Different conditions	**Re:** Large range of values **Nu:** Large Range of values	***h:*** Large range of values	[68]
PVDF membrane without spacer	**Flowrate:** (LPM) (0.5-2.5)	**Re:** (840-4700)	***h:*** (186 – 1509)	[89]
PTFE membrane (70% porosity)	**Flowrate:** (LPM) 2.0	**Re:** 2233	***h:*** (22490 – 26230)	[115]
PTFE/ PVDF membrane (porosity 62 – 90 %)		**Re: (laminar)** (762-2094) **Re: (turbulent)** (12217-19198)	***h: (laminar flow)*** (480 to 1240) ***h: (turbulent flow)*** (7100 to 16000)	[74]
Hollow Fiber Membrane				
PVDF membrane (82-85% porosity)	**Flowrate:** (LPM) (1.0 - 5.6)	**Re:** less than 1901	***h: (random pack)*** (943) ***h: (curly fibers)*** (2300)	[85]

Membrane	Operating Conditions	Re Nu	Heat Transfer Coefficient (W/m² K)	Ref.
PP membrane (more 70% porosity)	**Velocity:** (m/s) (0.86)		***h: (unaltered)*** (2600) ***h: (window baffle)*** (3150) ***h: (helical baffle)*** (3750)	[84]
PVDF/PTFE/PP membrane (more 70-90% porosity)	**Velocity:** (m/s) (1.6)	**Nu:** (8.5 – 9.3)	***h:*** (6000 – 7000)	[161]
(Air Gap) PP membrane (porosity 67%)	**Flowrate:** (LPM) (0.17-0.5)		***h:*** (1518.9 – 3239.8)	[164]
Polymeric membrane			***h:*** (75 – 200)	[108]
PP membrane (75% porosity)	**Velocity:** (m/s) (0.02-0.05)	**Re:** (840-4700)	***h:*** (190 – 238)	[72]